8-27-2009

Timing and emplacement of the Philipsburg batholith, SW Montana, and a comparison of two magnetic fabric techniques

Travis James Naibert

Travis James Naibert
Candidate

Earth and Planetary Sciences
Department

This thesis is approved, and it is acceptable in quality and form for publication:

Approved by the Thesis Committee:

, Chairperson

TIMING AND EMPLACEMENT OF THE PHILIPSBURG BATHOLITH, SW MONTANA, AND A COMPARISON OF TWO MAGNETIC FABRIC TECHNIQUES

BY

TRAVIS JAMES NAIBERT

B.S., EARTH SCIENCES, MONTANA STATE UNIVERSITY

THESIS

Submitted in Partial Fulfillment of the
Requirements for the Degree of

Master of Science
Earth and Planetary Sciences

The University of New Mexico
Albuquerque, New Mexico

August, 2009

ACKNOWLEDGEMENTS:

I acknowledge the Geological Society of America, the Office of Graduate Studies, and the Department of Earth and Planetary Sciences for their financial aid

I am grateful to the faculty and staff of the Earth and Planetary Sciences Department for their help and support, for great instruction, and for the opportunity to learn more about science and about myself through teaching and research. I would especially like to thank my committee members, Dr. Mousumi Roy and Dr. Jane Selverstone for their time, knowledge, and encouragement over the last three years.

I am grateful for the friendships I have made amongst my fellow UNM students. I sincerely hope and believe that many of these relationships will last well into the future.

I must extend a special thanks to the paleomagnetism research group: to Steph Mason, Kate Zeigler and Linda Donohoo-Hurley, to Jack Grow for assistance both in the field and through three years of classes, and to Scott Muggleton for lab assistance and close friendship. Thank you to Tim Wawryniec, lab manager and pizza maker extraordinaire. It has been great working with you all.

A huge thank you to my parents for always being proud of my accomplishments. I love you and it is easy to list you as my role models.

Special thanks to my best friend Christina Carr.

And finally, thank you to my advisor and good friend, Dr. John Geissman, for leading me to New Mexico. I have seen many spectacular places in the last three years, and I owe much of it to you.

TIMING AND EMPLACEMENT OF THE PHILIPSBURG BATHOLITH, SW MONTANA, AND A COMPARISON OF TWO MAGNETIC FABRIC TECHNIQUES

BY

TRAVIS JAMES NAIBERT

ABSTRACT OF THESIS

Submitted in Partial Fulfillment of the
Requirements for the Degree of

Master of Science
Earth and Planetary Sciences

The University of New Mexico
Albuquerque, New Mexico

August, 2009

TIMING AND EMPLACEMENT OF THE PHILIPSBURG BATHOLITH, SW MONTANA, AND A COMPARISON OF TWO MAGNETIC FABRIC TECHNIQUES

By

Travis James Naibert

B.S., Earth Sciences, Montana State University, 2006

M.S., Earth and Planetary Sciences, University of New Mexico, 2009

Abstract

Magnetic anisotropy is widely used for measuring the orientation of minerals in many rock types. The anisotropy of magnetic susceptibility (AMS) is used extensively to determine magma flow fabrics in both intrusive and extrusive igneous rocks. The anisotropy of anhysteretic remanent magnetization (AARM) allows determination of the anisotropy of ferro/ferrimagnetic minerals in igneous rocks, which have a strong control on AMS. Chapter One investigates the relationship of magma flow to local structures in the Philipsburg Batholith, a Late Cretaceous intrusion that cross-cuts the Georgetown-Princeton Thrust in the Flint Creek Range of southwest Montana. Well defined, mostly subhorizontal AMS fabrics were measured from 119 sites in the Philipsburg Batholith. Areas with steep magnetic foliations along the Georgetown-Princeton Thrust and the Bungalow Fault are interpreted as zones of magma ascent. Rising magma was emplaced along the Georgetown-Princeton thrust at the top of a ramp. $^{40}Ar/^{39}Ar$ dates from 13

biotite separates suggest that the Philipsburg Batholith was emplaced over about two millions years, with an average age of 74.6 ± 0.3 Ma. These data suggest that Sevier-age thrust belt development in SW Montana had shifted to the east by ~75 Ma. Paleomagnetic data from 28 accepted sites in the Philipsburg Batholith show 9 to 16 ± 8° of west-down tilting compared to reference directions for the North American Craton. Tilting is due to further Sevier thrust belt development to the east or uplift in the hanging wall of the Anaconda Metamorphic Core Complex to the east. Chapter Two compares AMS and AARM fabric data in the Philipsburg Batholith, two intrusions from the Central Montana Alkalic Province, and dikes from the Spanish Peaks Igneous Complex, Colorado. Rock magnetic tests show that the Philipsburg Batholith contains a large population of multi-domain magnetite. The Shonkin Sag and Square Butte Laccoliths contain a mixture of multi-domain and pseudo single-domain magnetite. Four relationships between AARM and AMS fabrics are recognized. All three intrusions have more than one AARM/AMS relationship, suggesting that multi-domain magnetite is not the only control on AARM/AMS relationships. Varying degrees of anisotropy within different size fractions of magnetite may also affect AMS and AARM fabrics.

Table of Contents

Table of Contents vii
List of Figures ix
List of Tables x
Introduction 1
Chapter One 6
Abstract 6
Introduction 7
Regional Geology and Setting of the Philipsburg Batholith 10
Location and Local Structures 10
Petrography 14
Previous Emplacement Models 18
Previous Geochronologic Studies 19
Methods 19
Anisotropy of Magnetic Susceptibility 19
Anisotropy of Anhysteretic Remanent Magnetization 22
Paleomagnetism and Rock Magnetism 23
^{40}Ar / ^{39}Ar Geochronology 24
Results 25
$^{40}Ar/^{39}Ar$ Geochronology 25
Paleomagnetism 33
Rock Magnetism 38
AMS Fabrics in the Philipsburg Batholith 44
AARM Fabrics in the Philipsburg Batholith 51
Discussion 52
Timing of Emplacement and Sevier Fold-Thrust Belt Development 52
Emplacement of the Philipsburg Batholith 57
Comparison of AARM and AMS Fabrics 62
Conclusions 63
Chapter One Acknowledgements 65
References Cited 65
Appendix: Calculating Horizontal-Axis Tilt and Associated Uncertainty 69
Chapter Two 74
Abstract 74
Introduction 75
AMS background 77
AARM background 80
Geologic Background of the Sampling Areas 82
Methods 83
AMS Methods 84
AARM Methods 85
Partial AARM methods 85
Results 87
Average Bulk Susceptibility 87
Rock Magnetic Results 88

AMS and AARM Results 91
Comparison of T and P' values from AMS and AARM Data 96
Comparison of AMS and AARM fabrics 97
Fabric Relationship Types 97
Philipsburg Batholith Fabrics 99
Square Butte and Shonkin Sag Laccolith Fabrics 100
SPIC Dike Fabrics 104
pAARM Results 105
Discussion 107
Conclusions 112
Chapter Two Acknowledgements 113
References Cited 114

List of Figures

Figure 1. Hypothetical ramp-top emplacement model for the Philipsburg Batholith..... 8
Figure 2. Regional map of SW Montana showing Cretaceous intrusions 10
Figure 3. Geologic map of the Flint Creek Range and Philipsburg Batholith..... 12
Figure 4. Modal variation of felsic minerals in the Philipsburg Batholith 15
Figure 5. Philipsburg Batholith photomicrographs under transmitted light 16
Figure 6. Philipsburg Batholith photomicrographs under reflected light 17
Figure 7. Schematic magnetic fabric ellipsoid..... 21
Figure 8. $^{40}Ar/^{39}Ar$ biotite age spectra from the Philipsburg Batholith 28
Figure 9. Age probability diagram for Philipsburg Batholith biotite age dates..... 32
Figure 10. Map of $^{40}Ar/^{39}Ar$ dates from Philipsburg Batholith samples 33
Figure 11. Orthogonal vector diagrams of representative Philipsburg Batholith samples 35
Figure 12. Equal-area plot of all paleomagnetic directional data and grand mean direction from the Philipsburg Batholith 38
Figure 13. IRM acquisition curves for representative Philipsburg Batholith samples 39
Figure 14. Representative modified Lowrie-Fuller plots..... 40
Figure 15. Median destructive field ratio (MDF_{arm}/MDF_{irm}) vs. bulk susceptibility..... 41
Figure 16. Representative hysteresis curves for Philipsburg Batholith samples 43
Figure 17. Coercivity ratio vs. magnetic saturation ratio plot 44
Figure 18. Bulk susceptibility plot of all Philipsburg Batholith sites..... 45
Figure 19. Shape parameter vs. degree of anisotropy for all sampling sites 45
Figure 20. Contours of the degree of anisotropy in the Philipsburg Batholith..... 46
Figure 21. Equal-area plots of AMS data from representative sites..... 48
Figure 22. Map of AMS lineations and foliations in the Philipsburg Batholith..... 50
Figure 23. Contours of the magnitude of dip of AMS foliations..... 51
Figure 24. Mean paleomagnetic directions from sections of the Philipsburg Batholith... 54
Figure 25. Comparison of the grand mean paleomagnetic direction to three expected directions from published paleomagnetic poles..... 56
Figure 26. Geometric representation of the variables used to calculate tilt between two paleomagnetic directions. 70
Figure 27. Geometric representation of the dependence of tilt error on the inclination of the measured and expected paleomagnetic directions 73
Figure 28. Schematic AMS and AARM fabric ellipsoid..... 78
Figure 29. Fifteen measurement positions for AARM and pAARM measurements..... 86
Figure 30. Median destructive field ratio (MDF_{arm}/MDF_{irm}) of twenty-six sites 89
Figure 31. Equal-area plots of representative AMS data from the four field areas..... 91
Figure 32. Equal-area plots of representative AARM data from the four field areas..... 92
Figure 33. Comparison of degree of anisotropy (P') of AMS and AARM ellipsoids..... 94
Figure 34. Comparison of the shape parameter (T) of AMS and AARM ellipsoids..... 95
Figure 35. Four model fabric relationships between AMS and AARM..... 96
Figure 36. AARM/AMS fabric relationships in the Philipsburg Batholith 98
Figure 37. AARM/AMS fabric relationships in the Square Butte Laccolith..... 99
Figure 38. AARM/AMS fabric relationships in the Shonkin Sag Laccolith 101
Figure 39. AARM/AMS fabric relationships in the Spanish Peaks Igneous Complex .. 102
Figure 40. Equal-area plots of pAARM and AARM ellipsoids from site PB58 104

List of Tables

Table 1. $^{40}Ar/^{39}Ar$ biotite dates from the Philipsburg Batholith 26
Table 2. Site mean paleomagnetic directional data 36
Table 3. AMS and AARM fabric directions from the Philipsburg Batholith 52
Table 4. Mean paleomagnetic directions from sections of the Philipsburg Batholith 53
Table 5. Comparison of observed and expected paleomagnetic directions 55
Table 6. Average bulk susceptibility for twenty-six sites 87
Table 7. AMS and AARM fabrics and calculated ellipsoid parameters 93

Introduction

This thesis encompasses two related research projects, which the author has worked on since starting at UNM in Fall 2006. The bulk of this thesis is work conducted by the author, with assistance in sample preparation and laboratory procedures by the co-authors of each chapter and by Mr. Nick George and Mr. Will Woodruff.

The anisotropy of magnetic susceptibility (AMS) is a widely used measurement approach for examining the fabrics, or the preferred orientation, of mineral species in a very wide range of rock types, including igneous, sedimendary and metamorphic rocks. Although AMS has many applications, one of the most useful is for determining the alignment of elongate or platy minerals in igneous rocks to determine the direction of magma flow during cooling. Flow fabrics are often too weak to see with the unaided eye in the field, but AMS data give researchers the ability to quantitatively measure very weak mineral fabrics in three dimensions. AMS data from multiple samples at each site also allow statistical examination of the robustness of the measured mineral fabrics.

The emplacement of large bodies of silicic magma into the crust in convergent settings is a long-standing problem in the geosciences. Horizontal compressive stress would seemingly prohibit the space required for magma ascension and emplacement. The Late Cretaceous Philipsburg Batholith in the Flint Creek Range of southwest Montana is an example of a moderate sized (122 km^2 surface area) silicic igneous intrusion, which was emplaced in the upper crust during a period of crustal shortening. To better understand the pattern of magma flow within the Philipsburg Batholith, and to determine if magma emplacement was related to local faults and folds, AMS fabric data were obtained from sampling sites throughout the Philipsburg Batholith. Paleomagnetic

directions recorded in the same samples also allow the assessment of whether the Philipsburg Batholith has undergone vertical axis rotation or horizontal tilting due to deformation in SW Montana since the time of magma emplacement. The magnitude of rotation, or more likely tilting, was determined by comparing paleomagnetic directions recorded in the Philipsburg Batholith with three expected directions based on previously published Late Cretaceous paleomagnetic poles for the North American Plate. Additionally, $^{40}Ar/^{39}Ar$ age spectra on biotite were used to accurately determine the emplacement age of the Philipsburg Batholith to more fully understand the timing and duration of magma emplacement relative to regional crustal shortening events in the Late Cretaceous.

Philipsburg Batholith data are presented in Chapter One of this thesis. Samples were collected during July/August of 2007, with three weeks of assistance in the field by Mr. Jack Grow and one week of assistance by Ms. Christina Carr. The author prepared all samples during the summer/fall of 2007. AMS measurements were conducted during the Fall 2007, and presented by the author at the 2007 American Geophysical Union Fall Feeting in San Francisco, CA. Paleomagnetism and geochronology of the Philipsburg Batholith were measured through the spring/summer, 2008. Rock magnetic data were collected by the author, with minor assistance by Mr. Will Woodruff. The author and Dr. John Geissman interpreted the AMS, paleomagnetic, and age data for the Philipsburg Batholith. The Chapter One manuscript was written by the author with editing by Dr. John Geissman, and will be submitted for publication in either the Geological Society of America Bulletin, or the new GSA journal Lithosphere.

The use of AMS fabrics to determine magma flow direction is predicated on an understanding of the key minerals contributing to the measured AMS fabrics. Measuring the anisotropy of anhysteretic remanent magnetization (AARM) allows an additional measure of magnetic mineral fabrics in igneous rocks, which may be dissimilar to AMS fabrics under some circumstances. AMS is a measure of the combined orientations of all diamagnetic, paramagnetic mineral species in a sample, as well as minerals capable of retaining a permanent magnetization. AARM measures only the preferred orientation of ferro/ferrimagnetic minerals, such as magnetite, which likely exert a strong control on the AMS fabric, due to their high susceptibilities compared to paramagnetic phases like biotite. It is therefore helpful to understand their preferred orientation in order to interpret their contribution to the measured AMS fabrics. AARM measurements were made for eight sites from the Philipsburg Batholith for comparison with AMS data. AARM measurements were also made for eleven sites from the Early Tertiary Shonkin Sag Laccolith and four sites from the Early Tertiary Square Butte Laccolith, both in north-central Montana, and for three dikes from the Mid-Tertiary Spanish Peaks Igneous Complex in southern Colorado. AARM and AMS fabrics from each of these sample sites were compared in order to make general observations about the relationship between the preferred orientations of magnetite and the overall AMS fabric orientations in these very different intrusive igneous rocks.

Chapter Two is a presentation of the fabric relationships between AARM and AMS from the three Montana intrusions and the Spanish Peaks dikes. The Philipsburg Batholith samples used in Chapter Two are the same as presented in Chapter One. Dr. John Geissman of UNM, Dr. Daniel Holm of Kent State University, and the author

conducted field sampling in the Shonkin Sag and Square Butte Laccoliths during August, 2006, and 2007. We were joined by Mr. Nick George in 2007. Shonkin Sag and Square Butte sample preparation and AMS measurements were performed by Nick George and the author. AMS samples from the Spanish Peak Igneous Complex dikes were collected, prepped, and measured by Mr. Scott Muggleton for his MS thesis at UNM, completed in 2006. AARM measurements of the eleven Shonkin Sag Laccolith and four Square Butte Laccolith sites were performed by Dr. Daniel Holm. The AARM data of all Philipsburg Batholith and Spanish Peaks dikes were measured by the author during the summer/fall of 2008. AARM data reduction was completed by the author during the Fall, 2008. Prelinimary results were presented at the 2008 American Geophysical Union Fall Meeting in San Francisco. The Chapter Two manuscript was written by the author, with editing by Dr. John Geissman, for submission to the Journal of Geophysical Research or Earth and Planetary Science Letters.

The project described in Chapter Two of this thesis marks the first time AARM measurements were performed at the University of New Mexico Paleomagnetism Laboratory. AARM measurement procedures were developed and documented for future use by the author with help from Dr. John Geissman and heavy reliance on Tauxe (1998). AARM ellipsoids were calculated and plotted using a MatLab script developed by the author.

AMS data from Shonkin Sag and Square Butte Laccolith samples presented in Chapter Two are part of a larger research project to determine the emplacement history and paleomagnetism of intrusions in the Central Montana Alkalic Province. This project

is primarily being conducted by Dr. John Geissman and Dr. Daniel Holm, with assistance by the author.

Chapter One

Timing and emplacement mechanisms of the Philipsburg Batholith from $^{40}Ar/^{39}Ar$ geochronology and magnetic fabrics.

T.J. Naibert and J.W. Geissman
Dept. of Earth and Planetary Sciences – University of New Mexico

Abstract

The Late Cretaceous Philipsburg Batholith in southwest Montana offers an ideal location to study the emplacement of silicic plutons in the Sevier fold-thrust belt of the western US Cordillera. Magnetic fabrics, determined using the anisotropy of magnetic susceptibility from 119 sites, suggest that the Philipsburg Batholith is a tabular body generally characterized by subhorizontal magma flow away from local thrust faults, including the Georgetown-Princeton Thrust, which served as conduits for magma ascent. Field relations and magnetic fabrics suggest that the Philipsburg Batholith was emplaced within a fault-bend fold at the top of a ramp in the Georgetown-Princeton thrust system. New $^{40}Ar/^{39}Ar$ geochronologic data indicate that the entire Philipsburg Batholith was emplaced rapidly around 74.6 ± 0.3 Ma. Paleomagnetic directional data indicate that the Philipsburg Batholith has experienced 9 to 16 ± 8° (tilt estimate and associated error based on a new method described here) of west-side down tilt since the Late Cretaceous. The data do not support any internal deformation of the batholith since emplacement. These results suggest that Sevier-age thin-skinned deformation in the Flint Creek Range had ceased by ~75 Ma and that the observed tilt could be associated with subsequent Cenozoic extension.

Introduction

Emplacement of silicic plutons is an important component in the growth of continental crust. Most silicic intrusions are emplaced within convergent plate boundaries where the principal stresses causing crustal shortening would seemingly prohibit emplacement of large magma bodies (Hutton, 1997). This long-standing room problem is a fundamental question in understanding the role of plate tectonics and attending magma generation in the formation of continental crust. Many workers have suggested emplacement mechanisms that may explain magma rise and intrusion during crustal shortening, typically requiring dilational space being formed by some component of oblique faulting (Tikoff and Teyssier, 1992; Karlstrom et al., 1993; Castro and Fernandez, 1998; Titus et al., 2005). Although deformation of the crust undoubtedly plays a major role in the ascent and emplacement of large, typically silicic, magma bodies, the actual mode of emplacement during crustal shortening is poorly understood. Knowledge of the internal architecture of granitic intrusions in relation to structures and deformation of the host rocks will lead to more accurate models for the growth of continental crust during orogeny.

The Late Cretaceous geologic history of Southwest Montana is marked by thin-skinned fold-and-thrust belt development (Sevier Orogeny) and higher-angle Laramide style reverse faulting involving Precambrian basement rocks (Schmidt et al., 1990). Contemporaneous granitic intrusions of a range of dimensions were emplaced to the east of the main magmatic arc (exposed in the Idaho Batholith), the largest intrusion being the composite Boulder Batholith (Hamilton and Myers, 1974). This temporal and spatial

overlap between magma emplacement and foreland thrust belt development offers an ideal setting for the study of plutonism associated with crustal shortening.

The geometry of the Boulder Batholith and other intrusions in SW Montana, whether tabular or prismatic, has been extensively debated (Klepper et al., 1971, 1974; Hamilton and Myers, 1974; Schmidt et al., 1990). Kalakay et al. (2001) mapped three tabular intrusions in Southwest Montana and developed a field-based model for shallow crustal intrusions (emplaced at 1-10 km depth) involving injection into fault-bend folds at the top of thrust fault ramps. The Kalakay et al. (2001) model proposes that ramp-flat geometry of thrust faults allows magma to fill space created by local extension, possibly aided by backthrusting (figure 1). Implicit in their model is the migration of magma along the thrust surface to the top of the ramp instead of magma flow by sub-vertical diking.

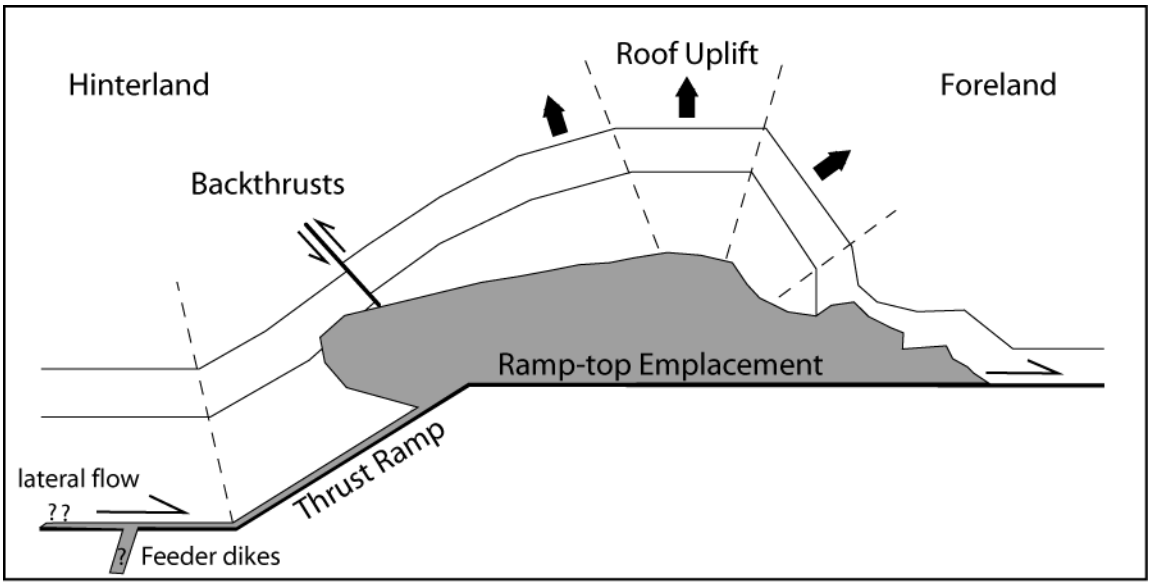

Figure 1. Ramp-top emplacement model for SW Montana intrusions proposed by Kalakay et al. (2001). Magma fills space within a fault-bend fold due to roof uplift and backthrusting.

The Philipsburg Batholith is a Late Cretaceous intrusion in the Flint Creek Range (figure 2), west of the Boulder Batholith and lies in a similar structural position as the Boulder Batholith, as well as the three intrusions studied by Kalakay et al. (2001). In the

current study, anisotropy of magnetic susceptibility (AMS) data are utilized as a measure of magma flow fabric to determine the internal architecture and emplacement mode of the Philipsburg Batholith. $^{40}Ar/^{39}Ar$ geochronologic data were obtained to better understand the emplacement history of the batholith and to determine if emplacement occurred in multiple pulses. Paleomagnetic data were used to examine post-emplacement deformation and to assess the possibility of internal deformation in the Philipsburg Batholith to ensure the validity of AMS interpretations. Estimated mean paleomagnetic directions reveal no statistically resolvable component of internal deformation of the batholith and, hence no corrections to AMS fabrics are required due to internal deformation. AMS data show mostly subhorizontal fabrics radiating away from local thrusts and are interpreted to suggest that emplacement was largely concentric away from at least one magma channel centered along the Georgetown-Princeton thrust. Our interpretation supports application of the model of Kalakay et al. (2001) to the emplacement of the Philipsburg Batholith.

Lageson et al. (2001) discussed the influence of large-volume intrusions on the development of the Sevier-age orogenic wedge in SW Montana and argued that critical wedge taper is promoted by the intrusion of large magma bodies, leading to further propagation of the thrust belt. If magma emplacement atop thrust ramps is common, then the added mass of plutons emplaced into the foreland may have similarly influenced the development of thrust belts in other orogens throughout the geologic past.

Regional Geology and Setting of the Philipsburg Batholith

Location and Local Structures

The Philipsburg Batholith is one of three large granitic intrusions in the Flint Creek Range, which lies ~40 km west of Butte, Montana (figure 2). The 122 km^2 surface area Philipsburg Batholith crops out to the west of the Mount Powell Batholith and Royal Stock (figure 3). All three bodies were intruded into metasedimentary and sedimentary rocks of the Precambrian Belt Supergroup through the Lower Cretaceous Kootenai Formation. The Flint Creek Range is separated from the Boulder Batholith to the east by the Deer Lodge Valley, a Cenozoic normal fault bounded valley.

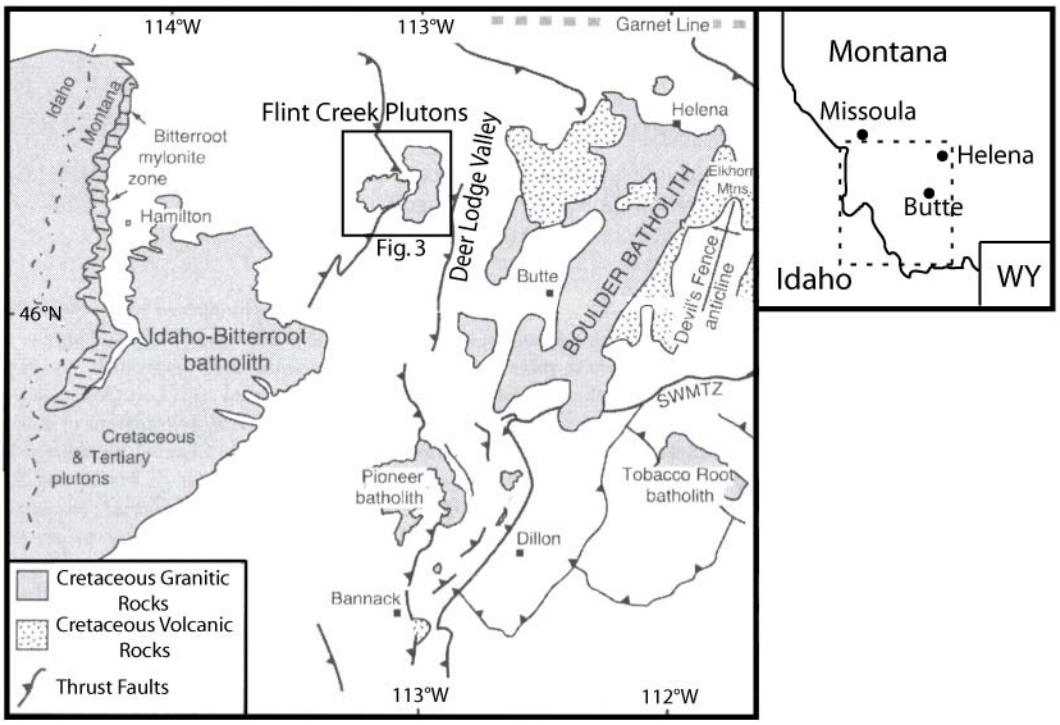

Figure 2. Map of Late Cretaceous granitic intrusions in SW Montana showing the location of the Flint Creek Range Plutons relative to regional tectonic features. SWMTZ – Southwest Montana Transverse Zone. Modified from Lageson et al., 2001.

The sedimentary sequence in the Flint Creek Range was intensely deformed during regional development of the Sevier fold and thrust belt in the Late Cretaceous

(Hyndman et al., 1972; O'Neill et al., 2004). The principal fault in the western Flint Creek Range is the west-dipping Georgetown-Princeton Thrust (figure 3), which places Belt Supergroup rocks over Paleozoic rocks as young as the Mississippian Madison Group (Hyndman et al., 1982). The fault trace runs roughly north-south, except where the fault swings to the east as it nears the contact with the Philipsburg Batholith. There is no evidence that the Georgetown-Princeton Thrust cuts the Philipsburg Batholith and therefore intrusion must have occurred during or after final movement on the Georgetown-Princeton Thrust. The fault segment south of the Philipsburg Batholith ends at the center of the southern batholith margin (Ehinger, 1971; Hyndman, 1982; O'Connell, 2000). An eastern splay of the Georgetown-Princeton Thrust is exposed south of the Philipsburg Batholith, is very steeply dipping and has been mapped by some workers as a high-angle normal fault (Lonn et al., 2003).

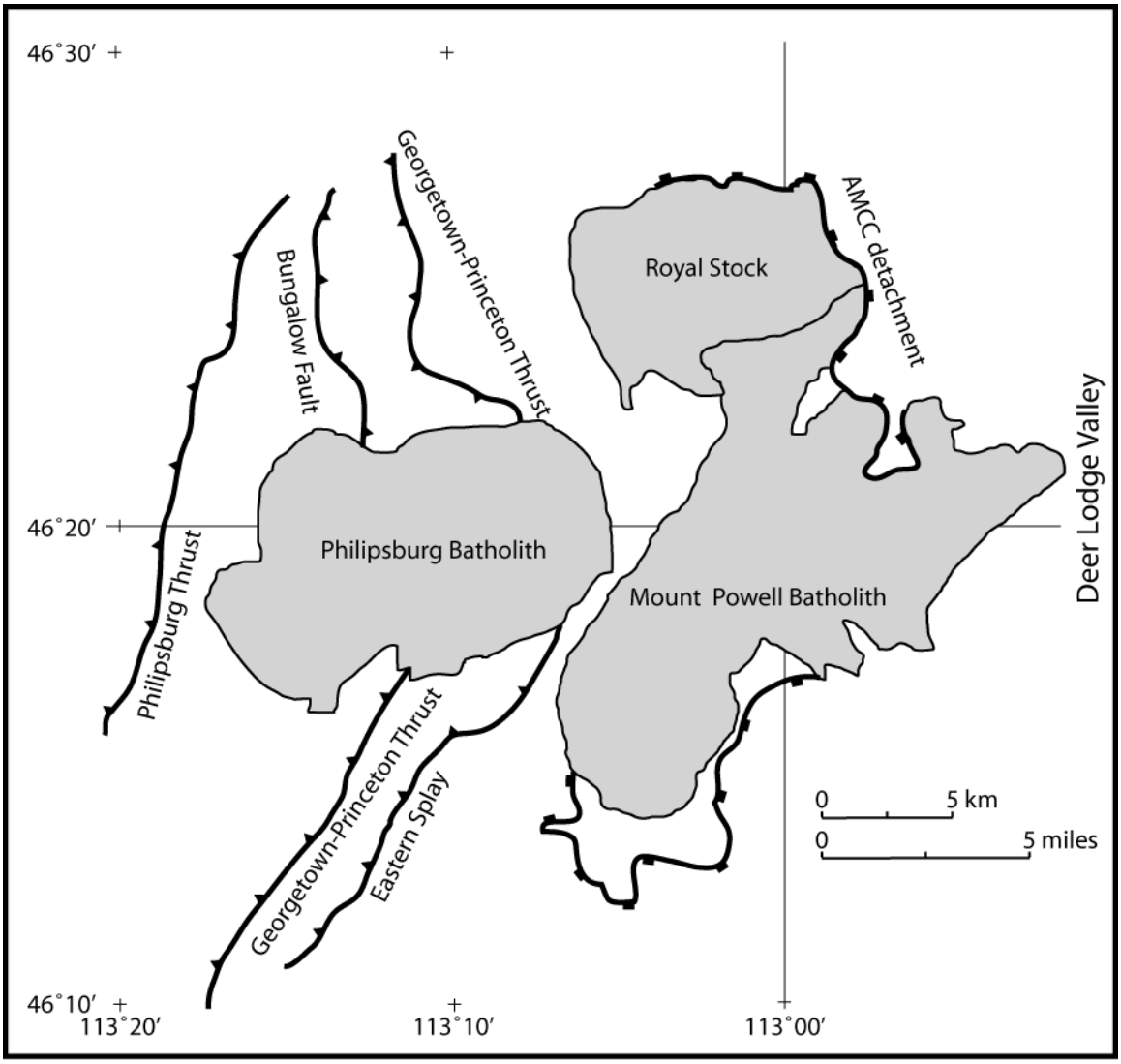

Figure 3. Generalized structural map of the Flint Creek Range showing relative positions of the three large Flint Creek plutons, major Sevier-age thrust faults, and the low-angle detachment of the Cenozoic Anaconda Metamorphic Core Complex. Modified from Hyndman et al., 1982 and O'Neill et al., 2004.

At its northern margin, the Philipsburg Batholith cuts the high-angle Bungalow Fault, a few kilometers west of the Georgetown-Princeton Thrust (figure 3). Interpretations of movement sense on the Bungalow fault are unclear due to poor exposure; both normal and reverse motion has been reported (Lonn et al., 2003; Lewis, 1998; Hyndman et al., 1982). In this study, the Bungalow Fault is interpreted as a backthrust accompanying Late Cretaceous displacement along the Georgetown-Princeton

thrust. This movement sense is suggested by near vertical dips of the thrust plane, movement prior to intrusion, and fault contacts between Belt Supergroup rocks on the east side of the fault and Upper Paleozoic through Mesozoic units west of the fault.

Folds in country rocks are present in both the hanging wall and the footwall of the Georgetown-Princeton Thrust system. The Philipsburg Anticline, runs N-S along the western margin of the Philipsburg Batholith and is cut by the intrusion. The Royal Gold Creek Anticline, the Finley Basin Anticline, and the Racetrack Folds are in the footwall of the Georgetown-Princeton Thrust. The Racetrack folds are a series of anticlines and synclines within an overall synclinorium between the Philipsburg Batholith and the Mount Powell Batholith and Royal Stock to the east. The synclinorium widens to the north. The fold axis of the Royal Gold Creek Anticline changes from N-S to NW-SE closer to the Philipsburg Batholith. The Cable Mountain Anticline is located between the main Georgetown-Princeton Thrust and the eastern thrust splay south of the Philipsburg Batholith. The N-S fold axis of the Cable Mountain Anticline is also deflected to the east closer to the Philipsburg Batholith.

The two intrusions in the eastern Flint Creek Range have been interpreted by O'Neill et al. (2004) as the uplifted footwall of the Anaconda Metamorphic Core Complex (AMCC), which developed during the Middle Eocene. The detachment fault for the AMCC dips shallowly to the east. The trace of the detachment is mapped on the eastern edge of the Flint Creek Range (figure 3) and extends south along the east side of the Anaconda Range. The Philipsburg Batholith is exposed ~15 km west of the detachment and no evidence of extension within the batholith was observed in the field.

Petrography

The composition of the Philipsburg Batholith ranges from granite to granodiorite and quartz monzodiorite (figure 4). Samples contain quartz, plagioclase feldspar, K-feldspar, biotite and hornblende. The Philipsburg Batholith was originally mapped as a single intrusion with some internal gradations in biotite, hornblende, and K-feldspar content (Ehinger, 1971). Hyndman et al. (1982) divided the Philipsburg Batholith into the more mafic Bimetallic Stock to the west and the more felsic Dora Thorn Pluton to the east (figure 3). The modal percentage of Fe-Mg silicate minerals varies considerably throughout the Philipsburg Batholith, especially within the Dora Thorn Pluton. The Bimetallic Stock averages 25 percent mafic phases, with hornblende often more abundant than biotite (figure 5). The Dora Thorn Pluton averages 15 percent Fe-Mg silicates but some samples are as low as 5 percent biotite and have no hornblende (figure 5). Overall, the percentage of hornblende is higher in samples from the Bimetallic Stock. Hyndman et al. (1982) report an apparent gap in SiO_2 content of ~10 percent between the two proposed plutons, but the gap is based on a limited number of samples. The composition grades from quartz diorite to granodiorite over 100-300 m near the head of Summer Gulch, which was interpreted by Hyndman et al. (1982) as the contact between the Bimetallic Stock and Dora Thorn Pluton in the southwest part of the field area. This gradation is difficult to trace north along the proposed contact between the two intrusions and other spatially restricted compositional gradations exist throughout the field area, suggesting that the Philipsburg Batholith may have been formed by multiple pulses of magmatism over a short span of time.

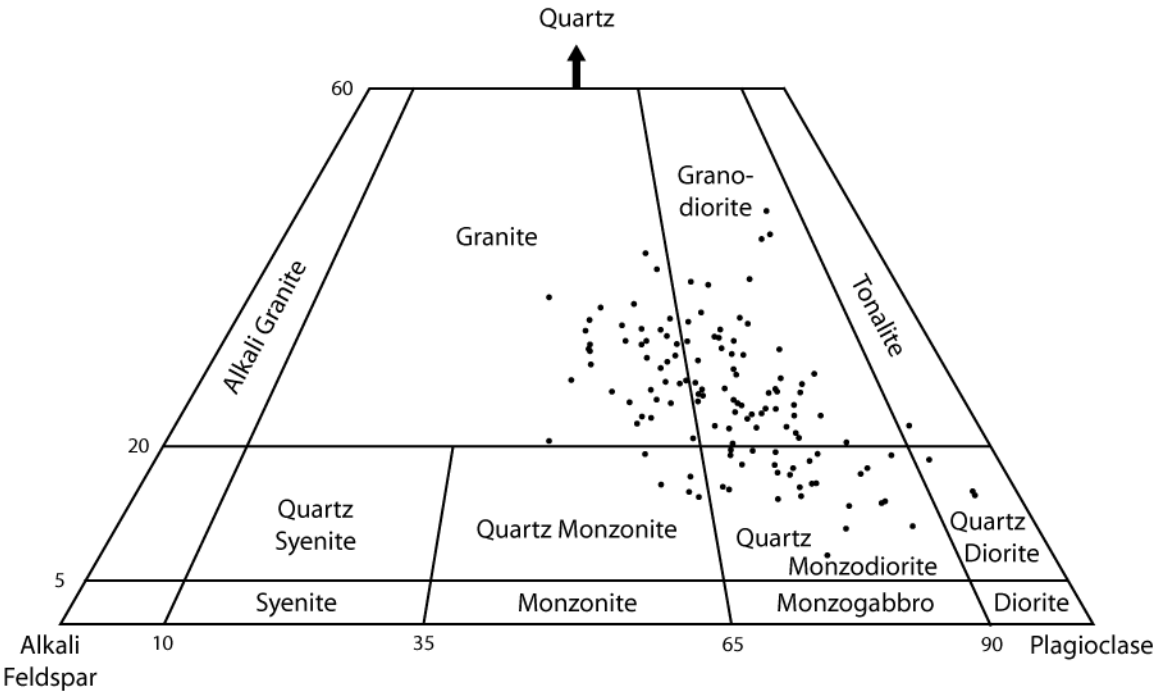

Figure 4. Modal variation of felsic minerals in the Philipsburg Batholith using the classificatin of Streckeisen, 1973. Modified from Hyndman et al., 1982.

Samples examined in reflected light show that magnetite is the most abundant oxide phase. Representative reflected light photomicrographs (figure 6) show that magnetite grains are located within biotite, feldspar, and amphibole, as well as along grain boundaries. Observed magnetite grains range in approximate diameter from about 4 to 200 μm, and often form clusters of large grains up to 2 mm. Most magnetite grains are equant, but some are about twice as wide along one axis in thin section and some are irregularly shaped. Ilmenite lamellae in magnetite are very uncommon. Trace amounts of pyrite are present in some thin sections.

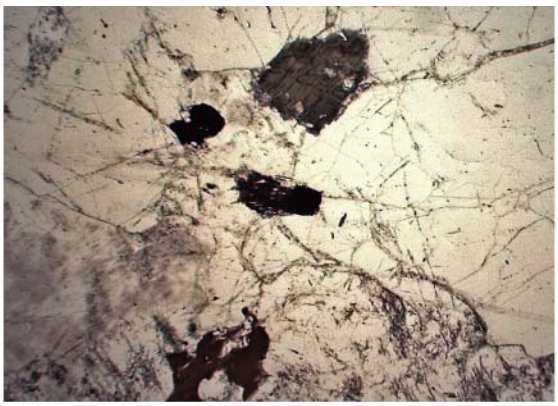

PB2 2.5x transmitted 1 mm

PB4 2.5x transmitted 1 mm

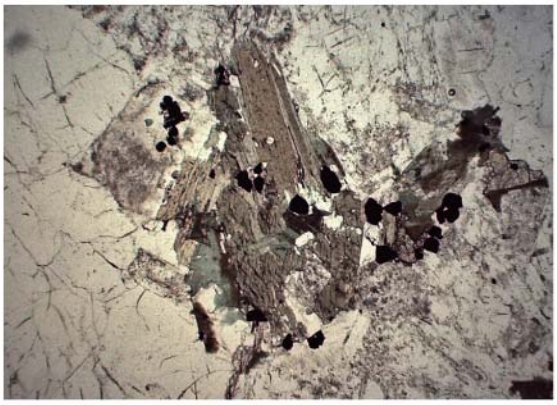

PB29 2.5x transmitted 1 mm

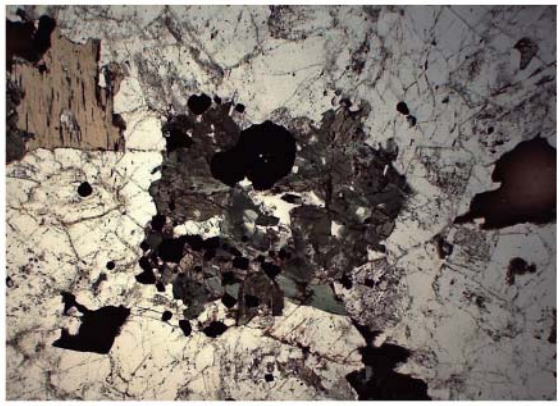

PB40 2.5x transmitted 1 mm

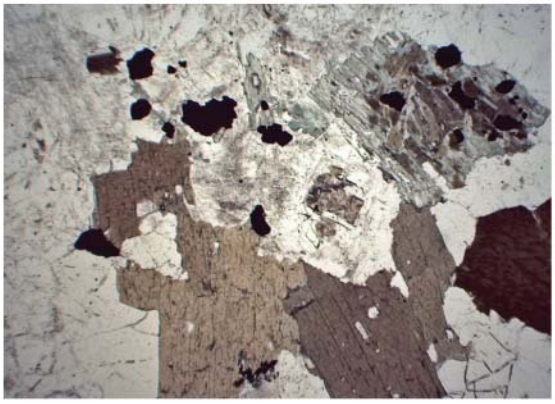

PB43 2.5x transmitted 1 mm

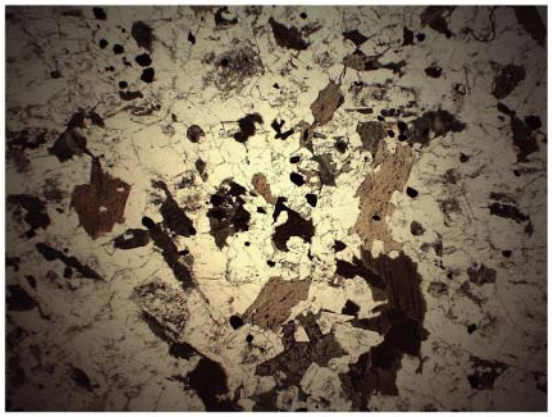

PB110 2.5x transmitted 1 mm

Figure 5. Representative photomicrographs of Philipsburg Batholith samples taken with transmitted light showing average size of major silicate minerals and the relation of large opaque (magnetite) grains to biotite and hornblende.

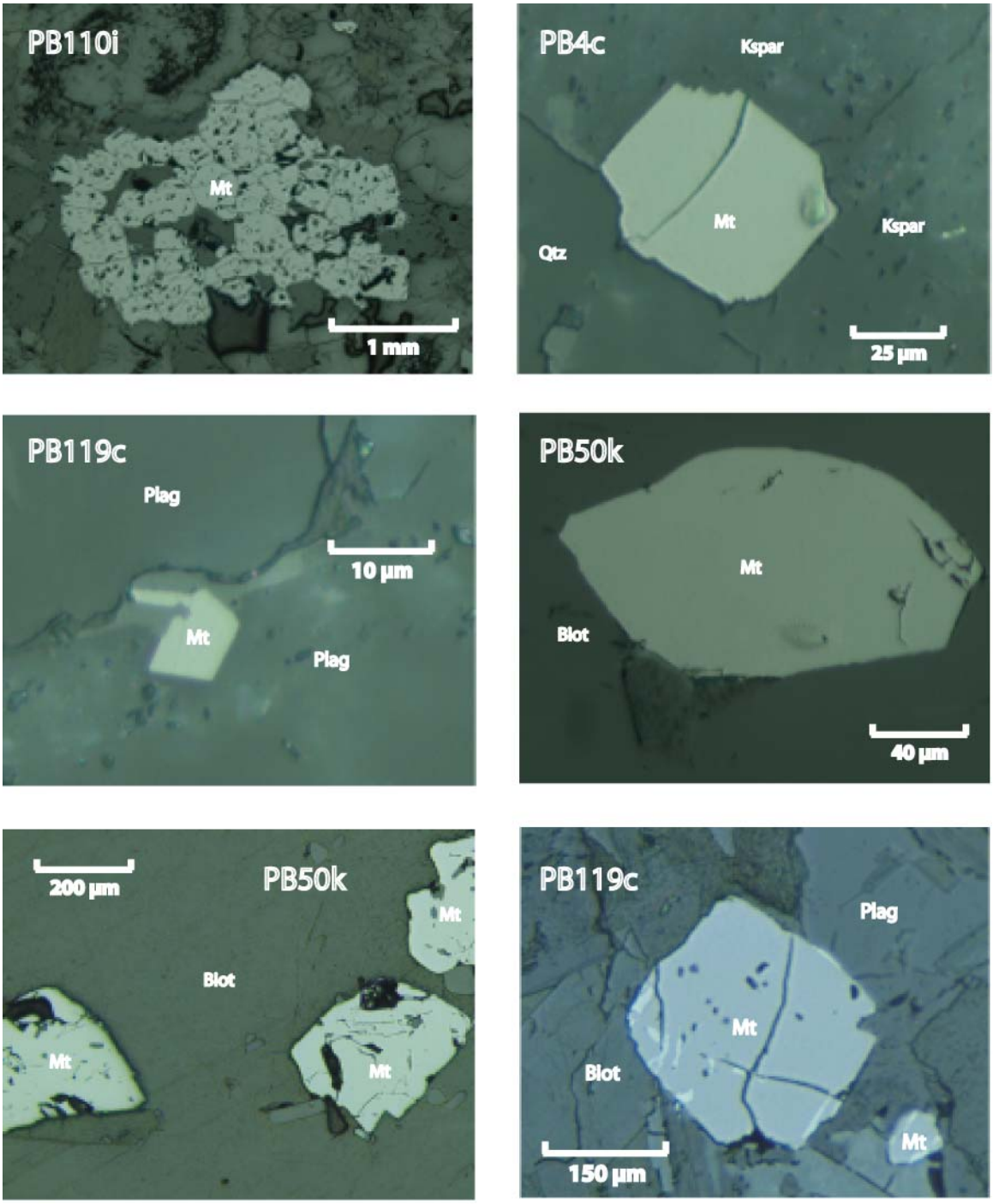

Figure 6. Representative photomicrographs taken under reflected light showing the range of magnetite size and shape in samples from the Philipsburg Batholith.

Typical silicate mineral crystal size in the Philipsburg Batholith is 0.5-2mm and is consistent throughout the field area (figure 5) with minimal fining towards the margins. Hyndman et al. (1982) report some coarsening in the Bimetallic Stock near the contact

with the Dora Thorn Pluton. The metamorphic aureole around the Philipsburg Batholith is about 2 km wide and wall rocks are metamorphosed to the hornblende-hornfels facies (Hyndman et al., 1982). O'Connell (2000) placed the metamorphic assemblages of two samples from the eastern contact aureole in P-T space and inferred temperatures of 500-650ºC and pressures of 1.2-2.7 kbar. Aluminum-in-hornblende geobarometry and hornblende-plagioclase geothermometry on four batholith samples indicate intrusion temperatures of ~720-820ºC and pressures of 0. 9-2.0 kbar, although no confidence limits were reported (O'Connell, 2000). Hyndman et al. (1982) report a maximum pressure of 0.6 kbar based on the presence of miarolitic cavities at the shallowest levels of intrusion. These observations suggest that the Philipsburg Batholith was intruded at depths less than ~6 km.

Previous Emplacement Models

Numerous emplacement mechanisms have been proposed for the Boulder Batholith and other contemporaneous intrusions in SW Montana. Hamilton and Myers (1974) argued that the Boulder Batholith was emplaced as a tabular sheet under the Elkhorn Mountain volcanics and thus questioned earlier interpretations of the Boulder Batholith as a steep-sided, thick intrusion (Klepper et al., 1971). Proposed emplacement mechanisms include lateral magma flow from the Idaho Batholith along major decollement surfaces beneath Sevier thrust plates (Hyndman et al., 1975) or emplacement within a pull-apart space created by intersecting fault sets in the Helena Salient (Schmidt et al., 1990). More recently, Late Cretaceous intrusions in SW Montana have been interpreted to have filled volumes of minimal differential stress within fault-bend folds above thrust ramps (Kalakay et al., 2001).

Previous Geochronologic Studies

Two samples from the Philipsburg Batholith were dated using the K-Ar method by Hyndman et al. (1972). One sample, from the southwest part of the intrusion, yields a hornblende K-Ar date of 76.7 ± 2.5 Ma and a biotite K-Ar date of 74.0 ± 2.1 Ma. The other sample, from the central part of the intrusion, has a hornblende date of 72.0 ± 2.5 Ma and a biotite date of 73.4 ± 2.1 Ma. The age determinations are all within error of ~74 Ma. The slightly older dates in the southwest were used to support the division of the Philipsburg Batholith into the Bimetallic Stock and Dora Thorn Plutons (Hyndman et al., 1982).

Three apatite fission track dates for the Philipsburg Batholith give an average age of 65.9 Ma (Baty, 1973), about 8 Ma younger than K-Ar dates. Fission tracks in apatite become annealed at temperatures well below granitoid crystallization and therefore these dates are not useful as estimates of intrusion ages.

Methods

Anisotropy of Magnetic Susceptibility

Low-field anisotropy of magnetic susceptibility (AMS) is a fast and quantitative method for determining the orientation and degree of development of preferred fabrics of Fe-bearing minerals and has been applied to a range of different rock types and geologic problems (Hrouda, 1982). The AMS technique is sensitive enough to measure preferred mineral fabrics that are far too weak to observe in the field. AMS has been extensively utilized to approximate magma flow fabrics in granitic rocks and to define emplacement models for granitic intrusions (Bouchez et al., 1990; Bouchez, 1997; Aranguren et al., 2003; Titus et al., 2005; Gebelin et al., 2006).

The magnetic susceptibility, K, is a proportionality constant relating the induced magnetization of a solid to the strength of an applied magnetic field. The value of K for most minerals varies depending on the orientation of the mineral in the applied magnetic field. This anisotropy is related to the crystal structure or the shape of the mineral grains (Hrouda, 1982). The susceptibility of a rock combines the contributions to K from all minerals making up the rock and AMS is therefore the result of preferential alignment of anisotropic minerals in the sample. The anisotropy in K for a mineral or a collection of minerals in a sample can be expressed as a symmetric second-rank tensor with eigenvectors K_{max}, K_{int}, and K_{min}. These eigenvectors can be visualized as the principal axes of a susceptibility ellipsoid (figure 7). K_{max} is the AMS lineation and K_{min} is normal to the AMS foliation. The bulk susceptibility, K, for a sample is the mean of the three susceptibility eigenvalues. The degree of anisotropy, P', and the shape parameter, T, are used to describe the relative strengths of K_{max}, K_{int}, and K_{min}. P' ranges from 1 (isotropic) to infinity and T ranges from -1 to 1, with negative values for prolate and positive values for oblate susceptibility ellipsoids. P' and T are calculated following Jelinek (1978) as:

$$P' = \exp(2[(\ln K_{max} - \eta)^2 + (\ln K_{int} - \eta)^2 + (\ln K_{min} - \eta)^2])^{0.5}$$

$$T = 2(\ln K_{int} - \ln K_{min})/(\ln K_{max} - \ln K_{min}) - 1$$

where

$$\eta = (\ln K_{max} + \ln K_{int} + \ln K_{min}) / 3$$

All minerals acquire an induced magnetization when placed in a magnetic field. Diamagnetic and paramagnetic minerals are only magnetized in an applied field. Diamagnetic minerals acquire an induced magnetization opposite to the applied field and have low negative susceptibilities. An example is quartz, which has a susceptibility of -0.8×10^{-7} SI (Butler, 1992). Paramagnetic minerals, such as biotite and hornblende,

acquire induced magnetizations parallel to the applied field and have susceptibilities two to three orders of magnitude higher than diamagnetic minerals. Ferromagnetic or ferrimagnetic minerals have susceptibilities that are orders of magnitude higher than dia- and paramagnetic minerals. Ferromagnetic or ferrimagnetic minerals also acquire a remanent magnetization that remains in the absence of an applied magnetic field.

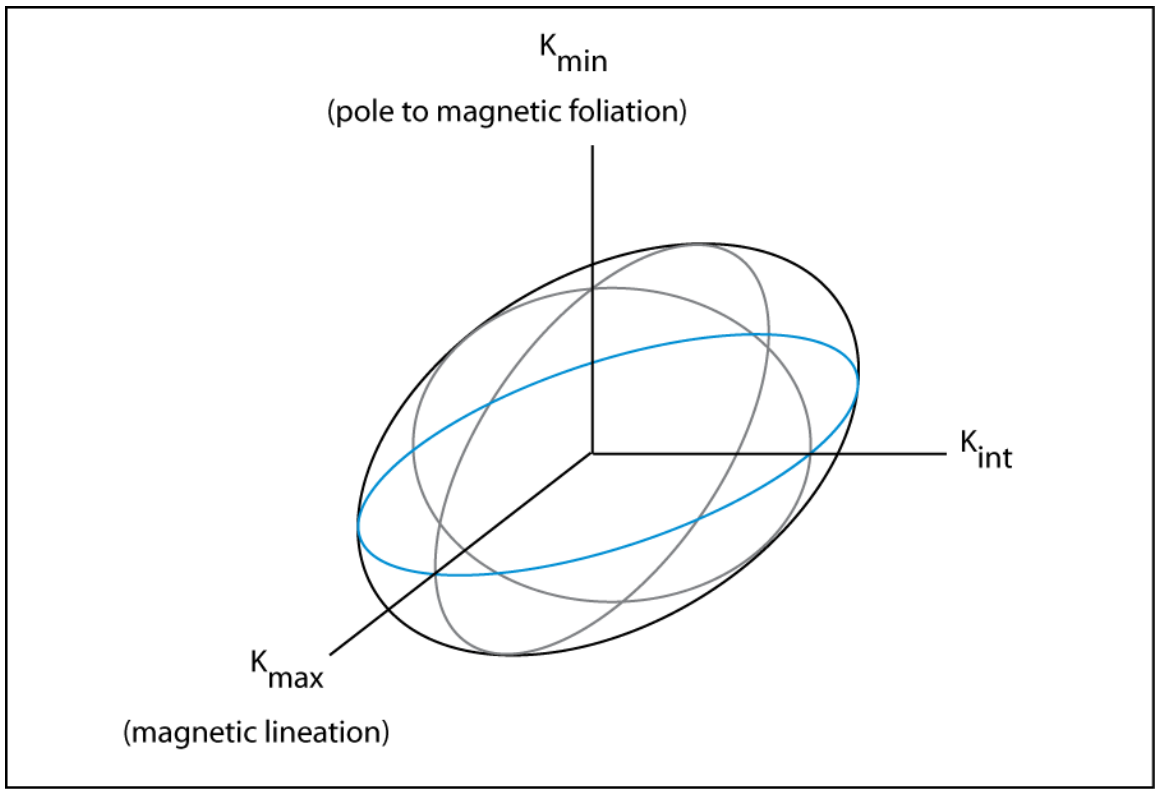

Figure 7. Schematic magnetic fabric ellipsoid showing the relationship of the three principal susceptibility directions to the magnetic lineation and magnetic foliation planes. A similar ellipsoid can be used to visualize both AMS data and AARM data.

A total of 1316 samples from 119 field sampling sites (6-15 samples/site) were collected in the Philipsburg Batholith. Roughly half the AMS samples were also used for paleomagnetic study. In all cases, AMS was measured before discrete specimens were demagnetized for paleomagnetic measurements. Sites were located near logging roads/trails or within stream valleys and were spaced ~1 km apart. Sampling density is

lower in the northern and eastern parts of the batholith due to limited accessibility. Site locations were defined with a hand-held GPS unit with an accuracy of ±10 m. Samples at each site were collected within ~50 m^2 (a single outcrop). All samples were collected using a portable-gas drill with a nonmagnetic diamond drill bit and were oriented with magnetic and sun compasses. The samples were cut into 25 x 22mm right cylinder specimens with a non-magnetic diamond blade before measuring to best approximate the volume of a sphere. At least one specimen from each sample was measured using a Kappabridge KLY-4S. Susceptibility axes $K_{max}>K_{int}>K_{min}$, degree of anisotropy P', and shape parameter T were calculated using the program Anisoft (v4.2) from Agico Inc.

Anisotropy of Anhysteretic Remanent Magnetization

The anisotropy of anhysteretic remanent magnetization (AARM) of samples can be measured to produce a second rank tensor or AARM ellipsoid, similar to the AMS ellipsoid. AARM measures only the preferred fabric of minerals capable of retaining a remanent magnetization after removal of a magnetic field, and therefore the preferred orientation of diamagnetic or paramagnetic minerals does not contribute to AARM.

The AARM of 63 samples from 8 sampling sites was measured to compare with AMS measurements from the same sites. AARM measurements were performed after specimens were AF demagnetized to 100 mT. The specimens for AARM measurement were cut into 15 x 13 mm right cylinders (~2.5 cm^3). An ARM was imparted along the first of fifteen specific axes in a direct field of 0.1 mT superimposed on an alternating field decaying from 100 mT. The specimen was then measured and AF demagnetized to 100 mT. This process was repeated with ARM being measured for the fifteen sample positions described in Tauxe (1998). The AARM ellipsoid and principal axes

$AARM_{max}>AARM_{int}>AARM_{min}$ were then calculated and errors were calculated using the Jelinek method of linear perturbation analysis (Tauxe, 1998).

Paleomagnetism and Rock Magnetism

Paleomagnetic data from 516 independently oriented samples from 63 sites (8-10 samples per site) were collected in order to evaluate post-emplacement deformation of the Philipsburg Batholith. At least one specimen per sample was measured using a 2G Enterprises superconducting rock magnetometer at the University of New Mexico Paleomagnetism Laboratory. Specimens were progressively demagnetized in a series of alternating fields (20-30 steps) until at least 90 percent of the natural remanent magnetization (NRM) had been removed. Most Philipsburg Batholith specimens were 90 percent demagnetized in a range of peak fields from 15 to 35 mT, and few specimens required demagnetizing at fields above 60 mT. For a selected number of samples, an additional specimen was first demagnetized by low temperature demagnetization (LTD) to 77K using liquid nitrogen and warming in a low-field space. 3-4 steps of LTD were followed by progressive alternating field (AF) demagnetization. LTD takes advantage of the change in the crystal structure of magnetite, from cubic to monoclinic at the Verwey transition (~120K). As the structure changes, the crystalline anisotropy in magnetite decreases and remanent magnetization is only retained by elongate SD grains due to shape anisotropy (Dunlop and Ozdemir, 1997). For at least half of the selected samples from the Philipsburg Batholith, over 70 percent of NRM was demagnetized using the LTD technique. The high percentage of NRM reduced in these samples suggests that the NRM is largely held by multi-domain (MD) magnetite. The other population of samples subjected to LTD from the Philipsburg Batholith show less than 10 percent reduction in

NRM. These samples were subsequently AF demagnetized over a range of low alternating fields similar to other Philipsburg Batholith samples.

The direction of characteristic remanent magnetization (ChRM) was determined using at least three sequential demagnetization steps chosen by visual inspection of orthogonal vector diagrams. ChRM was calculated using principal component analysis (Kirschvink, 1980). For eight specimens from one site, no linear demagnetization interval defined by three or more demagnetization steps could be identified. In these cases, great circles were fit to curvilinear demagnetization intervals. Site means were calculated using Fisher (1953) statistics when ChRMs were well determined for all samples, or by using a combination of stable endpoint and great circle analysis (McFadden and McElhinny, 1988).

Several rock magnetic experiments were employed to determine the carriers of magnetic remanence and these included acquisition of an isothermal remanent magnetization (IRM) to saturation, direct field demagnetization of the IRM, AF demagnetization of anhysteretic remanent magnetization (ARM) acquired in a direct field of 0.1 mT and an alternating field decaying from 98 mT, and AF demagnetization of a 98 mT isothermal remanent magnetization (IRM). These tests were performed on a small, but representative, group of samples from 14 sites in the Philipsburg Batholith.

^{40}Ar / ^{39}Ar Geochronology

The ^{40}Ar/^{39}Ar method was used to acquire additional geochronologic data on the Philipsburg Batholith, to test the proposed age difference, as defined by K-Ar data, between the Bimetallic Stock and Dora Thorn Pluton and to place a minimum age on movement of the Georgetown-Princeton thrust. ^{40}Ar/^{39}Ar measurements were obtained

for thirteen biotite separates from the Philipsburg Batholith at the New Mexico Geochronology Research Laboratory, New Mexico Tech. Nine of the samples were from the Dora Thorn Pluton, two were from the Bimetallic Stock, and two were collected near the proposed contact between the two intrusions (figure 4). All samples were analyzed by incremental heating in a furnace using nine heating steps.

All thirteen samples were irradiated in a single irradiation tray with seven standards of Fish Canyon sanidine, with an assigned age of 28.02 Ma (Renne et al., 1998). Six crystals from each standard position were analyzed by laser fusion to calculate J-values for the irradiation tray. Four crystals were excluded from J-value calculations due to K/Ca ratios lower than for typical sanidine. Blank bracketing and linear interpolation were both attempted for some sample blanks with little effect on the assigned age. Therefore, preceding blanks were used for background calculations for all the samples in this study.

Results

$^{40}Ar/^{39}Ar$ Geochronology

Age spectra for the 13 biotite samples are generally well defined, with younger apparent ages in the first few steps and age plateaux defined by heating steps above 800°C. Plateau ages are defined as three or more overlapping heating step ages (at 2σ) that contain greater than 50 percent total ^{39}Ar released (figure 8). Plateaux with mean square weighted deviates (MSWD) <3 were considered to be well-defined. K_2O values for most of the 13 samples are between 10 and 15 percent, indicating that the biotite separates are not significantly chloritized. Some spectra have a slightly higher apparent age for the 1075˚C heating step, which is usually still within the plateau. This increase in

age creates a saddle similar to spectra from chloritized biotite, as discussed by Lo and Onstatt (1988), and corresponds to a few samples with lower K_2O values discussed later in this section. The assigned dates for the 13 Philipsburg Batholith samples are summarized in Table 1.

Table 1. Assigned Ages for Philipsburg Batholith samples

Sample	Age (Ma)	Method	MSWD	Sample Location
PB4	74.0 ± 0.3	Plateau	0.78	Dora Thorn Pluton
PB17	65.4 ± 0.3	Plateau	2.57	Dora Thorn Pluton
PB19	75.6 ± 0.4	Integrated	---	Dora Thorn Pluton
PB30	73.5 ± 0.3	Plateau	1.37	Dora Thorn Pluton
PB42	74.6 ± 0.3	Plateau	1.82	Near Contact
PB50	74.4 ± 0.3	Plateau	3.27	Bimetallic Stock
PB73	75.1 ± 0.3	Plateau	1.57	Bimetallic Stock
PB76	74.9 ± 0.3	Plateau	1.23	Near Contact
PB81	74.9 ± 0.3	Plateau	---	Dora Thorn Pluton
PB97	74.6 ± 0.4	Integrated	4.39	Dora Thorn Pluton
PB105	74.5 ± 0.3	Plateau	3.72	Dora Thorn Pluton
PB111	67.4 ± 0.2	Plateau	2.93	Dora Thorn Pluton
PB122	74.7 ± 0.2	Plateau	0.47	Dora Thorn Pluton

Six samples (PB4, PB30, PB42, PB73, PB76, PB122) have well-defined plateau ages between 73.5 and 75.1 Ma. With the exception of PB122, all samples in this group have 13 to 15 percent K_2O, indicating that the samples are unaltered. The plateau ages have low MSWD values and are determined to be the best age estimates for these six samples.

Samples PB50 and PB81 have plateau ages of 74.9 ± 0.3 Ma and 74.9 ± 0.4 Ma, respectively. The MSWD values are high for both samples, meaning that the plateau step ages are non-normally distributed. In both cases, the 1075˚C temperature step (step G) is older than the rest of the plateau. These samples both have about 12 percent K_2O, indicating some alteration of biotite to chlorite. The older apparent age for the 1075˚C step is probably caused by recoil of ^{39}Ar out of biotite that is degassing around 1075˚C

(Lo and Onstatt, 1988). The older 1075˚C steps are still part of the plateaux and therefore the plateau ages are determined to be the best age estimates for samples PB50 and PB81, though the MSWD values are not ideal. Sample PB105 also has a plateau with a high MSWD value, but the K_2O value of 14.9 percent does not suggest chloritization. The plateau age of 74.5 ± 0.3 Ma is considered to be the best age estimate for sample PB105.

Samples PB19 and PB97 yield an older apparent age for step G (1075˚C). In these two cases, the 1075˚C step is significantly older than surrounding heating steps so the spectra do not have plateaux. The shapes of the spectra suggest that recoil of ^{39}Ar from biotite to chlorite was substantial during irradiation. The K_2O contents of samples PB19 and PB97, 10.5 and 8.5 percent respectively, confirm substantial chloritization of biotite separates. The integrated age was determined to be the best age estimate for these samples. PB19 has an integrated age of 75.6 ± 0.4 Ma and PB97 has an integrated age of 74.6 ± 0.3 Ma. Both of these assigned dates are similar to samples with well-defined plateaux.

Eleven of the samples measured in this study yield $^{40}Ar/^{39}Ar$ biotite dates between 73.6 and 75.6 Ma. Samples PB17 and PB111 have younger dates of 65.4 ± 0.3 and 67.4 ± 0.2 Ma, respectively. PB17 has an age spectrum with a well-defined plateau and MSWD of 2.57. PB111 also has a well-defined plateau with an MSWD of 2.93, but the final step (I) is about 1 Ma older than the plateau. This older step at the end of the spectrum may be the result of ^{39}Ar recoil out of biotite or it may be due to degassing of inclusions of sphene or other high-Ca accessory minerals, leading to low K/Ca ratios observed in age spectra.

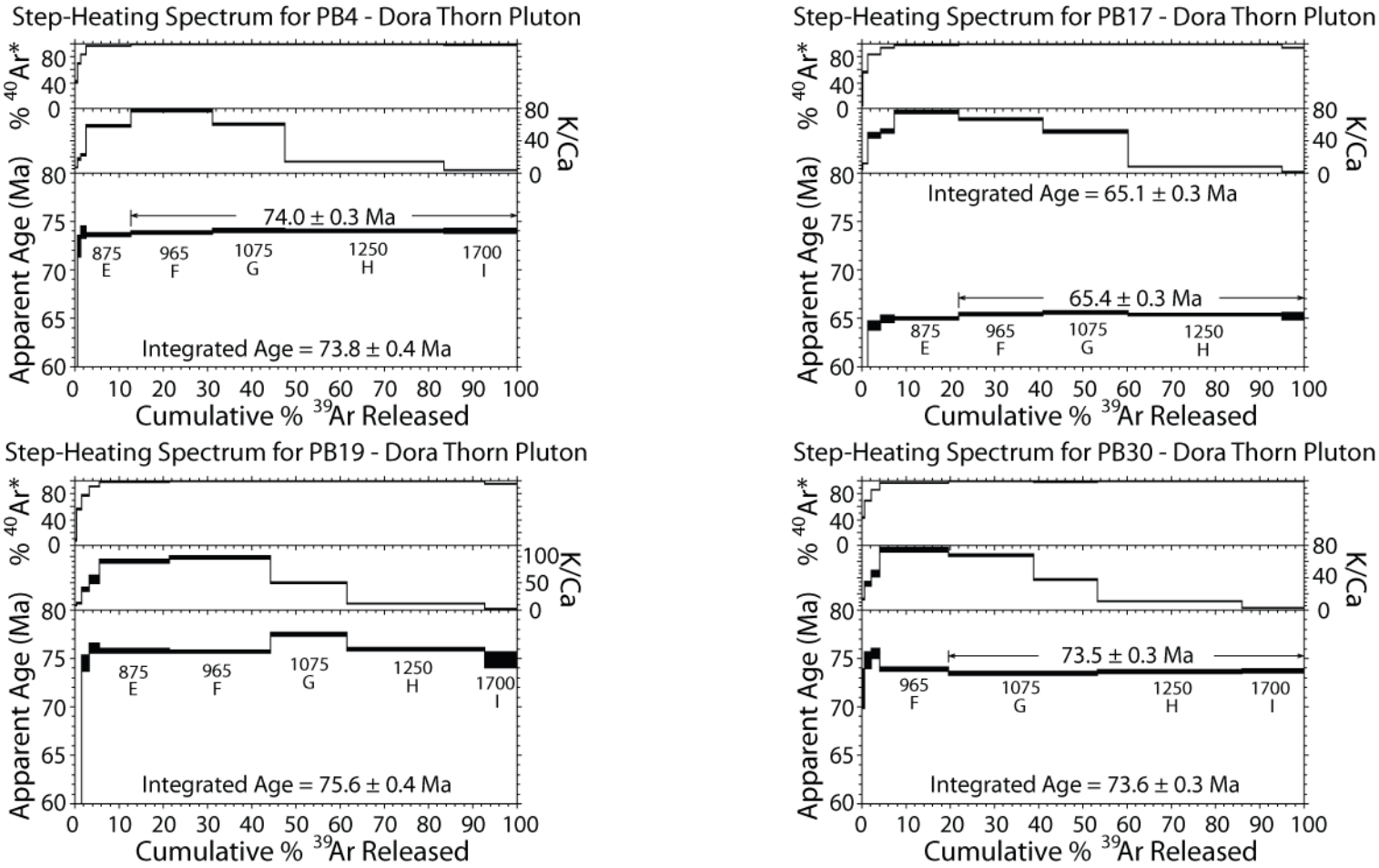

Figure 8. $^{40}Ar/^{39}Ar$ step-heating spectra for Philipsburg Batholith samples showing apparent step ages, K/Ca ratio, and % $^{40}Ar^*$ released. Temperatures for heating steps are reported in degrees celsius. Plateau dates are reported for samples with acceptable plateaux.

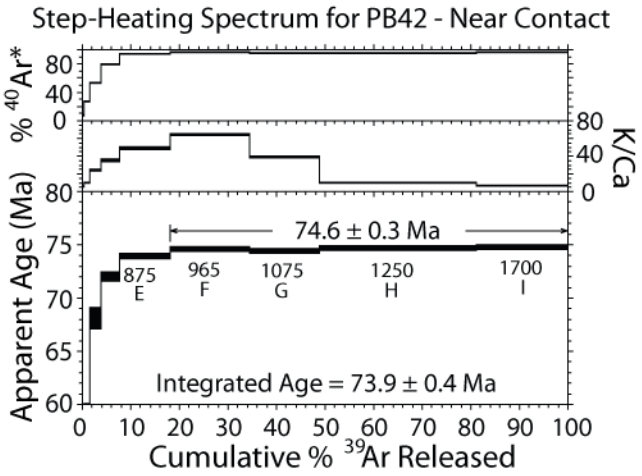

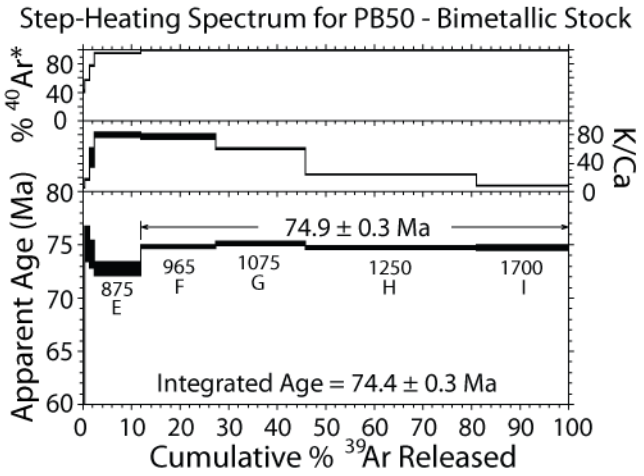

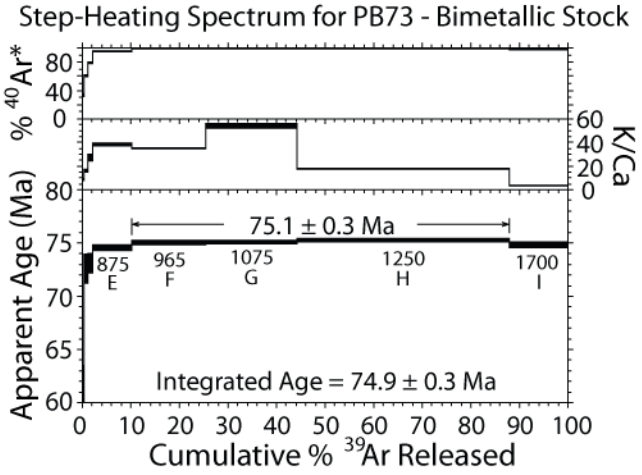

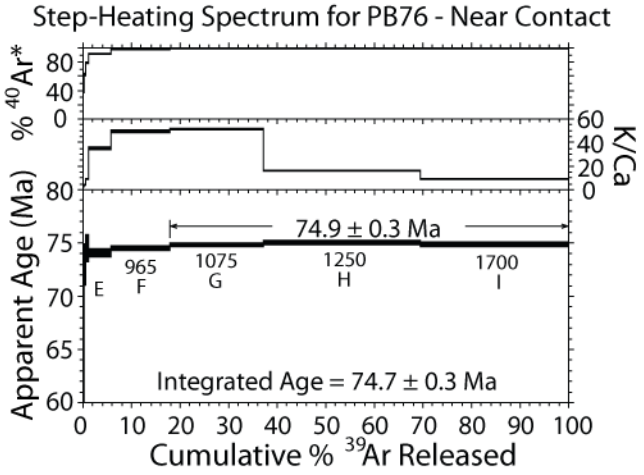

Figure 8. continued.

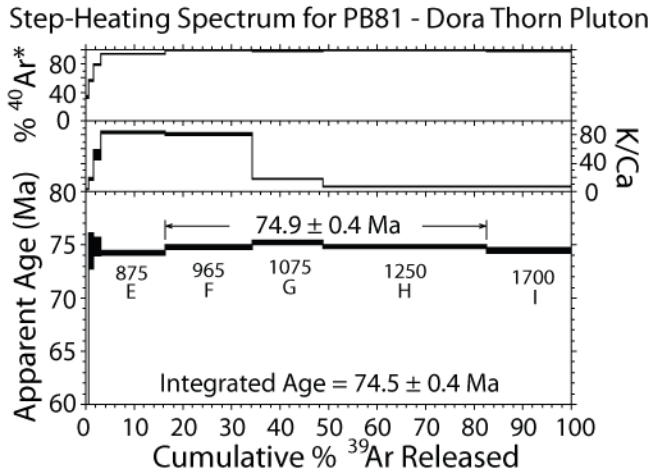

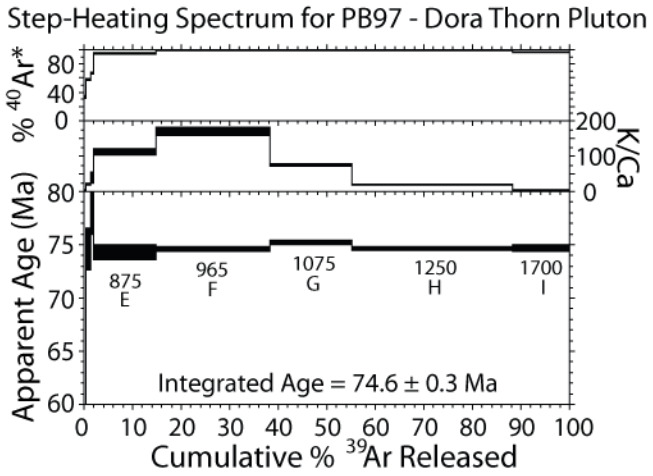

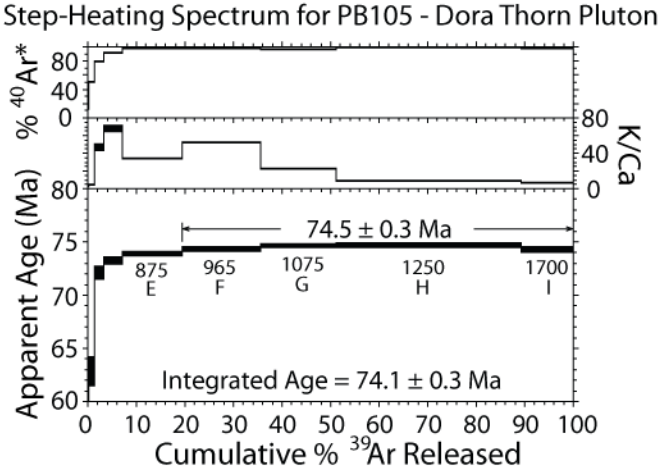

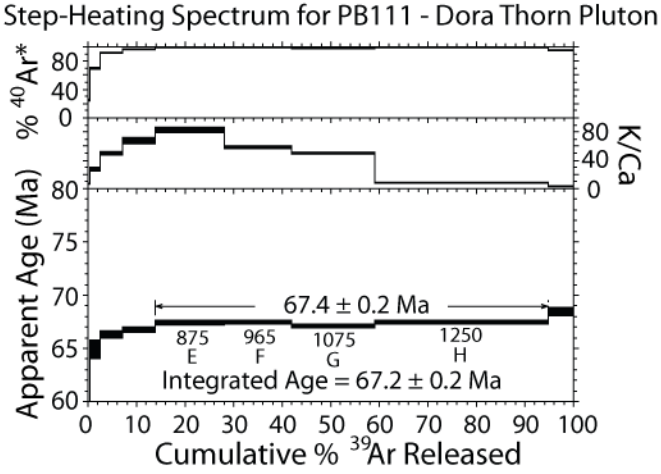

Figure 8. continued.

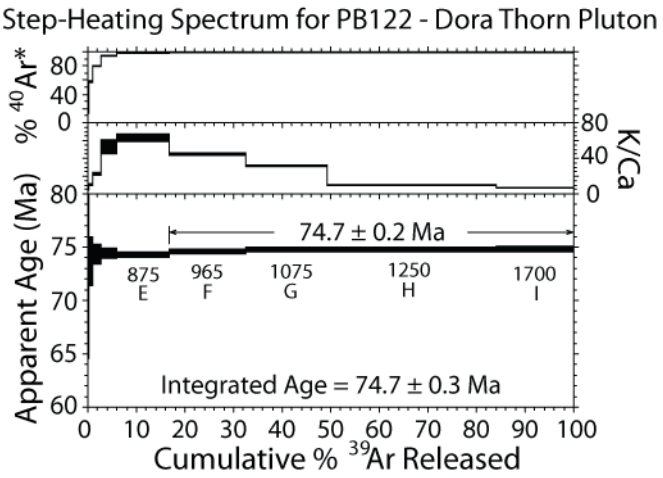

Figure 8. continued.

An age probability diagram of assigned dates shows a peak at 74.6 ± 0.3 Ma for the eleven older samples as well as two young outlying peaks (figure 9). The confidence limits of both previously reported K-Ar biotite ages overlap the average age estimate provided by this study. The two samples with dates over 75 Ma were obtained from the southern and western parts of the batholith (figure 10). In general, $^{40}Ar/^{39}Ar$ dates are slightly younger towards the center and eastern parts of the batholith. Given the overlap in age estimate errors and the gradational nature of the contact, the geochronologic data suggest that intrusion of the Bimetallic Stock and Dora Thorn Plutons occurred nearly contemporaneously.

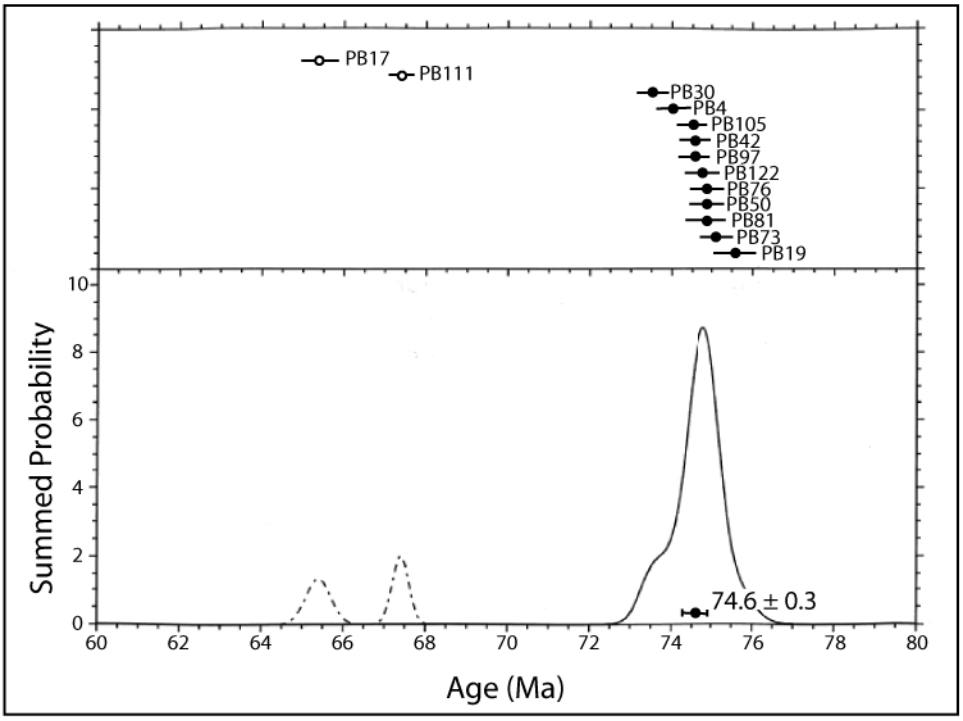

Figure 9. Summed age probability density functions for thirteen 40Ar/39Ar dates from the Philipsburg Batholith showing an age peak at 74.6 Ma and two young outliers. The area under the curve is thirteen, the total number of samples.

The samples yielding relatively young dates are both from near the eastern margin of the Philipsburg Batholith and their dates do not overlap at 2σ. There is no textural or mineralogic evidence from these sampling sites that would indicate a separate intrusion from the rest of the Philipsburg Batholith. It is likely that the dates from these samples have been reset, possibly due to intrusion of the Mount Powell Batholith ~1.5km to the east, which has also been mapped as Late Cretaceous but the age of emplacement is unknown. Eight AFT dates from the Mount Powell Batholith have an average of 62.1 Ma, which is ~4 Ma younger than AFT dates for the Philipsburg Batholith, suggesting that the Mount Powell Batholith may be younger than the Philipsburg Batholith (Baty, 1973). More geochronologic data from the eastern margin of the Philipsburg Batholith

and from the Mount Powell Batholith are needed to better explain the young age determinations of samples PB17 and PB111.

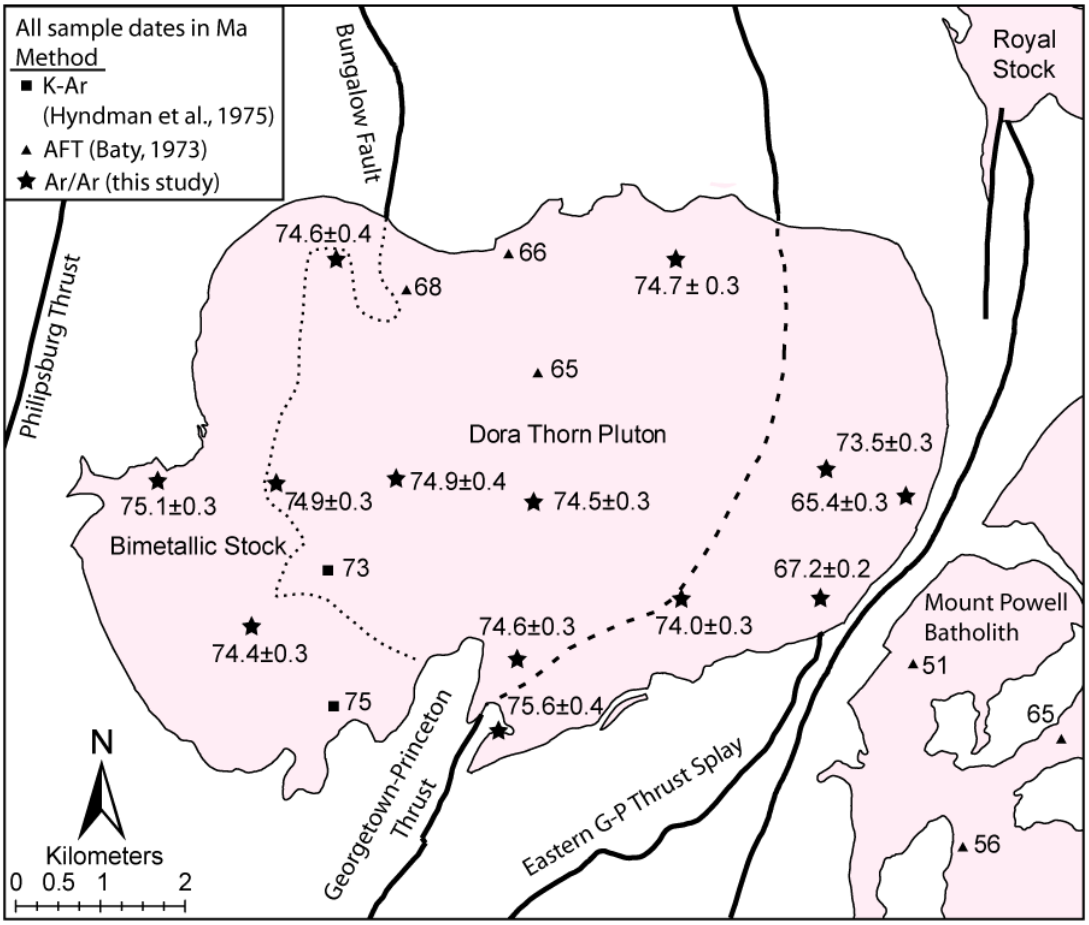

Figure 10. Age map of the Philipsburg Batholith and nearby Mount Powell Batholith showing previously published K-Ar and apatite fission track ages and $^{40}Ar/^{39}Ar$ dates from this study.

Paleomagnetism

Most specimens demagnetized with alternating field (AF) demagnetization yield coherent linear demagnetization trends (figure 11), allowing the calculation of characteristic remanent magnetizations (ChRMs) and estimates of site mean directions. Magnetizations isolated over the lowest range of peak fields, and thus carried by lowest coercivity materials, are similar to present-day field directions. For most samples from most sites, a north-northeast directed, moderate positive inclination magnetization was

isolated over a range of moderate coercivities, and is interpreted as a normal polarity ChRM for the batholith. Site means of the ChRM were estimated for 63 sites (table 2). Six sites yielded magnetizations of moderate negative inclination and these magnetizations are considered to be of reverse polarity. ChRMs of all accepted samples from one reverse polarity site were determined using great circle analysis. Five sites yielding reverse polarity magnetizations also had a subset (up to three) of samples that yielded normal polarity magnetizations and these were inverted to reverse polarity data for the calculation of estimated site means. Thirty-one sites provided α95 values associated with estimated site mean directions that are greater than 15° and these sites were excluded from further calculations. Five sites yielding reverse polarity ChRMs had α95 values greater than 15°, and were excluded. The remaining 32 site mean directions are moderately well defined, with α95 values ranging from 4.7 to 14.9 degrees and precision parameter (k) values of 12 to 108. The dominance of normal polarity magnetizations in the Philipsburg Batholith is consistent with an emplacement age of slightly older than ca 74.6 Ma, which is during Chron C33n, having a duration of about 5.5 Ma between ca. 79.1 and 73.6 Ma (Cante and Kent, 1995). The high number of rejected sites is due to the control of multi-domain magnetite on the characteristic remanent magnetization (next section), which is not an ideal recorder of the geomagnetic field.

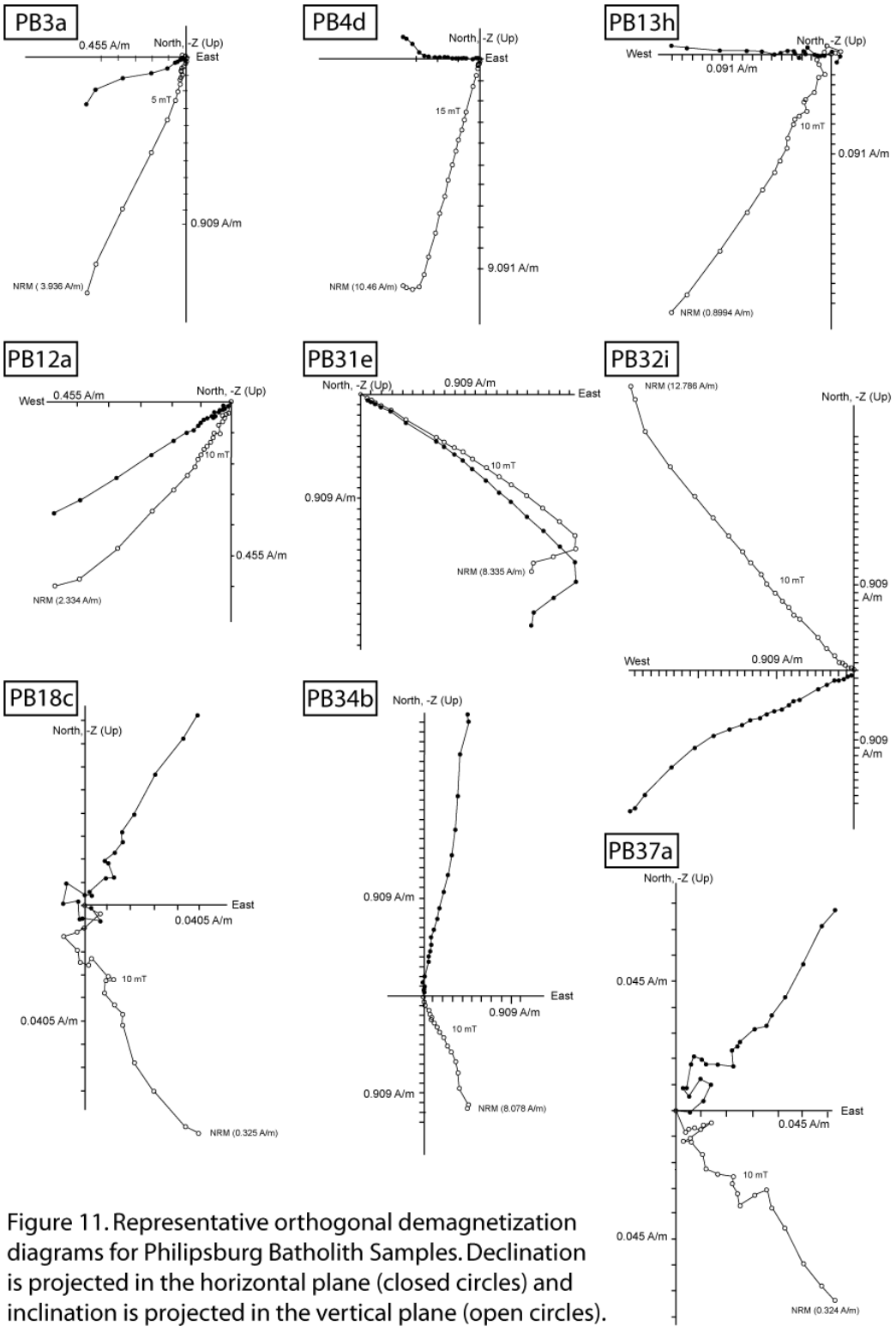

Figure 11. Representative orthogonal demagnetization diagrams for Philipsburg Batholith Samples. Declination is projected in the horizontal plane (closed circles) and inclination is projected in the vertical plane (open circles).

Table 2 – Site mean paleomagnetic directional data

Site	$N_{collected}$	$N_{measured}$	k	a_{95} (degrees)	Declination	Inclination
PB1*	11	9	3.74	28.01	174.8	74.8
PB2	12	12	46.92	6.12	64.4	72
PB3*	11	10	1.41	61.21	7.7	52.3
PB4*	10	6	2.52	44.98	317.6	56.8
PB5*	11	11	5.19	20.96	71.1	54.6
PB6	12	12	15.65	10.81	35.7	75.9
PB7*	10	8	8.32	18.94	260.8	42.7
PB8*	8	5	9	23.84	82.5	73.2
PB9*	10	7	5.11	26.97	0.4	49.8
PB10*	10	10	7.35	18	85.6	74.6
PB11	10	10	31.62	8.26	50.3	71.8
PB12*	10	8	12.73	15.03	227.6	58.1
PB13*	10	7	12.16	16.59	0.8	66.8
PB14	10	10	16.8	11.48	57.7	64.3
PB15*	12	8 (circle fits)	n/a	2.35 / 5.82	50.7	-23.9
PB17	10	10	69.2	5.54	354.2	64.7
PB18	11	10	22.89	9.76	14.9	61
PB19	10	10	31.97	8.22	15.3	79
PB20	12	9	11.53	14.85	300.1	41.2
PB21*	10	5	9.75	22.83	52.4	24.8
PB22	12	10	66.89	5.64	340.4	79.4
PB23	12	11	28.38	8.3	358.1	69.7
PB24*	8	5	16.65	17.17	30.8	72.7
PB25*	11	10	1.15	84.81	286.7	26.5
PB26*	10	6	10.04	20.11	66.8	-68.7
PB27*	10	9	8.15	17.97	98.4	-54.9
PB28*	10	9	11.23	15.07	13.9	82.8
PB29*	8	7	11.69	16.94	27.4	59.4
PB30	8	6	47.55	8.94	19.1	73.3
PB31*	8	7	10.66	17.81	267.8	81
PB32*	4	4	12.61	23.08	20.9	60.7
PB33*	14	6	7.19	24.18	194.1	-49.5
PB34*	10	7	12.71	16.21	196.3	47.9
PB35*	6	6	15.4	16	168.6	-54.9
PB36*	7	6	6.58	25.42	350.9	63.4
PB37	8	8	20.75	11.61	27.7	47.6
PB38*	8	7	3.87	31.13	39.4	36.6
PB40	10	9	27.26	9.44	202.9	81.8

Table 2 – continued

Site	$N_{collected}$	$N_{measured}$	k	a_{95} (degrees)	Declination	Inclination
PB41	11	10	13.39	12.95	15.2	46.7
PB42**	11	9	14.13	13.32	302.7	-6.2
PB43*	12	6	10.99	19.15	175.5	36.7
PB44**	12	12	16.01	10.69	285.6	29.2
PB45**	9	9	107.67	4.7	83.8	4.6
PB46	11	11	27.54	8.43	32.8	62.6
PB47	10	9	22.8	10.36	2.3	57.1
PB48	8	7	25.62	11.22	18.7	62.2
PB49	12	10	17.77	11.15	358.2	82.6
PB50	12	11	30.29	8.03	21.3	79.8
PB51	9	6	21.35	13.49	-27.7	69.7
PB52	10	10	27.12	8.94	345.8	73.8
PB53	10	10	17.81	11.13	14.6	73
PB54*	3	3	26.18	19.94	80.3	83.3
PB55	11	7	17.5	13.68	120.5	64.7
PB56	12	8	22.3	11.18	4.3	70.7
PB57	10	9	28.23	9.28	37.9	49
PB58	10	10	25.98	9.15	26.4	66.6
PB59*	10	9	9.98	16.07	34.3	57.3
PB60	10	8	26.89	10.15	5	54.9
PB61**	10	7	16.31	14.2	190.2	41.3
PB62*	10	7	6.26	23.94	124.3	57.5
PB63*	10	5	18.95	16.05	27.3	64.9
PB64*	8	6	4.74	29.79	339.5	30.2
PB65	10	7	17.48	13.69	16.4	69.2

* - sites omitted from grand mean calculation due to high 95 percent conf. angle.
** - sites greater than two angular standard deviations from the grand mean.

The 32 accepted site means were used to calculate a grand mean assuming a Fisherian distribution (Fisher, 1953). Four site mean directions were more than two angular standard deviations (59°) from the grand mean. These sites were omitted and a grand mean for the remaining 28 sites (figure 12) was calculated (Dec.=015.7, Incl.=70.6, k=21.8, s = 17.3, a_{95} = 5.7).

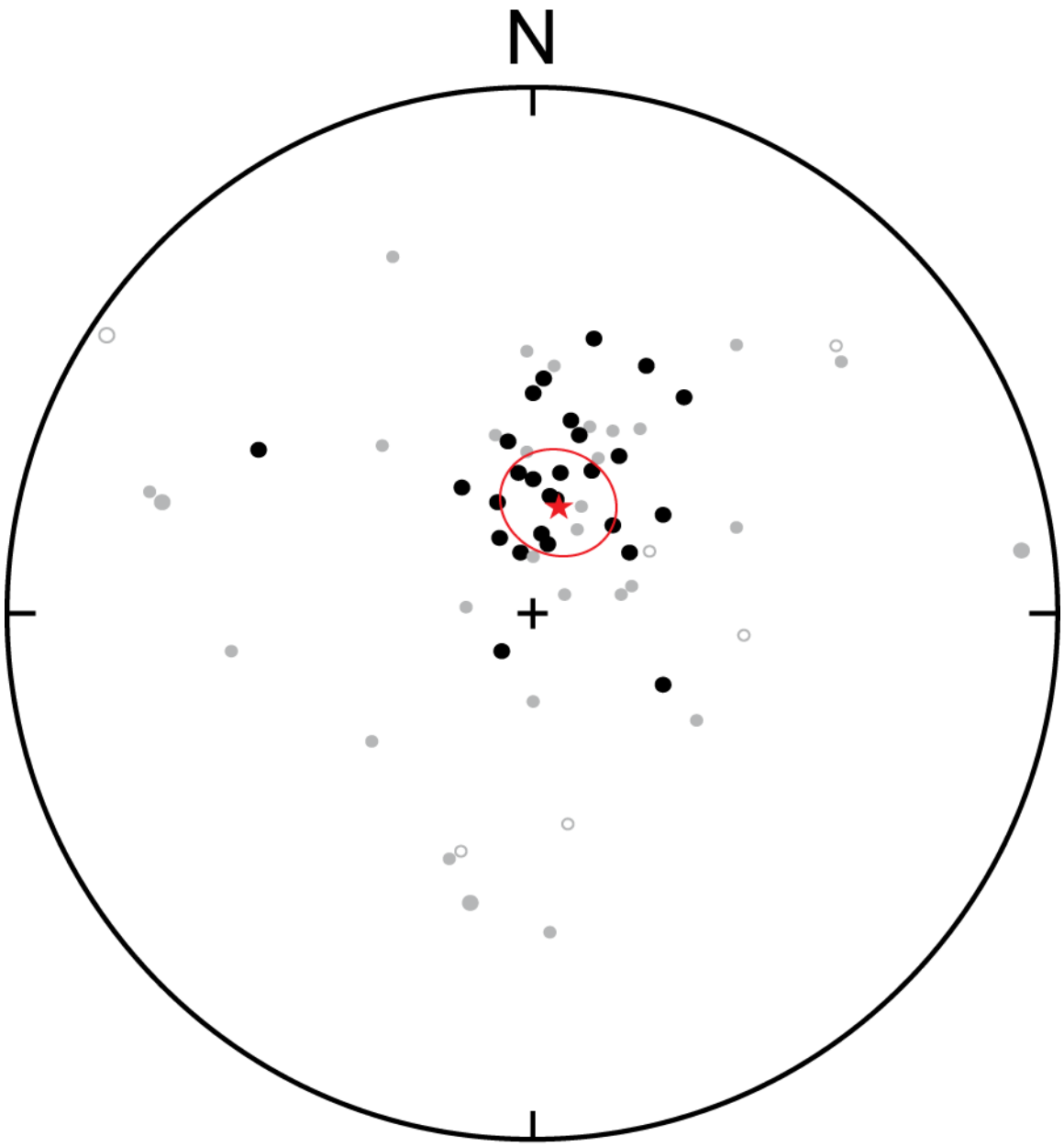

Figure 12. Stereographic projection of observed site mean paleomagnetic directions from the Philipsburg Batholith. Open circles represent upper hemisphere directions. The grand mean (star) was calculated using site directions with 95% confidence cones < 15° (black circles). Sites with 95% confidence cones > 15° (grey circles) were not used for grand mean calculations.

Rock Magnetism

Isothermal remanent magnetization (IRM) acquisition data for selected specimens from the Philipsburg Batholith approach complete saturation in fields below 150 mT,

with most samples ~80% saturated by 50 mT (figure 13). Backfield demagnetization of saturation IRM yield coercivity of remanence (H_{cr}) from 12 to 24 mT. The low fields required for saturation of IRM and the low coercivities for all samples imply multi-domain (MD) magnetite is the dominant magnetic phase in the Philipsburg Batholith and is an important carrier of ChRM.

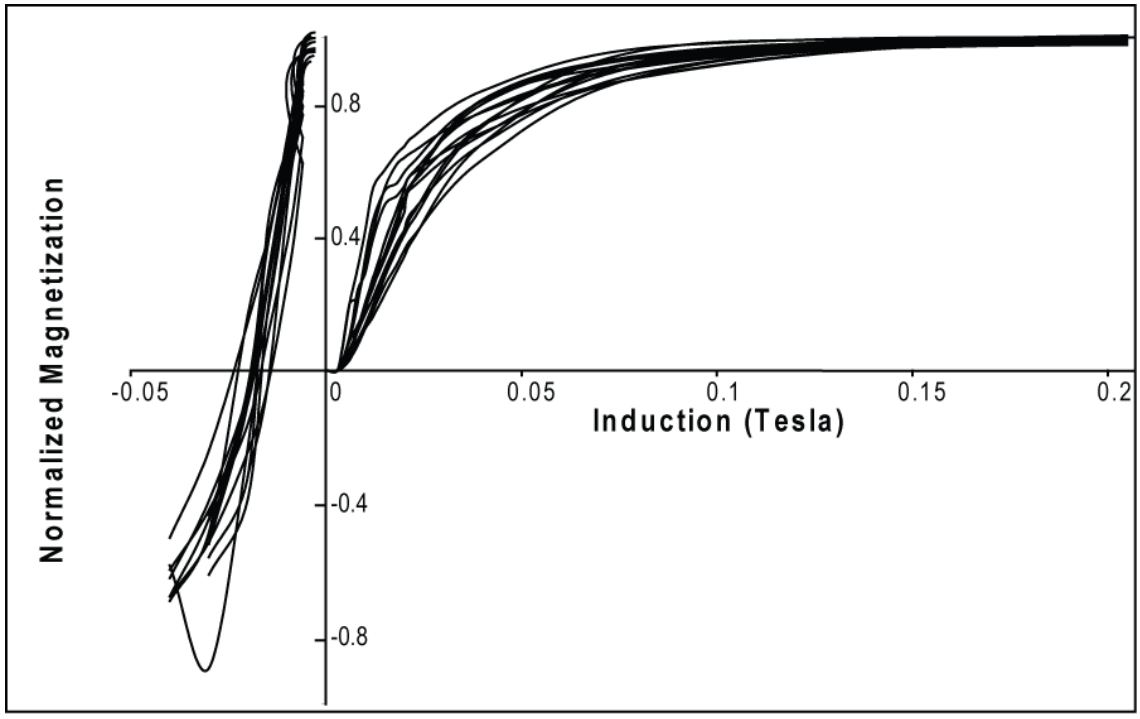

Figure 13. IRM acquisition curves and backfield IRM demagnetization curves for representative Philipsburg Batholith samples.

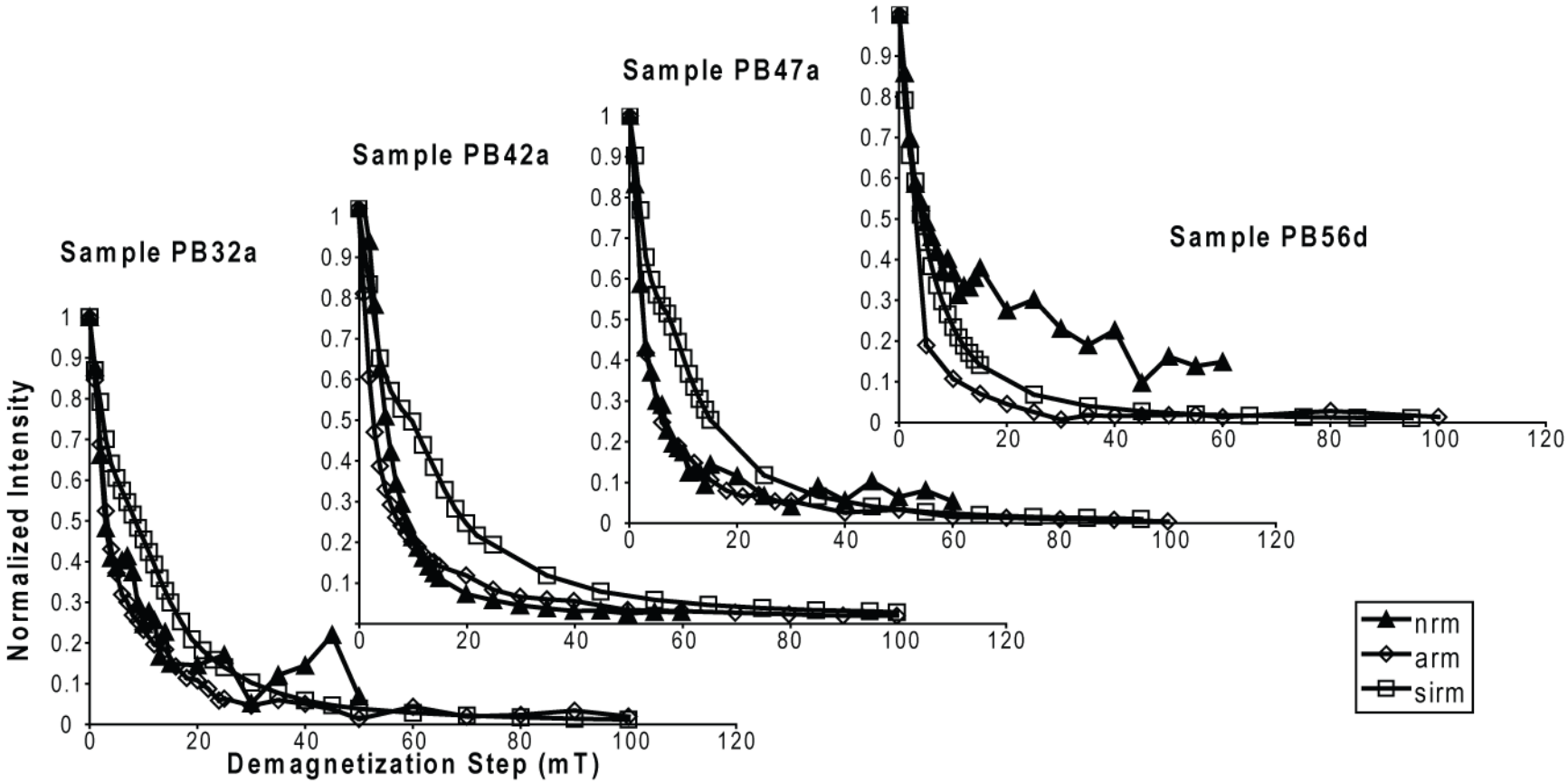

Figure 14. Modified Lowrie-Fuller Plots for representative Philipsburg Batholith samples showing relationship of ARM and IRM demagnetization curves.

Modified Lowrie-Fuller tests (Johnson et al., 1975), which compare normalized AF demagnetization curves of anhysteretic remanent magnetization (ARM) and IRM acquired in a DC field identical to the peak AF used for ARM, were performed to assess the dominance of MD magnetite in samples from the Philipsburg Batholith. For all but two specimens, higher destructive fields were required to demagnetize 98 mT IRM than were required to demagnetize ARM, a result characteristic of dominance by MD magnetite (figure 14). The normalized NRM demagnetization curves nearly match the ARM demagnetization curves for about half of the specimens, indicating that ARM is a good proxy for low-field thermoremanent magnetization (TRM). The Philipsburg Batholith ChRM is assumed to be a TRM acquired in Earth's magnetic field during subsolidus cooling. For other specimens, the NRMs do not exponentially demagnetize, but have more complex curves and are often demagnetized at higher fields than both ARM and SIRM.

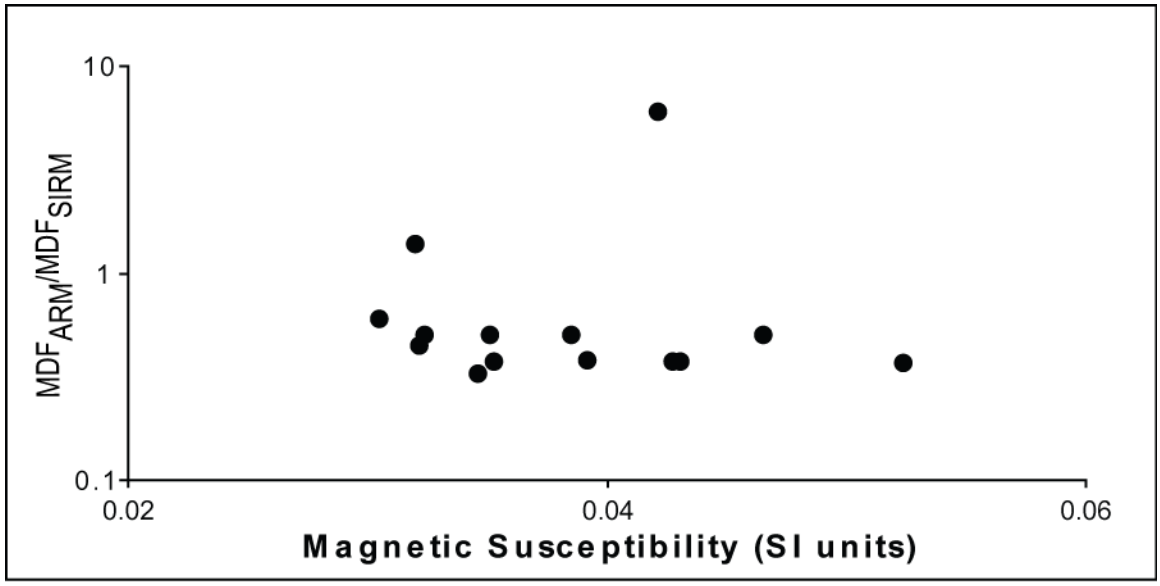

Figure 15. Median destructive field ratio versus magnetic susceptibility for representative Philipsburg Batholith samples.

The median destructive field (MDF) is that required to demagnetize 50% of a magnetization. The ratio $MDF_{ARM}/MDF_{SIRM,}$ plotted against bulk susceptibility of Philipsburg Batholith samples (figure 15) shows that Philipsburg Batholith samples are dominated by MD magnetite, due to MDF ratios <1, over the entire range of bulk susceptibilities.

Hysteresis curves for twelve selected samples were obtained using a vibrating sample magnetometer at the Institute for Rock Magnetism, University of Minnesota. Saturation magnetization, M_s, ranges from 1.12 to 1.89 Am^2/kg, saturation remanence (M_{rs}) ranges from 0.007 to 0.021 Am^2/kg, coercity (H_c) ranges from 0.6 to 1.5 mT, and coercivity of remanence (H_{cr}) ranges from 7.4 to 12.0 mT. Representative hysteresis loops for the Philipsburg Batholith (figure 16) show the ramp-shaped curves typical of dominance by MD magnetite grains (Dunlop and Ozdemir, 1997). The Philipsburg Batholith samples have low M_{rs}/M_s and high H_{cr}/H_c (figure 17), which further suggests that the intrusion is dominated by MD magnetite (Day et al., 1977).

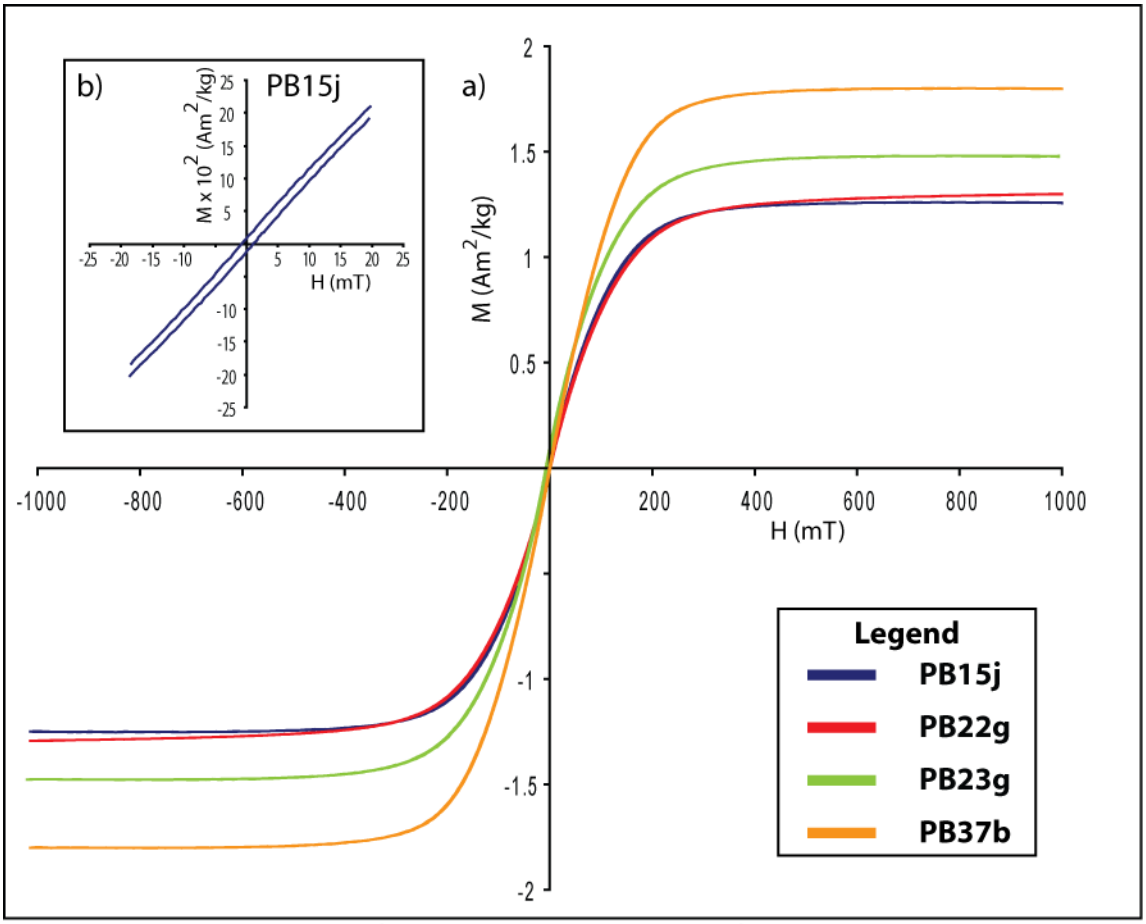

Figure 16. Hysteresis curves for representative samples from the Philipsburg Batholith showing typical ramp-like shape of multi-domain magnetite (a). A close up of the center of a hysteresis curve for sample PB15j is shown in (b).

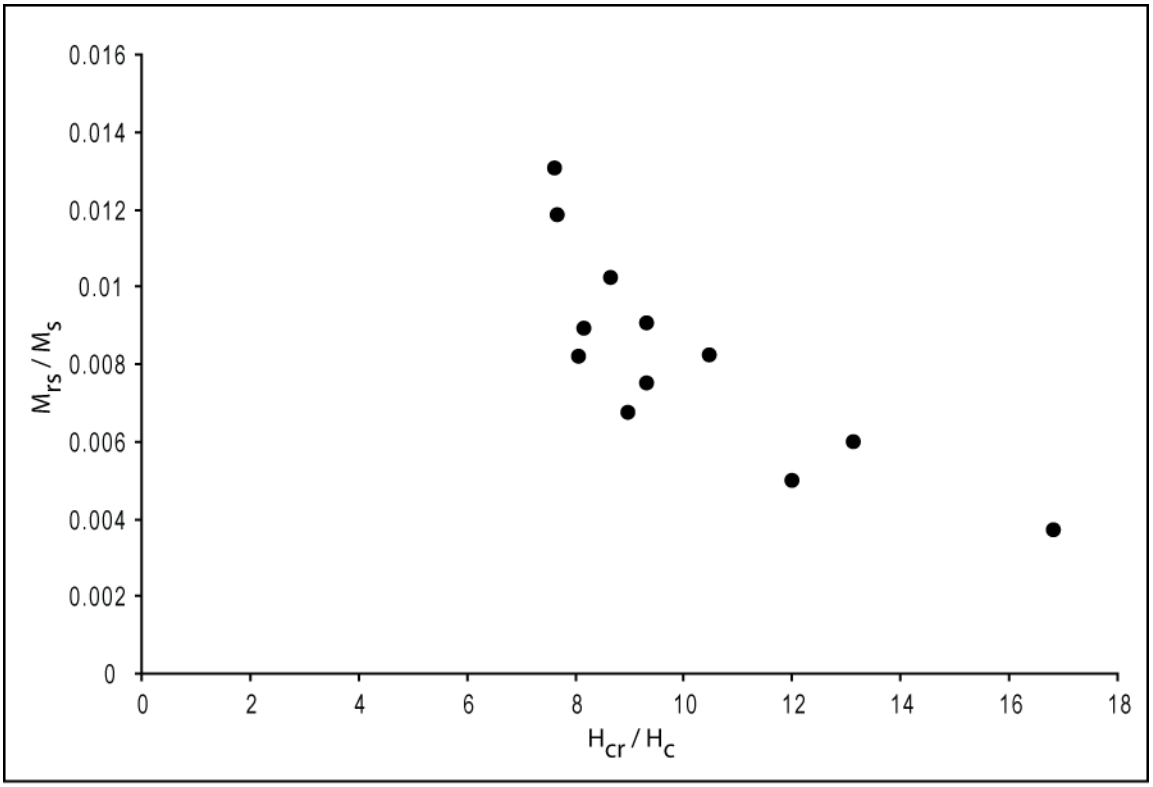

Figure 17. Plot of coercivity ratio versus magnetic saturation ratio, after Day et al. (1977) for Philipsburg Samples. High Hcr/Hc and very low Mrs/Ms suggest dominance of multi-domain magnetite in the samples.

AMS Fabrics in the Philipsburg Batholith

Average bulk susceptibility for all 119 sites ranges from 2 to 6 x 10^{-2} SI/volume (figure 18), indicating that the AMS measurements are dominantly recording ferro/ferrimagnetic mineral fabrics, most likely defined by magnetite (Hrouda, 1982).

The degree of anisotropy, P', at the site level ranges from 1.02 – 1.33, with an average of 1.11 or 11 percent anisotropy (figure 19). Hrouda (1982) suggests that magma flow usually produces P' values <1.2 and because there is no evidence for subsolidus deformation in thin section, all Philipsburg Batholith AMS fabrics are assumed to be magmatic in character. P' values are fairly uniform across the intrusion, although values seem to increase slightly from west to east. Map view contours of P' (figure 20) reveal two areas of higher anisotropy in the SE and SW corners of the Philipsburg Batholith.

The shape parameter, T, is positive for most sites, indicating that AMS foliation generally dominates AMS lineation. No relationship is apparent between T and P' values (figure 19).

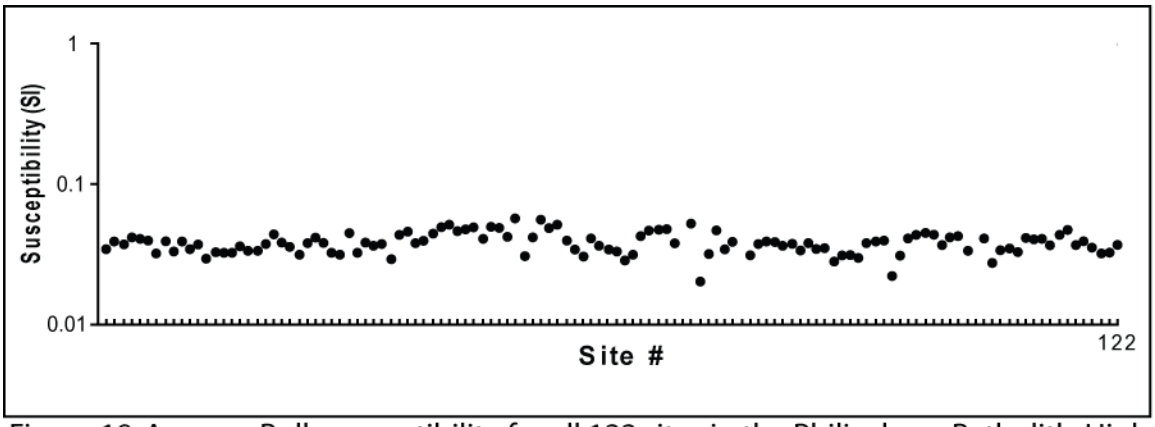

Figure 18. Average Bulk susceptibility for all 122 sites in the Philipsburg Batholith. High bulk susceptibilities suggest AMS fabrics controlled by ferro/ferrimagnetic minerals such as magnetite.

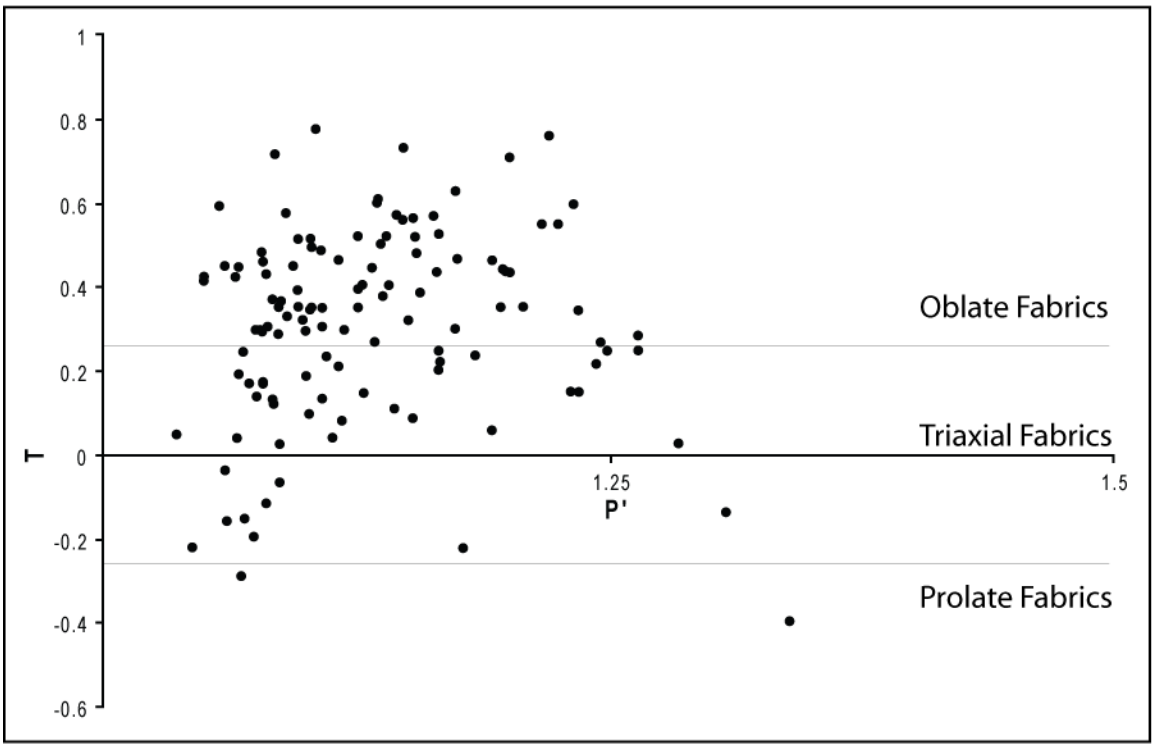

Figure 19. Degree of anisotropy, P', verses shape parameter, T, for all Philipsburg Batholith sites.

Figure 20. Contoured degree of anisotropy values for the Philipsburg Batholith showing areas of high anisotropy in the southwest and southeast parts of the batholith. P′ values >1.2 are shown in grey and P′ values > 1.3 are shown in dark grey.

Principal AMS directions for sample ellipsoids are generally well clustered at the site level (figure 21), meaning that fabrics are consistent over the scale of individual outcrops. Sites with $T > 0.25$ are considered oblate, $T < -0.25$ are considered prolate, and $-0.25 < T < 0.25$ are considered triaxial. Foliation data for oblate and triaxial sites and lineation data for triaxial and prolate sites (figure 22) allow assessment of magma flow. AMS Foliations generally show shallow dips in the center and steeper dips near the eastern margin of the batholith, although there is considerable scatter in dip values across the map area. AMS foliations generally dip away from an area in the center of the Dora Thorn Pluton. Foliations in the Bimetallic Stock are, on average, steeper than those of the Dora Thorn Pluton. Lineation data are generally subparallel or oblique to the strike of foliations, with most rakes less than 50°. Lineations are rarely in the foliation dip direction. Strike-parallel lineations are especially common near the margins of the batholith.

Contours of AMS foliation dips (figure 23) show that the steepest dip values (75-90°) are concentrated in three areas near the estimated position of the Georgetown-Princeton thrust, and at several sites near the proposed contact between the Dora Thorn Pluton and the Bimetallic Stock. An area of shallow dips exists near the southeast margin of the batholith. The shallowest dip in this area is from one of the two sites yielding samples with relatively young $^{40}Ar/^{39}Ar$ dates.

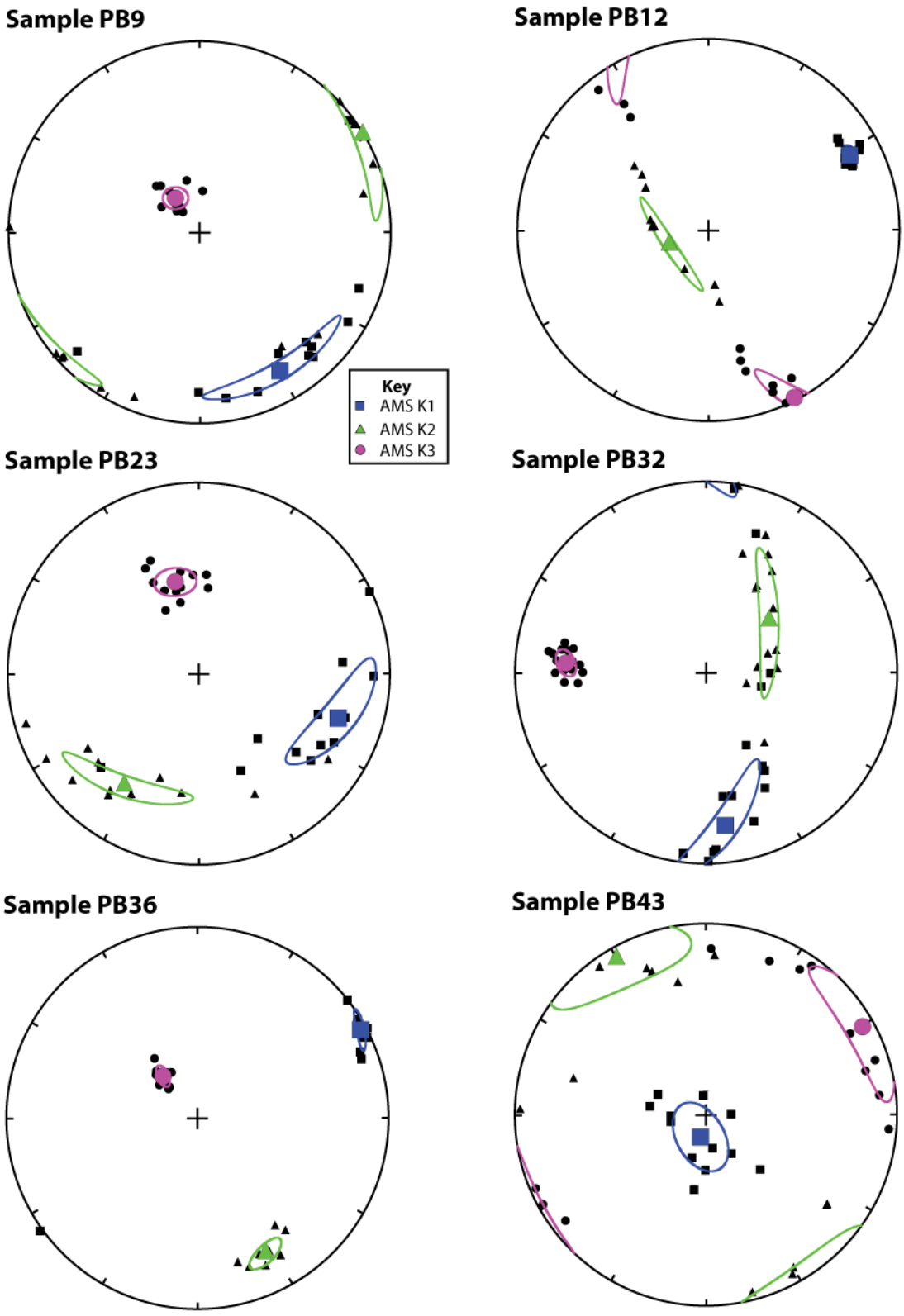

Figure 21. Individual AMS measurements (black points) and site mean principal axes (colored points) for representative sites from the Philipsburg Batholith.

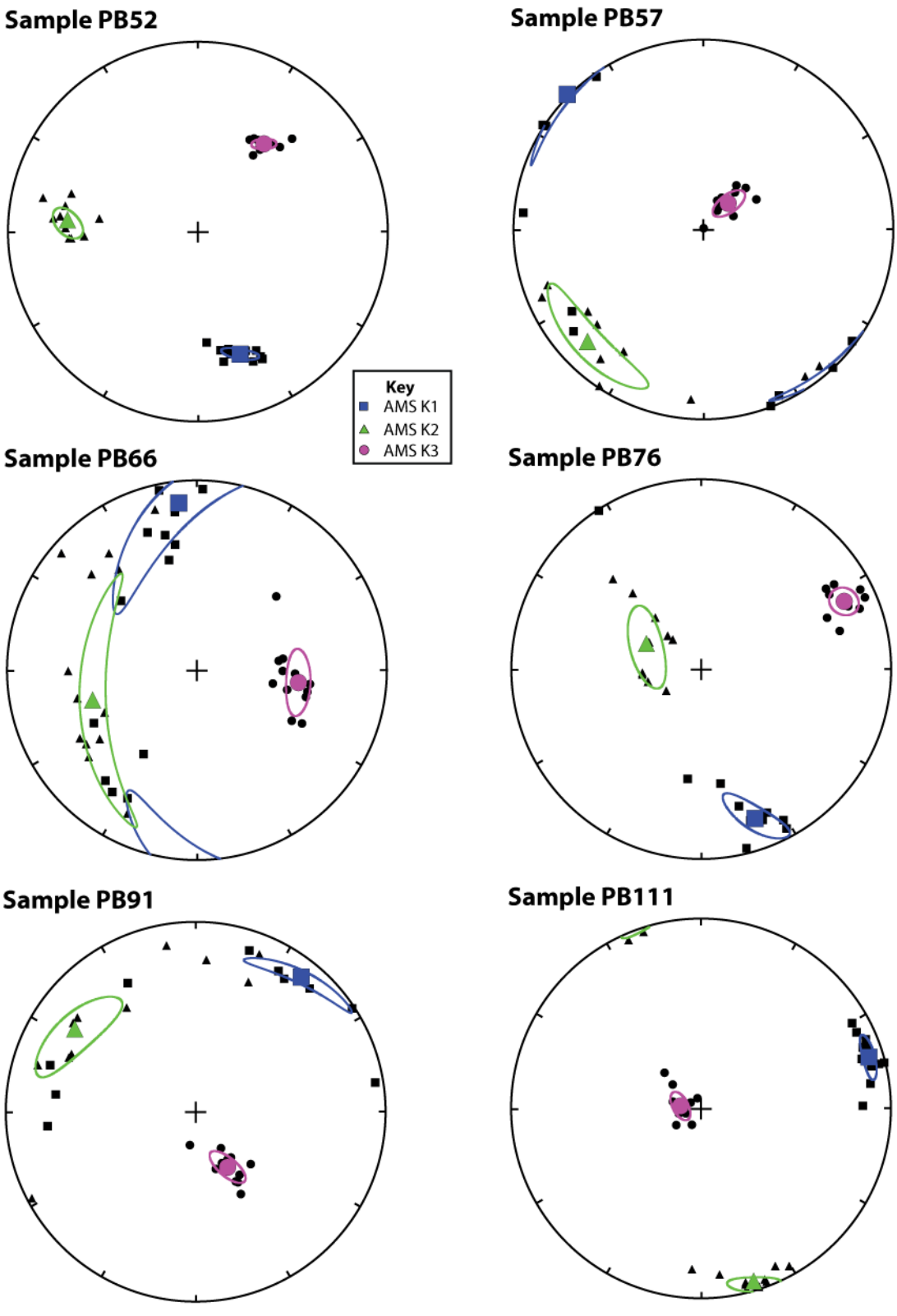

Figure 21. continued.

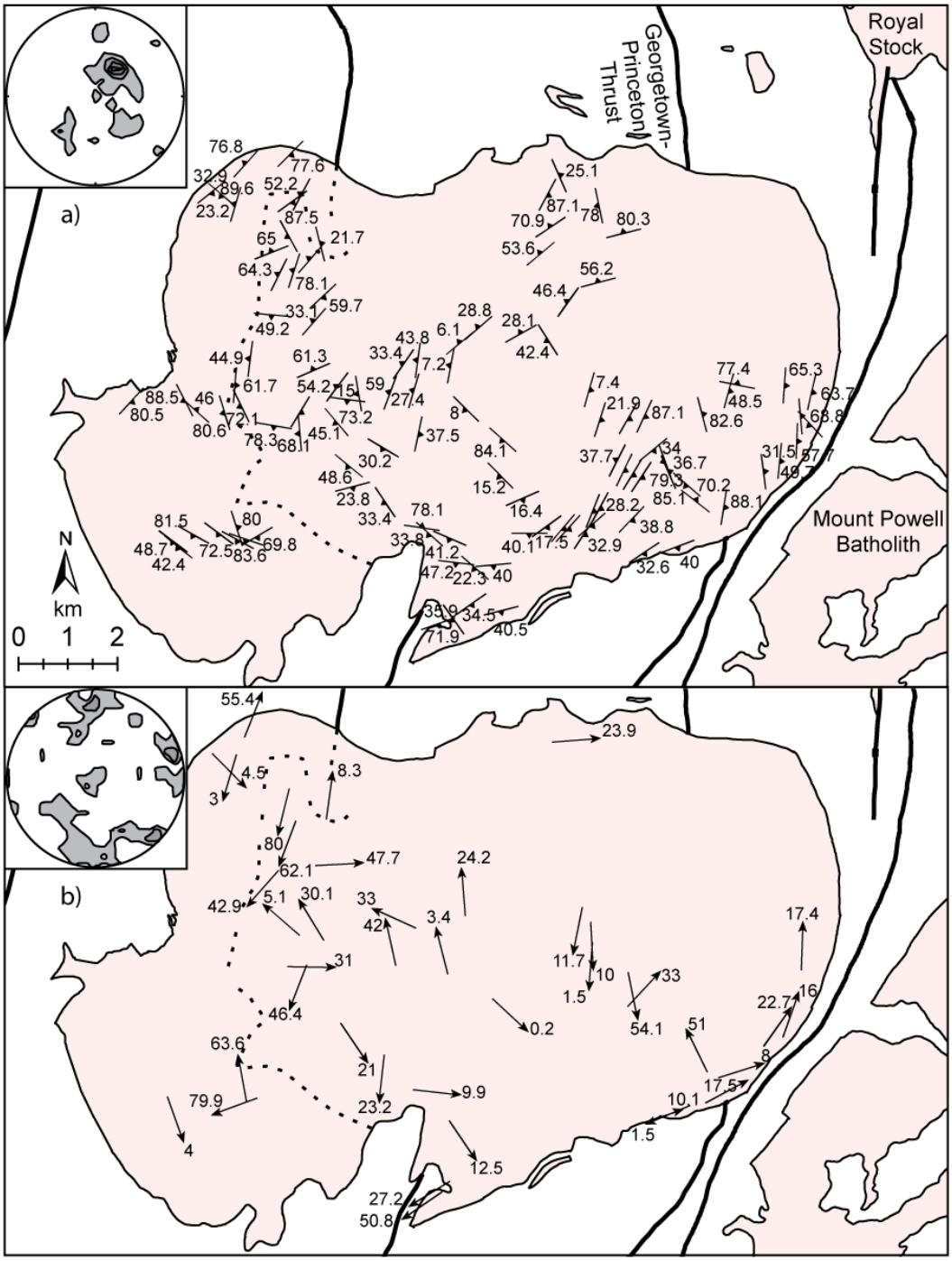

Figure 22. Foliations (a) and lineations (b) from AMS measurements in the Philipsburg Batholith. Foliations are plotted for sites with oblate or triaxial AMS ellipsoids and lineations are plotted for sites with prolate or triaxial AMS ellipsoids, as defined in the text. Insets show contours of poles to foliation and of lineation directions plotted in stereographic projection.

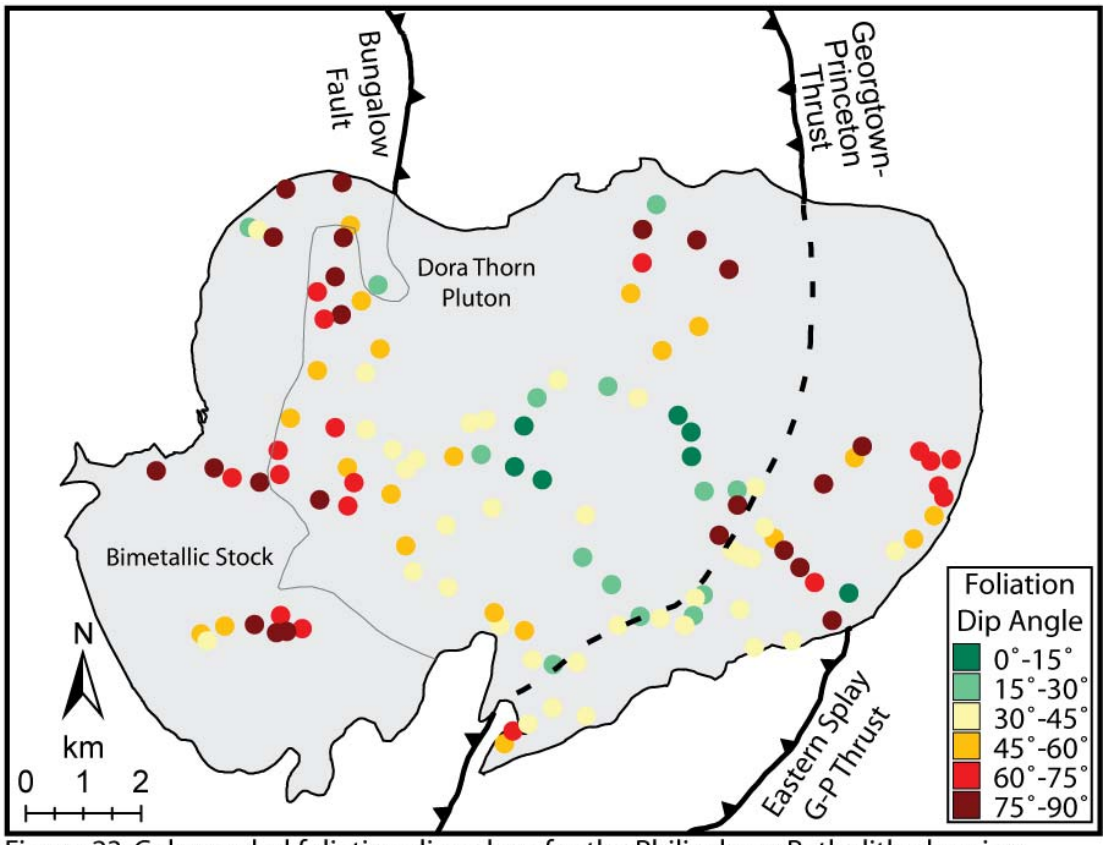

Figure 23. Color-coded foliation dip values for the Philipsburg Batholith, showing areas of steeply dipping foliations (warm colors) and subhorizontal foliations

AARM Fabrics in the Philipsburg Batholith

AARM ellipsoids from six sites in the Philipsburg Batholith have principal axes that are coaxial with AMS ellipsoid axes. One of the samples (PB12) has parallel axes, but the $AARM_2$ axis and the K_3 axis of AMS ellipsoid are parallel. The last AARM site that was measured in the Philipsburg Batholith has an AARM fabric that is oblique to the AMS fabric. Two sites have prolate AARM ellipsoids, two are triaxial, and four sites have oblate AARM ellipsoids. All of the oblate sites have coaxial AMS and AARM ellipsoids. AARM foliations and lineations are similar to AMS fabrics (Table 3). Both AMS and AARM foliations have strikes that are roughly parallel to the margins of the Philipsburg Batholith for all sites located near the margins, except for site PB 12, which

has an AARM foliation striking perpendicular to the southeast margin. The AARM results from the eight measured sites generally fit the pattern of steeper, margin parallel foliations near the batholith margins and shallower foliations in the interior of the batholith.

Table 3 - Comparison of AMS and AARM fabric directions

site	AARM Lineation	AMS Lineation	AARM Foliation	AMS Foliation
PB12	54.9/21.4	062.1/17.5	112.9/24.8	062.7/88.1
PB23	126.4/27.0	107.9/24.2	366.1/38.2	075.8/40.5
PB32	205.1/43.7	172.8/20.3	231.4/65.1	003.8/62.8
PB43	185.5/67.6	193.7/80	312.1/71.9	150.8/83.1
PB52	301.1/4.5	160.7/32.4	306.6/41.5	127/48.7
PB57	313.1/6.0	314.7/0.2	009.1/7.3	135.3/15.2
PB58	315.2/40.2	133/10	322.5/81.7	132/84.1
PB59	238.6/17.4	184.2/6.1	277.1/26.8	134.7/8

Discussion

Timing of Emplacement and Sevier Fold-Thrust Belt Development

$^{40}Ar/^{39}Ar$ biotite ages between 73.5 ± 0.3 and 75.6 ± 0.4 Ma from eleven age spectra results (average 74.6 ± 0.3 Ma) suggest that the Philipsburg Batholith was intruded over about 2 Ma or less. These new age determinations are consistent with previous K-Ar ages. A division of the Philipsburg Batholith into two or more separate magma pulses, as proposed by Hyndman et al. (1982), is not ruled out by the age data and the trend of slightly younger ages from west to east may still imply that the Bimetallic Stock was intruded before the Dora Thorn Pluton. The analytical error of the $^{40}Ar/^{39}Ar$ technique shows that, though Philipsburg Batholith ages cluster around 75 Ma, individual sample errors often do not overlap. This suggests that the Philipsburg Batholith may be an amalgamation of multiple intrusive events (Glazner et al., 2004). The amalgamation hypothesis is supported by subtle variations in mafic mineral content throughout the

batholith and by model cooling times for moderate sized intrusions, which are much less than two million years (Glazner et al., 2004).

To assess the possibility of internal deformation of the Philipsburg Batholith, the sampling area was divided into six sections (figure 24). Estimates of mean paleomagnetic directions for individual section means were then calculated for each of the four sections with a sufficient number of accepted site mean directions. The grand mean direction and section mean directions are recorded in Table 4. The grand mean 95 percent confidence cone overlaps the confidence cones for each of the four section means, indicating a lack of post-emplacement deformation between different sections of the Philipsburg Batholith (figure 24).

Table 4 - Section means for Philipsburg Batholith paleomagnetic data

Section	Nsites	Trend (deg)	Plunge (deg)	a95 (deg)	k
Grand Mean	32	10.4	71.4	10	7.4
NW Mean	9	2.9	58.5	34.6	3.6
SW Mean	7	13.2	79	11.1	35.7
S Mean	9	5.3	69.6	12.6	19.9
SE Mean	5	36.6	71.4	10.8	63.7

The lack of field relations or paleomagnetic evidence supporting any internal, post-emplacement deformation of the Philipsburg Batholith suggests that Sevier-age deformation in the Flint Creek Range had ceased and thrust-belt development had shifted farther to the east by ~75 Ma. This result is consistent with previous work on the timing of folding and thrusting in the Helena Salient east of the Boulder Batholith, which generally started at ~80 Ma (Schmidt et al., 1990) and ended prior to ~50 Ma (Harlan et al., 1988).

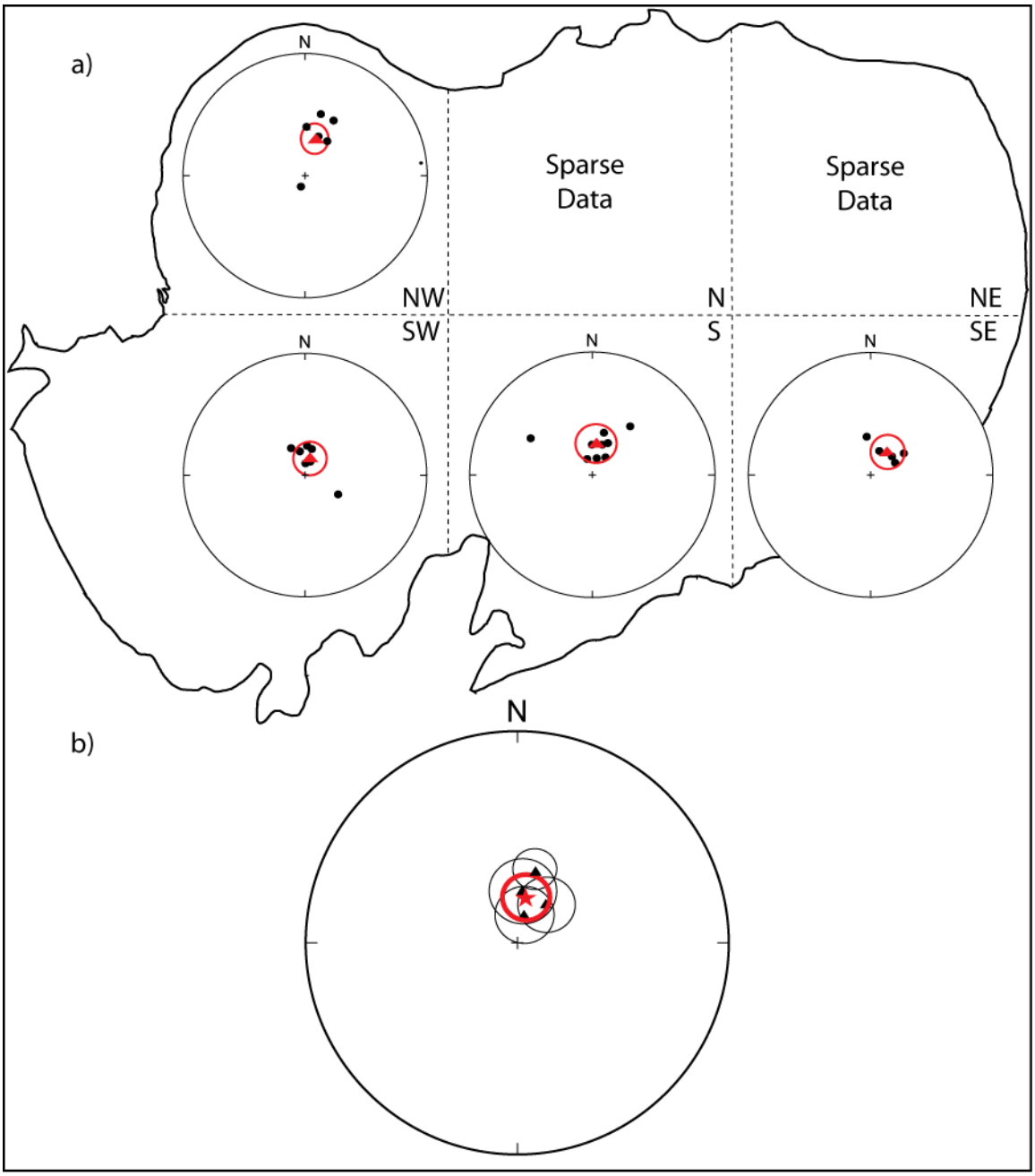

Figure 24. Section means (triangles) calculated from accepted paleomagnetic site mean directions in the Philipsburg Batholith (a). Means were not calculated for sections with less than three accepted site means. The grand mean (star) and all sections means (b) are not significantly different, indicating that the Philipsburg Batholith has not experienced any internal deformation since emplacement.

To evaluate post-emplacement rotation and tilt of the entire Philipsburg Batholith, the grand mean was compared to expected paleofield directions calculated from three published paleomagnetic poles for the Late Cretaceous (Besse and Courtillot, 2003;

Gunderson and Sheriff, 1991; Van der Voo, 1993). Calculated rotation and flattening, as well as tilt are given in Table 5. Comparisons between the grand mean and each of the three Late Cretaceous expected directions suggest that the Philipsburg Batholith has experienced 23 to 48 ± 19° of clockwise vertical axis rotation and minimal inclination shallowing since emplacement. Rotation and flattening error values were calculated as in Beck (1980) with modification by Demarest (1983).

Table 5 – Comparison of the observed paleomagnetic grand mean to expected directions.

Reference Pole	Besse and Courtillot, 2003	Gunderson and Sheriff, 1991	Van der Voo, 1993
Pole Latitude	74.7 N	82.2 N	68 N
Pole Longitude	207.4 E	209.9 E	192 E
Expected Dec.	342.1	352.4	327.7
Expected Incl.	72	68.9	70.8
α95	3.6	4.3	3.1
Rotation (R)	33.6	23.3	48
ΔR	18.5	18.6	18.1
Flattening (F)	1.4	-1.7	0.2
ΔF	8.9	9.1	8.8
W-down Tilt (T)	11.3	8.7	16.2
Tilt Axis	352.1	15.1	351.1
ΔT	7.1	7.6	6.8

All major structures in the western Flint Creek Range are oriented roughly N-S, including the Georgetown-Princeton Thrust. No strike-slip or oblique-slip motion has been reported in or around the Philipsburg Batholith. Estimated vertical-axis rotations of 23 to 48 ± 19° are therefore inconsistent with the local geology. A more plausible explanation for the difference between the observed paleomagnetic direction for the Philipsburg Batholith and the expected paleofield directions from previously published paleomagnetic poles is crustal tilt around a horizontal axis. Using the error calculation method described in appendix A, depending on the reference direction selected, the grand mean paleomagnetic direction for the Philipsburg Batholith can be explained by a 9 to 16 ± 8° west-side down tilt around a horizontal tilt axis with an azimuth between 351˚ and

015˚ (figure 25). West-side down tilt in the western Flint Creek Range could be explained by further crustal shortening related to eastward propagation of the Sevier thrust-belt following emplacement of the Philipsburg Batholith. Tilting due to continued Sevier thrusting to the east must have occurred prior to the cessation of thrust/fold shortening at about 50 Ma (Harlan et al., 1988). Alternatively, the inferred modest west-down tilting in the western Flint Creek Range could have taken place after ca. 50 Ma, due to flexural uplift of the footwall, including the Philipsburg Batholith, below the east-dipping Anaconda Metamorphic Core Complex detachment. The data are presently insufficient to distinguish between these two styles of deformation that could have resulted in modest amounts of west-side down tilting. Notably, both explanations are more consistent with the local and regional geology than vertical-axis rotation.

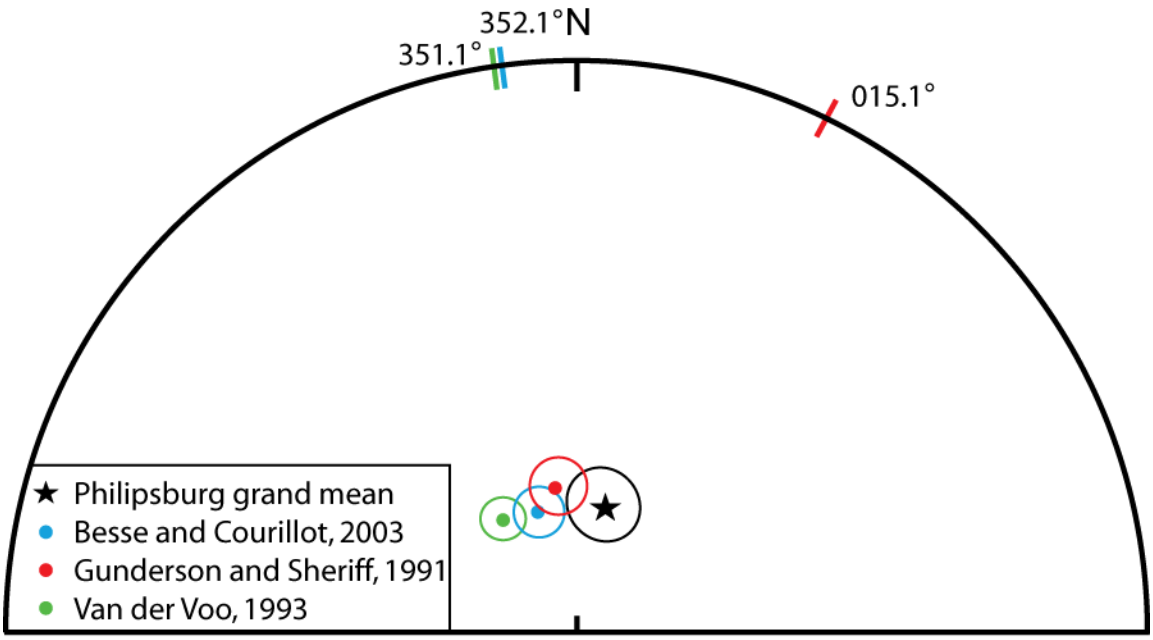

Figure 25. Stereographic projection of the observed Philipsburg Batholith grand mean direction (star) and expected paleofield directions calculated from previously published Late Cretaceous paleomagnetic poles. Horizontal tilt axes for the observed direction and each expected direction are plotted along the edge of the plot.

Lageson et al. (2001) suggested that intrusion of the ca. 70 to 80 Ma Boulder Batholith and coeval eruption of the Elkhorn Mountain volcanics into the active Late Cretaceous fold-thrust belt in SW Montana created a supercritical orogenic wedge, which then led to increased deformation in the Helena Salient. The intrusion of the Philipsburg Batholith and other Late Cretaceous intrusions in the Flint Creek Range to the west of the Boulder Batholith may have also led to an over-thickened orogenic wedge. Over-thickening in the western part of the fold-thrust belt may have accentuated deformation to the east in the vicinity of the Boulder Batholith. Alternatively, over-thickening of the orogenic wedge in the Flint Creek Range may have led to orogenic collapse and extension resulting in formation of the Anaconda Metamorphic Core Complex in the Eocene, as proposed by O'Neill et al. (2004).

Emplacement of the Philipsburg Batholith

There is no field evidence indicating that the Georgetown-Princeton thrust offsets the Philipsburg Batholith, implying that intrusion occurred after movement on the fault. The position of the fault prior to intrusion of the Philipsburg Batholith (figure 23) is critical in interpreting the relationship between the structures related to crustal shortening and magma emplacement in the Philipsburg Batholith. The trace of the Georgetown-Princeton Thrust swings east near both the northern and southern margins of the Philipsburg Batholith, though deflection of the fault trace is more pronounced near the northern margin. The eastward deflection of the trace of the Georgetown-Princeton Thrust near the Philipsburg Batholith suggests that the footwall of the thrust was depressed during intrusion and that the magma not only filled space due to roof uplift but also space due to depression of the footwall.

The AMS fabric data obtained in this study are interpreted to reflect major silicate mineral fabrics acquired by supersolidus magma flow during emplacement of the Philipsburg Batholith. High bulk susceptibilities for Philipsburg Batholith AMS samples indicate that the AMS fabrics are controlled by magnetite, rather than paramagnetic silicates. Sites in the batholith exhibit degrees of anisotropy (P') typical of magma flow fabrics from other plutonic rocks (Hrouda, 1982). Rock magnetic data indicate that the pluton is dominated by MD magnetite, with resulting AMS fabrics due to shape anisotropy of elongate magnetite grains. Magnetite is typically located within hornblende or biotite, or situated on grain boundaries of Fe-Mg silicates. These spatial relations suggest that the magnetite-dominated AMS fabrics most likely reflect preferred orientation of the silicate mineral network. A magmatic origin for AMS fabrics is corroborated by orientations of previously measured mafic enclaves in the southeast part of the Philipsburg Batholith, which are elongate parallel to the margin of the intrusion and roughly parallel to AMS lineations in the same area (O'Connell, 2000).

We interpret the AMS data to indicate that during emplacement of the Philipsburg Batholith, magma spread horizontally from a limited number of locations. Most AMS lineations and foliations in the Philipsburg Batholith are subhorizontal. Average foliation dip is shallow to the south-southwest. If dips are corrected for ~10º of estimated west-side down tilt of the pluton, the average is even closer to horizontal. AMS foliations dip concentrically, with values less than 30º, away from an area around Fred Burr Lake in the center of the Dora Thorn Pluton. Contours of foliation dips show an overall pattern of shallow values in the Dora Thorn Pluton, except around the estimated subsurface location of the Georgetown-Princeton Thrust and near the eastern margin of the intrusion. Near

intrusion margins, foliation dips range from shallow to steep, yet all foliation strikes are parallel to the margins. Subhorizontal AMS lineations are roughly parallel to foliation strike and to the batholith margins, and are interpreted as stretching lineations due to magma flow impinging on wall rock contacts. AMS fabrics due to interaction of magma flow with pluton margins are best illustrated in the southeast part of the Philipsburg Batholith, where all lineations trend parallel to the margin, are subhorizontal, and P' values are very high compared to the rest of the intrusion. These strong fabrics resulted from west to east magma flow impinging on the southeast margin of the intrusion.

The Bimetallic Stock exhibits much steeper foliation dips than the Dora Thorn Pluton. The steepest dips are along the proposed contact between the Bimetallic Stock and Dora Thorn Pluton suggesting that the Bimetallic Stock was fed by magma conduits in the vicinity of the internal contact. There is a close spatial relationship between the gradational internal contact between the Dora Thorn Pluton and the Bimetallic Stock, and inferred subsurface location of the Bungalow fault, interpreted as a backthrust associated with the Georgetown-Princeton Thrust, implying that magma feeding the Bimetallic Stock used the Bungalow Fault as a conduit during emplacement.

AMS data are interpreted to indicate that the Georgetown-Princeton Thrust served as a conduit for rising magma feeding the Dora Thorn Pluton. Shallowly dipping foliations abruptly change to steeply dipping foliations above the estimated location of the Georgetown-Princeton Thrust, with two areas in the southeast and one area in the north of the Dora Thorn Pluton having near vertical foliations (figure 23). In the same two areas of the southeast Dora Thorn Pluton, AMS lineations have plunges above 50º (figure 22b). One of the areas with near vertical foliations and steep lineations lies

between the main Georgetown-Princeton Thrust and an eastern thrust splay. Magma may have risen along both these faults during emplacement of the Dora Thorn Pluton.

Steeply dipping foliations do not completely characterize the estimated location of the Georgetown-Princeton Thrust or the contact between the Bimetallic Stock and Dora Thorn Pluton. An area of steep dips in the Fred Burr Creek drainage in the south of the Bimetallic Stock is separated from steep dips near South Boulder Creek in the north of the Bimetallic Stock by an area of moderate dipping foliations. Near Fred Burr Creek, the modal percent hornblende is highest and the hornblende has slightly coarser grain size than in the northern Bimetallic Stock. In the southern Dora Thorn Pluton, AMS foliation dips are shallow along the Georgetown-Princeton Thrust. The limited areas of steep foliation dips along the internal intrusive contact and the Georgetown-Princeton Thrust are interpreted to indicate that magma did not rise in a sheet along faults during emplacement. Instead, magma is interpreted to have flowed in conduits near the fault surfaces before spreading horizontally during emplacement.

We interpret the Georgetown-Princeton Thrust in the vicinity of the Philipsburg Batholith as a thrust ramp. The thrust surface in this area steps to higher levels within the Belt Supergroup, as evidenced by the lack of carbonate strata of the lower Belt Supergroup exposed east of the thrust system. The Philipsburg Anticline on the west side of the Philipsburg Batholith is interpreted as a ramp-top anticline. A ramp geometry can explain the steep dips of the main Georgetown-Princeton Thrust and the eastern splay, which we interpret as an imbricate thrust typical of ramp-flat settings. In this interpretation, the Bungalow Fault would be considered a backthrust off the Georgetown-Princeton Thrust.

Kalakay et al. (2001) noted intrusion margin parallel footwall synclines with fold axes lying east of the McCartney Mountain Pluton and the Pioneer Batholith. They interpret these synclines as part of fault-propagation folds beneath structurally higher hanging-wall anticlines, and rely on this inferred relationship to support their ramp-top emplacement model for the two intrusions. The Racetrack Folds synclinorium, to the east of the Philipsburg Batholith, lies in a similar structural position to the footwall synclines discussed by Kalakay et al. (2001) and supports the ramp-flat geometry interpretation for the Georgetown-Princeton Thrust in the vicinity of the Philipsburg Batholith.

We propose that emplacement of the Philipsburg Batholith occurred after final movement along the Georgetown-Princeton Thrust system, facilitating magma transport to the level of emplacement via conduits along the thrust surface. AMS fabrics indicate that the magma utilized the Bungalow Fault, the main Georgetown-Princeton Thrust, and an eastern thrust splay to rise before laterally spreading atop the thrust ramp. The Philipsburg Batholith was emplaced as a tabular body fed from multiple areas of nearly vertical magma flow and the space for emplacement was made possible by roof uplift in the ramp-top setting due to previous fault-bend folding and backthrusting in the hanging wall of the Georgetown-Princeton Thrust. Depression of the footwall may have aided emplacement in the ramp-top setting. This emplacement model is similar to the ramp-top emplacement model of Kalakay et al. (2001) for other intrusions in SW Montana and AMS fabric results from the Philipsburg Batholith may support the application of a ramp-top emplacement model to other Late Cretaceous intrusions in SW Montana.

The difference in composition between the Bimetallic Stock and the Dora Thorn Pluton led Hyndman et al. (1982) to split the Philipsburg Batholith into two separate

intrusions. They proposed that the two magmas differentiated at depth from a common source. The $^{40}Ar/^{39}Ar$ age data and AMS data indicate that magma of the Bimetallic Stock was transported vertically along the Bungalow Fault and was emplaced within and adjacent to the Philipsburg Anticline very shortly before the Dora Thorn magma rose along the Georgetown-Princeton Thrust. The Dora Thorn magma spread laterally to the west of the Georgetown-Princeton Thrust due to roof uplift until reaching the still cooling Bimetallic stock, resulting in a gradational contact. Dora Thorn magma also spread laterally to the east of the Georgetown-Princeton Thrust, filling space caused by depression of the footwall. The high P' values for AMS fabrics east of the thrust suggest a more forceful emplacement of the magma near the eastern margin of the Dora Thorn Pluton

Comparison of AARM and AMS Fabrics

The high bulk susceptibilities of AMS samples suggest that AMS fabrics are dominated by the preferred orientation of magnetite grains. We interpret the data from sites with similar AARM and AMS fabrics to confirm the assumption that MD magnetite controls the observed AMS fabrics. The lack of parallel relationship between AARM fabrics and AMS fabrics for two of the eight studied sites in the Philipsburg Batholith suggests that the AMS technique may not exactly reflect the preferred orientation of ferro/ferrimagnetic minerals at all sites. It is possible, though these samples are dominated by MD magnetite, that a small population of SD magnetite may control the AMS fabrics. The different response of SD magnetite to induced and remanent magnetization methods could explain the difference between the AMS and AARM fabrics (Jackson, 1991). These results may call into question some of the underlying

assumptions of the AMS technique for measuring the magma flow fabrics of ferromagnetic-dominated granitoids, including the assumptions that high bulk susceptibility implies that fabrics are controlled by magnetite (Bouchez, 1997), and that samples dominated by MD magnetite have fabrics that are also controlled by MD magnetite and not by a small but important SD magnetite population. We assume that AMS fabrics in the Philipsburg Batholith reflect alignment of major silicate and oxide phases in the magma during emplacement. The relatively small number of sites studied using the AARM method in the Philipsburg Batholith precludes clear determination of the validity of these assumptions, but the similarity between AMS and AARM fabrics at six out of eight measured sites gives us confidence that the assumptions are reasonable in this study. More detailed comparison of AARM and AMS fabrics from granitic rocks may lead to a better understanding of the conditions under which the assumptions of the AMS technique are valid.

Conclusions

The emplacement and deformation history of the Philipsburg Batholith in the Sevier fold-thrust belt of SW Montana has been refined using $^{40}Ar/^{39}Ar$ age determinations on biotite mineral separates, paleomagnetic data, field relations, and AMS/AARM fabric data. Paleomagnetic data indicate that the Philipsburg Batholith has not been internally deformed, but may have experienced a small amount of west-side down tilt since emplacement. Sevier-age thin-skinned deformation in the western Flint Creek Range ceased before emplacement of the Philipsburg Batholith around 74.6 Ma. Emplacement of the Philipsburg Batholith occurred over ~2 Ma, possibly by amalgamation of multiple magma pulses, and the distribution of interpreted ages of

biotite cooling suggests emplacement generally progressed from west to east. These results are consistent with the gradational contacts previously reported between the more mafic Bimetallic Stock and the less mafic Dora Thorn Pluton. AMS fabrics are interpreted to reflect magma flow fabrics during emplacement and show that the Philipsburg Batholith magma utilized the Georgetown-Princeton Thrust system as a conduit for magma ascent. The Philipsburg Batholith is dominated by subhorizontal AMS fabrics and we interpret it to have been intruded as a tabular body, with magma filling space above a ramp in the Georgetown-Princeton Thrust within a fault-bend anticline, aided by backthrusting on the Bungalow Fault. The ramp-top emplacement of the Philipsburg Batholith is consistent with the similar thrust ramp emplacement models proposed for other intrusions in SW Montana by Kalakay et al. (2001) using field relations, suggesting that this is the dominant emplacement position for Late Cretaceous intrusions in SW Montana.

Our results suggest that the space required for the ascent and emplacement of large magma bodies within regions of crustal shortening is facilitated by step-overs or irregularities in the geometry of fault planes, which lead to areas of lesser compressive stress. These areas allow magma the space to rise buoyantly. Magma flow along fault surfaces is more likely than classic models of magma ascent such as diapirism and stoping, especially in regions of horizontal shortening, because magma could rise in smaller volumes. Releasing bends in strike-slip systems have previously been invoked as areas of lesser compressive stress allowing pluton emplacement in the Sierra Nevada Batholith (Titus et al., 2005). We expect magmas rising along thrust faults to also form

plutons in areas of lesser compressive stress, such as within fault-bend folds above thrust ramps, as shown for the Philipsburg Batholith.

A new method for calculating horizontal-axis tilt errors from paleomagnetic data is presented in appendix A. This tilt error calculation method is useful for comparing measured paleomagnetic directions to expected directions calculated using published paleomagnetic poles and is more accurate for tilt calculations than using the formula for vertical-axis rotation proposed by Beck (1980) and modified by Demarest (1983).

Chapter One Acknowledgements

We would like to thank Dr. Mike Jackson for help with hysteresis measurements at the University of Minnesota Institute of Rock Magnetism. $^{40}Ar/^{39}Ar$ geochronology was performed with the assistance of Dr. Matt Heizler, Dr. Bill McIntosh, and Lisa Peters, for which we are very thankful. We are grateful to Jack Grow and Christina Carr for field assistance during the summer of 2007. This project was funded by grants to T. Naibert from the Geological Society of America, and the Office of Graduate Studies and Dept. of Earth and Planetary Sciences at the University of New Mexico.

References Cited

Aranguren, A., Cuevas, J., Tubia, J.M., Roman-Berdiel, T., Casas-Sainz, A., Casas-Ponsati, A., 2003, Granite laccolith emplacement in the Iberian arc: AMS and gravity study of the La Tojiza pluton (NW Spain): Journal of the Geological Society London, v. 160, p. 435-445.

Baty, J.B., 1973, Fission track age dates from three granitic plutons in the Flint Creek range, Western Montana [M.S. Thesis]: Missoula, University of Montana, 37 p.

Beck, M.E., 1980, Paleomagnetic record of plate-margin tectonic processes along the western edge of North America: Journal of Geophysical Research, v. 85, p. 7115-7131.

Besse, J. and Courtillot, V., 2003**,** Correction to apparent and true polar wander and the geometry of the geomagnetic field over the last 200 Myr: Journal of Geophysical Research, v. 108, doi: 10.1029/2003JB002684. issn: 0148-0227.

Bouchez, J.-L., 1997, Granite is never isotropic: an introduction to AMS studies of granitic rocks, *in* Bouchez, J.-L., Hutton, D.H.W., and Stephens, W.E., eds., Granite: from segregation of melt to emplacement fabrics: Dordrecht, Holland, Kluwer Academic Publishers, p. 95-112.

Bouchez, J.-L., Gleizes, G., Djouadi, T., Rochette, P., 1990, Microstructure and magnetic susceptibility applied to emplacement kinematics of granites: the example of the Foix pluton (French Pyrenees): Tectonophysics, v. 184, p. 157-171.

Bulter, R.F., 1992, Paleomagnetism: magnetic domains to geologic terranes: Boston, Massachusetts, Blackwell Scientific Publishing. 336 p.

Cante, S.C. and Kent, D.V., 1995, Revised calibration of the geomagnetic polarity timescale for the Late Cretaceous and Cenozoic: Journal of Geophysical Research, v. 100, p. 6093-6095.

Castro, A., and Fernandez, C., 1998, Granite intrusion by externally induced growth and deformation of the magma reservoir, the example of the Plasenzuela pluton, Spain: Journal of Structural Geology, v. 20, p. 1219-1228.

Day, R., Fuller, M., Schmidt, V.A., 1977, Hysteresis properties of titanomagnetites: grain size and compositional dependence: Physics of the Earth and Planetary Interiors, v. 13, p. 260–267.

Demarest, H.H., Jr., 1983, Error analysis for the determination of tectonic rotation from paleomagnetic data: Journal of Geophysical Research, v. 88, p. 4321-4328.

Dunlop, D.J., and Özdemir, Ö., 1997, Rock Magnetism: Cambridge, United Kingdom, Cambridge University Press, 596 p.

Ehinger, R., 1971, Petrochemistry of the western half of the Philipsburg batholith, Montana [PhD thesis]: Missoula, University of Montana, 128 p.

Fisher, R.A., 1953, Dispersion on a sphere: Proceedings of the Royal Society of London, Series A, v. 217, p. 295–305.

Gebelin, A., Martelet, G., Chen, Y., Brunel, M., Faure, M., 2006, Structure of late Variscan Millevaches leucogranite massif in the French Massif Central: AMS and gravity modeling results: Journal of Structural Geology, v. 28, p. 148-169.

Glazner, A.F., Bartley, J.M., Coleman, D.S., Gray, W., and Taylor, R.Z., 2004, Are plutons assembled over millions of years by amalgamation or small magma chambers?: GSA Today, v. 14, p. 4-11.

Gunderson, J.A., and Sheriff, S.D., 1991, A new Late Cretaceous paleomagnetic pole from the Adel Mountains, West Central Montana: Journal of Geophysical Research, v. 96, p. 317-326.

Hamilton, W., and Myers, W.B., 1974, Nature of the Boulder Batholith of Montana: Geological Society of America Bulletin, v. 85. p. 365-378.

Harlan, S.S., Geissman, J.W., Lageson, D.R., Snee, L.W., 1988, Paleomagnetic and isotopic dating of thrust-belt development along the eastern edge of the Helena salient, northern Crazy Mountains Basin, Montana: Geological Society of America Bulletin, v. 100, p. 492-499.

Hrouda, F., 1982, Magnetic anisotropy of rocks and its application in geology and geophysics: Geophysical Surveys, v. 5, p. 37-82.

Hutton, D.H.W., 1997, Syntectonic granites and the principle of effective stress: a general solution to the space problem?, *in* Bouchez, J.-L., Hutton, D.H.W., and Stephens, W.E., eds., Granite: from segregation of melt to emplacement fabrics: Dordrecht, Holland, Kluwer Academic Publishers, p. 95-112.

Hyndman, D.W., Obradovich, J.D., Ehinger, R., 1972, Potassium-Argon age determinations of the Philipsburg Batholith: Geological Society of America Bulletin, v. 83, p. 475-480.

Hyndman, D.W., Talbot, J.L., Chase, R.B., 1975, Boulder batholith: a result of emplacement of a block detached from the Idaho batholith infrastructure?: Geology, v. 3, p. 401-404.

Hyndman, D.W., Silverman, A.J., Ehinger, R., Benoit, W.R., Wold, R., 1982, The Philipsburg Batholith, Western Montana: Montana Bureau of Mines and Geology Memior, v. 49, p. 1-37.

Jackson, M., 1991, Anisotropy of magnetic remanence: a brief review of mineralogical sources, physical origins, and geological applications, and comparison with susceptibility anisotropy: Pure and Applied Geophysics, v. 136, p. 1-28.

Jelinek, V., 1978, Statistical processing of magnetic susceptibility measured in groups of specimens: Studia Geophysica et Geodaetica, v. 22, p. 50–62.

Johnson, H.P., Lowrie,W., and Kent, D.V., 1975, Stability of anhysteretic remanent magnetization in fine and coarse magnetite and maghemite particles: Royal Astronomical Society Geophysical Journal, v. 41, p. 1–10.

Kalakay, T.J., John, B.E., Lageson, D.R., 2001, Fault-controlled pluton emplacement in the Sevier fold-and-thrust belt of southwest Montana, USA: Journal of Structural Geology, v. 23, p. 1151-1165.

Karlstrom, K.E., Miller, C.F., Kingsbury, J.A., Wooden, J.L., 1993, Pluton emplacement along an active ductile thrust zone, Piute Mountains, southeastern California: interaction between deformational and solidification processes: Geological Society of America Bulletin, v. 105, p. 213-230.

Kirschvink, J.L., 1980, The least-squares line and plane and the analysis of paleomagnetic data: Geophysical Journal of the Royal Astronomical Society, v. 62, p. 699-718.

Klepper, M.R., Robinson, G.D., and Smedes, H.W., 1971, On the nature of the Boulder Batholith of Montana: Geological Society of America Bulletin, v. 82, p. 1563–1580.

Klepper, M.R., Robinson, G.D., and Smedes, H.W., 1974, Nature of the Boulder Batholith of Montana: Discussion: Geological Society of America Bulletin, v. 85, p. 1953–1960.

Lageson, D.R., Schmitt, J.G., Horton, B.K., Kalakay, T.J., Burton, B.R., 2001, Influence of Late Cretaceous magmatism on the Sevier Orogenic wedge, western Montana: Geology, v. 29, p. 723-726.

Lewis, R.S., 1998, Geologic map of the Butte 1° x 2°quadrangle: Montana Bureau of Mines and Geology Open File Report MBMG 363, scale 1:250,000, 1 sheet.

Lo, C.H., and Onstott, T.C., 1988, ^{39}Ar recoil artifacts in chloritized biotite: Geochimica et Cosmochimica Acta, v. 53, p. 2697-2711.

Lonn, J.D., McDonald, C., Lewis, R.S., Kalakay, T.J., O'Neill, J.M., Berg, R.B., and Hargrave, P., 2003, Preliminary geologic map of the Philipsburg 30° × 60° quadrangle, western Montana: Montana Bureau of Mines and Geology Open-File Report 483, scale 1:100 000, 1 sheet, 29 p.

McFadden, P.L., McElhinney, M.W., 1988, The combined analysis of remagnetization circles and direct observations in paleomagnetism: Earth and Planetary Science Letters, v. 87, p. 161-172.

O'Connell, M.P., 2000, Geometry, kinematics, and emplacement mechanisms of the Philipsburg Batholith within the Sevier fold-and-thrust belt, Flint Creek Range, western Montana [M.S. Thesis]: Bozeman, Montana State University, 99 p.

O'Neill, J.M., Lonn, J.D., Lageson, D.R., Kunk, M.J., 2004, Early Tertiary Anaconda metamorphic core complex, southwestern Montana: Canadian Journal of Earth Sciences, v. 41, p. 63-72.

Renne, P.R., Swisher, C.C., Deino, A.L., Karner, D.B., Owens, T.L., DePaolo, D.J., 1998, Intercalibration of standards, absolute ages and uncertainties in ^{40}Ar/^{39}Ar dating: Chemical Geology, v. 145, p. 117-152.

Schmidt, C.J., Smedes, H.W., O'Neill, J.M., 1990, Syncompressional emplacement of the Boulder and Tobacco Root batholiths (Montana-USA) by pull-apart along old fault zones: Geological Journal, v. 25, p. 305-318.

Streckeisen, A., 1973, Plutonic rocks: Classification and nomenclature recommended by the IUGS subcommission on systematics of igneous rocks: Geotimes, v. 18, p. 26-30.

Tauxe, L., 1998, Paleomagnetic principals and practice: Dordrecht, Holland, Kluwer Academic Publishers, Modern Approaches in Geophysics, v. 17, 299 p.

Tikoff, B., and Teyssier, C., 1992, Crustal-scale, en echelon "P-shear" tensional bridges: A possible solution to the batholithic room problem: Geology, v. 20, p. 927-930.

Titus, S.J., Clark, R., Tikoff, B., 2005, Geological and geophysical investigation of two fine-grained granites, Sierra Nevada batholith, California: evidence for structural controls on emplacement and volcanism: Geological Society of America Bulletin, v. 117, p. 1256-1271.

Van der Voo, R., 1993, Paleomagnetism of the Atlantic, Tethys, and Iapetus Oceans: Cambridge, United Kingdom, Cambridge University Press, 411 p.

Appendix: Calculating Horizontal-Axis Tilt and Associated Uncertainty

A horizontal tilt axis is the vector normal to a vertical plane that includes a small circle containing the endpoints of both the observed and expected paleomagnetic vectors (Figure 26a). The tilt axis can be determined using the declination and inclination of the expected direction (D_x,I_x) and the observed direction (D_y,I_y) by first calculating the total declination difference between the two directions:

$$D_t = D_x - D_y$$

From figure 26:

Eq. 1 $\cos(I_x) = i_x$ (figure 26b)

Eq. 2 $\cos(I_y) = i_y$ (figure 26c)

Eq. 3 $\cos(I_r) = i_r$ (figure 26d)

Eq. 4 $\cos(D_a) = i_r/i_x = \cos(I_r)/\cos(I_x)$ (figure 26e)

Eq. 5 $\cos(D_b) = i_r/i_y = \cos(I_r)/\cos(I_y)$ (figure 26e)

Eq. 4 and eq. 5 can be rearranged to solve for $\cos(I_r)$ and set equal to each other in order to solve for D_a and D_b, using the relationship:

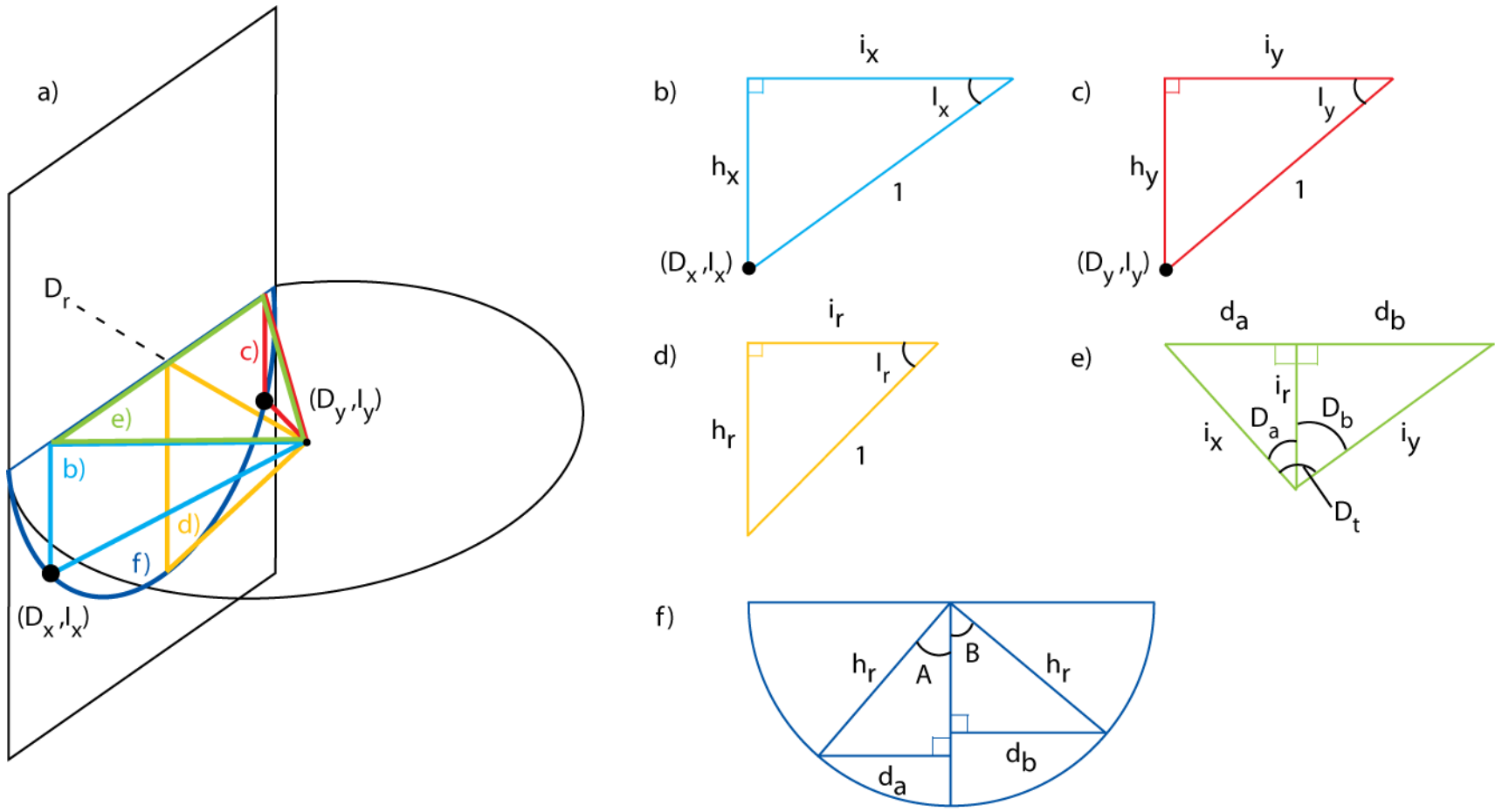

Figure 26. (a) A geometric representation of a small circle of rotation around a horizontal-tilt axis, Dr, for comparing paleomagnetic directions. Labeled line segments and angles are used for calculating total horizontal axis tilt and tilt uncertainty. Right triangles are formed outside the plane of rotation by the inclinations of the expected direction (b) and the observed direction (c), and by the azimuth of the tilt axis (d). Geometric relationships in the horizontal plane are shown in (e). Relationships in the vertical plane of rotation are shown in (f).

Eq. 6 $D_b = D_t - D_a$ (figure 26e)

$$\cos(D_a)\cos(I_x) = \cos(D_b)\cos(I_y)$$

$$\cos(D_a)\cos(I_x) = \cos(D_t-D_a)\cos(I_y)$$

Eq. 7 $$\cos(D_a)\cos(I_x)/\cos(I_y) = \cos(D_t-D_a)$$

Eq. 7 can be further simplified using the trigonometric identity for the cosine of the difference of two angles:

$$\cos(D_a)\cos(I_x)/\cos(I_y) = \cos(D_t)\cos(D_a) + \sin(D_t)\sin(D_a)$$

$$\cos(I_x)/\cos(I_y) = \cos(D_t) + \sin(D_t)\sin(D_a)/ \cos(D_a)$$

$$\cos(I_x)/\cos(I_y) - \cos(D_t) = \sin(D_t)\tan(D_a)$$

$$\tan(D_a) = [\cos(I_x)/\cos(I_y) - \cos(D_t)] / \sin(D_t)$$

Eq. 8 $$D_a = \tan^{-1}\{[\cos(I_x)/\cos(I_y) - \cos(D_t)] / \sin(D_t)\}$$

D_a is the declination angle between the expected direction and the tilt axis, so the azimuth of the tilt axis, D_r, is:

Eq. 9 $D_r = D_x + D_a$

To calculate the magnitude of tilt about the horizontal tilt axis, solve for the inclination, I_r, of the vector from the origin to the low point on the small circle using eq. 4 and the value calculated for D_a in eq. 8. It follows from figure 26(d,e) that:

Eq. 10 $h_r = \sin(I_r)$

Eq. 11 $d_a = i_x\sin(D_a) = \cos(I_x)\sin(D_a)$ (using eq. 1)

Eq. 12 $\sin(A) = d_a/h_r = \cos(I_x)\sin(D_a)/ \sin(I_r)$ (figure 26f)

and similarly:

Eq. 13 $d_b = i_y\sin(D_b) = \cos(I_y)\sin(D_b)$ (using eq. 2)

Eq. 14 $\sin(B) = d_b/h_r = \cos(I_y)\sin(D_b)/ \sin(I_r)$ (figure 26f)

The estimate of total tilt, T, between the expected and observed directions is:

Eq. 15 $T = A + B$

The error in the estimate of total tilt can be calculated by considering how the α_{95} confidence values for the expected and observed directions project onto the small circle around the tilt axis, similar to calculating ΔD for the expected and observed values when finding ΔR for vertical-axis rotation. The angular errors in the small circle of tilt, Δt_x and Δt_y for expected and observed directions respectively, are the projections of the α_{95} value on the small circle and can be found by scaling α_{95x} and α_{95y} by the radius, h_r, of the small circle of tilt. When the observed and expected directions lie in a small circle close to the edge of the unit sphere, h_r is small and the projection of α_{95} on the small circle, Δt, is much larger than α_{95} (figure 27b). Conversely, when the small circle of tilt, defined by the observed and expected directions, is further from the edge of the unit sphere, h_r is large and the projection of α_{95} on the small circle, Δt, is closer to α_{95} (figure 27c). In the case where tilt occurs along a great circle, $h_r = 1$ and $\Delta t = \alpha_{95}$. Eq. 10 states that $h_r = \sin(I_r)$, so the individual tilt errors can be calculated by:

Eq. 16 $\Delta t_x = \sin^{-1}(\sin(\alpha_{95x})/\sin(I_r))$

Eq. 17 $\Delta t_y = \sin^{-1}(\sin(\alpha_{95y})/\sin(I_r))$

The error in tilt, ΔT, can then be found by:

Eq. 18 $\Delta T = \sqrt{\Delta t_x^2 + \Delta t_y^2}$

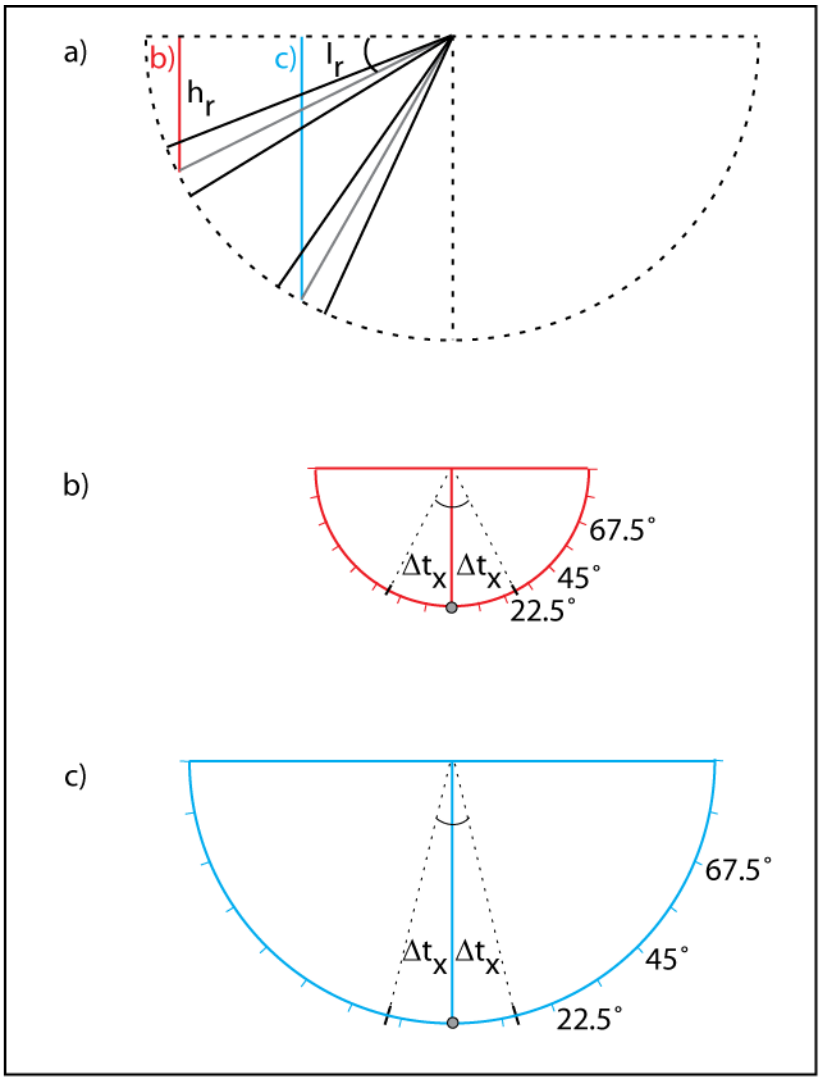

Figure 27. Diagram showing how Δt values are higher for shallow paleomagnetic directions (b) and lower for steeper paleomagnetic directions (c), if both directions have the same α_{95} value.

Chapter Two

Comparison of the anisotropy of anhysteretic remanent magnetization and the anisotropy of magnetic susceptibility in intrusive igneous rocks: implications for the interpretation of magma flow fabrics.

[1]T. J. Naibert, [2]D. K. Holm, [1]J. W. Geissman, and S. R. Muggleton
[1]Dept. Earth and Planetary Sciences – University of New Mexico
[2]Dept. Geology – Kent State University

Abstract

The anisotropy of anhysteretic remanent magnetization (AARM) and the anisotropy of magnetic susceptibility (AMS) have been compared for 26 sites (10-19 samples per site) from the Philipsburg Batholith, southwest Montana, the Square Butte and Shonkin Sag Laccoliths, north-central Montana, and radial and lamprophyre dikes of the Spanish Peaks Igneous Complex, Colorado. All of the rocks included in this study have high average bulk susceptibilities and AMS fabric data are controlled by the orientation of magnetite. Four relationships between AARM and AMS fabrics have been identified in the results from the 26 sites. Normal, inverse, and intermediate fabric relationships are similar to previously described comparisons of AMS foliations and dike wall orientations. Additionally, sites with AMS foliations that are oblique to AARM foliations have been identified in each of the intrusions. These complicated AARM/AMS data sets may be due to different anisotropies associated with different magnetite size fractions. More than one fabric relationship was identified in each of the studied intrusions, suggesting that the controls on AMS may not be consistent throughout individual intrusions. Partial anisotropy of anhysteretic remanent magnetization (pAARM) data obtained over three peak field windows (0-30, 30-60, 60-100 mT) for two

samples show that the lowest coercivity population of magnetite, presumably multi-domain, controls the AARM signal at site PB58, which has a normal AARM/AMS fabric relationship. In three studied dikes, AARM foliations were not parallel to dike margins, indicating that the inverse effect of single-domain (SD) magnetite is not necessarily the cause of inverse relationships between AMS fabrics and dike margins. Our results show that AARM can be utilized to better understand the control of magnetite on AMS data from igneous rocks with high susceptibility.

Introduction

Anisotropy of magnetic susceptibility (AMS) has been extensively used to determine mineral fabrics in igneous, sedimentary, and metamorphic rocks and is a common tool for defining the orientation of magma flow fabrics in intrusive igneous rocks, where petrofabrics are often too weak to be measured in the field (Hrouda, 1982; Bouchez, 1997). The anisotropy of anhysteretic remanent magnetization (AARM) has been utilized less frequently than AMS, mostly for analyzing strain in metamorphosed rocks or determining the effects of remanence anisotropy on paleomagnetic directional data. AMS is a fast and straightforward technique for measuring mineral fabrics in rocks and is more quantitative than traditional two dimensional fabric measurements made in the field. Many studies have successfully used AMS fabrics to interpret the interaction of magma flow with local structures during emplacement of igneous intrusions (Bouchez et al., 1990; Aranguren et al., 2003; Titus et al., 2005; Gebelin et al., 2006). AARM has not been extensively used to measure igneous fabrics due largely to prohibitively long measurement times compared to AMS and to the lack of standard laboratory procedures.

Magnetic fabric studies of magma flow rely on the assumption that the magnetic lineation and the magnetic foliation are parallel to the petrofabric lineation and petrofabric foliation, respectively. Because AMS fabrics reflect the combined preferred orientations of all anisotropic minerals in a sample, including diamagnetic, paramagnetic, and ferro/ferrimagnetic minerals, the orientation of the measured magnetic fabric may not coincide with the preferred orientation of major rock-forming silicate minerals aligned during magma flow. AMS fabrics may be primarily controlled by the orientation of high susceptibility ferrimagnetic minerals, such as magnetite, and the effect of paramagnetic silicates on the fabric may be insignificant. AMS fabrics controlled by magnetite are further complicated by the inverse effect of single-domain (SD) magnetite grains. Understanding the contributions of different magnetite size fractions to the AMS fabric is therefore important for assessing the validity of AMS studies in igneous rocks and for correctly assessing magma flow directions.

AARM fabrics reflect the preferred alignment of minerals capable of carrying a remanent magnetization, such as magnetite. Diamagnetic and paramagnetic silicates do not contribute to measurements of AARM fabrics. Additionally, AARM measurements are not affected by inverse magnetic fabrics (Jackson, 1991), which may be a common and confounding problem in AMS measurements of rocks containing single-domain (SD) magnetite. We have measured the AARM of samples from 26 sites used in AMS studies of three intrusions in Montana and three mafic dikes from the Spanish Peaks Igneous Complex, Colorado. These AARM data provide information about the orientation of the ferro/ferrimagnetic portion of the petrofabric to more fully assess the control of magnetite

on AMS in plutonic rocks. The results show four distinct relationships between AMS and AARM fabrics.

AMS background

All materials acquire an induced magnetization when placed in a magnetic field. Diamagnetic minerals, such as quartz and feldspars, acquire magnetization directions opposite the direction of the applied field. Paramagnetic minerals, including ferromagnesian silicates such as biotite and hornblende, are magnetized parallel to the applied field. Ferro/ferrimagnetic minerals acquire induced magnetizations parallel to the applied field, and also acquire a remanent magnetization that remains in the absence of the applied magnetic field (Hrouda, 1982).

The induced magnetization, **M**, of diamagnetic and paramagnetic materials is linearly related to the strength of the applied magnetic field, **H**. For relatively weak fields, the induced magnetization of ferro/ferrimagnetic minerals is also approximately linearly related to the applied field. This relationship can be expressed as:

$$M = K*H$$

where **K**, called the magnetic susceptibility, is the constant of proportionality relating the magnetization to the applied field. The susceptibility of materials can vary with the orientation of the magnetic field. In a three-dimensional Cartesian coordinate system, the magnetization, **M**, and the magnetic field, **H**, can be expressed as two vectors related by a second-rank susceptibility tensor.

$$\begin{bmatrix} M_1 \\ M_2 \\ M_3 \end{bmatrix} = \begin{bmatrix} K_{11} & K_{12} & K_{13} \\ K_{21} & K_{22} & K_{23} \\ K_{31} & K_{32} & K_{33} \end{bmatrix} \begin{bmatrix} H_1 \\ H_2 \\ H_3 \end{bmatrix}$$

This susceptibility tensor can be represented as a susceptibility ellipsoid (figure 28) with principal axes, K_1, K_2, and K_3, oriented along the maximum, intermediate, and minimum eigenvectors of the susceptibility tensor, respectively. The K_1 direction defines an AMS lineation and the plane perpendicular to K_3 defines an AMS foliation. The AMS lineations and foliations define the AMS fabric of the sample. The shape and overall degree of anisotropy of the AMS fabric can be determined by comparing the eigenvalues for the three principal axes. The shape parameter, **T**, ranges from -1 for infinitely prolate fabrics to 1 for infinitely oblate fabrics. The degree of anisotropy, **P'**, ranges from 1 to infinity, with greater values indicating greater anisotropy. Both values are calculated following Jelinek (1978).

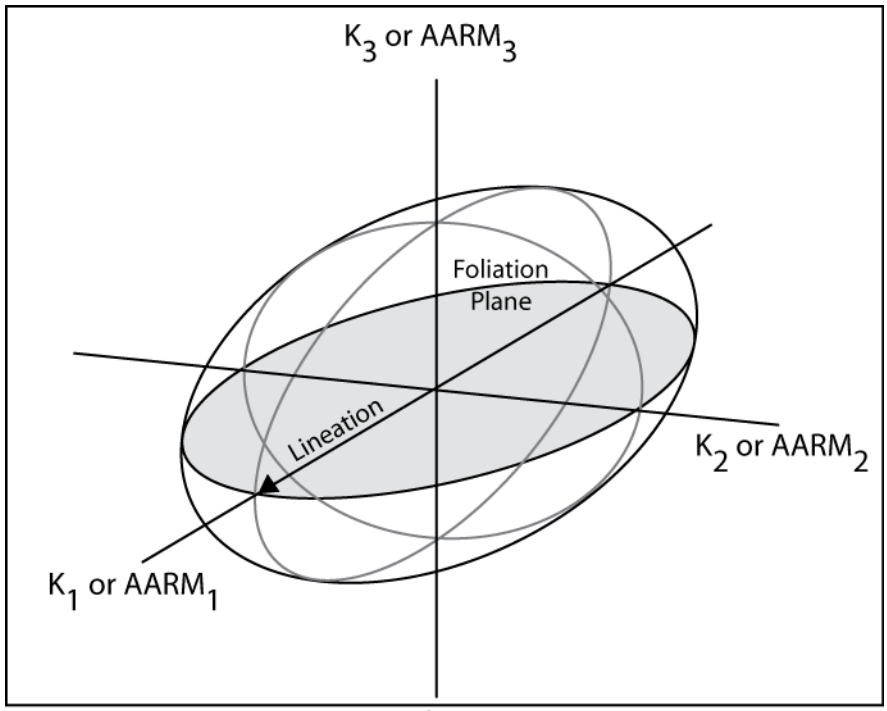

Figure 28. Schematic magnetic fabric ellipsoid showing the three principal AMS or AARM axes, the magnetic lineation, and the magnetic foliation plane.

Bulk susceptibility is the average of susceptibility along the three principal axes. Quartz and other diamagnetic minerals have low bulk susceptibilities around -0.8×10^{-7}

SI (Butler, 1992). Paramagnetic minerals have susceptibilities two to three orders of magnitude higher than quartz, therefore the diamagnetic contribution to the AMS fabric is not significant for most igneous rocks, even those with low ferromagnesian silicate contents. AMS fabrics in granitic rocks with bulk susceptibilities below 10^{-4} are primarily controlled by the preferred orientation of paramagnetic minerals, such as biotite and hornblende. Ferro/ferrimagnetic minerals have susceptibilities that are several orders of magnitude higher than paramagnetic minerals. Bulk susceptibilities of 10^{-3} or above therefore indicate that AMS fabrics are dominated by the preferred orientation of magnetite, the most abundant ferrimagnetic mineral in granitic rocks.

AMS in individual minerals is a function of both crystalline anisotropy and shape anisotropy. The dominant paramagnetic minerals in granite, biotite and hornblende, both have crystalline anisotropy. Biotite has minimum susceptibility along the c-axis, perpendicular to cleavage planes (Bouchez, 1997). Hornblende has maximum susceptibility along the c-axis (Hrouda, 1982). AMS fabrics in paramagnetic intrusions, with low bulk susceptibility, reflect foliations due to the preferred orientation of biotite cleavage planes and lineations due to the preferred orientation of elongate hornblende crystals or the intersection of multiple biotite foliations.

Magnetite has very weak crystalline anisotropy and the AMS of magnetite is largely controlled by shape anisotropy. For elongate multi-domain (MD) magnetite grains, the maximum susceptibility is parallel to the long axis of the magnetite grains. For elongate single-domain (SD) magnetite grains, the maximum susceptibility is perpendicular to the long axis of the magnetite grain. This behavior occurs because SD grains are magnetically saturated and the remanent magnetization of SD magnetite must

be oriented parallel to the long axis of the crystal in order to minimize magnetostatic energy (Jackson, 1991). A SD magnetite grain therefore cannot acquire additional induced magnetization parallel to its long axis. Applied fields that are perpendicular to the long axis of the grain will rotate the remanent magnetization away from the long axis leading to a component of magnetization parallel to the applied field.

In AMS studies of mafic dikes, AMS fabric orientations are often compared to the orientation of dike walls (e.g. Rochette et al., 1992; Rochette et al., 1999; Callot et al., 2001; Aubourg et al., 2002). It is assumed that magma flow in dikes will result in foliations roughly parallel to the dike margins. If the minimum susceptibility direction, K_3, is perpendicular to the dike margin (i.e. AMS foliation is margin parallel) the fabric is referred to as a 'normal magnetic fabric' (Rochette et al., 1992). Conversely, if the maximum susceptibility direction, K_1, is perpendicular to the dike margin then the fabric is termed 'inverse magnetic fabric' and if K_2 is perpendicular to the dike margin then the resulting fabric is termed an 'intermediate magnetic fabric' (Rochette et al., 1992). Inverse fabrics have been attributed to the control of SD magnetite on the AMS fabric, since K_1 is perpendicular to the long axis of SD grains. Intermediate fabrics have been attributed to a mixed population of SD and MD magnetite grains, which cause the principal axes of the susceptibility ellipsoid to interchange susceptibility values (Rochette et al., 1992).

AARM background

Because AMS studies of plutonic rocks rely on the assumption that AMS fabric data are a reflection of magmatic flow fabrics, it is critical to determine the effect of SD magnetite on AMS fabrics and correct for potential inverse fabrics before making

interpretations about magma flow direction. Unlike studies of dikes, most sampling sites are not spatially related to an intrusion margin in studies of larger plutons such as laccoliths and batholiths. Therefore AMS fabric orientations cannot be readily classified as normal, intermediate, or inverse by comparison to intrusion margins. Although rock magnetic tests can be utilized for magnetite-bearing samples to distinguish between populations dominated by SD and MD magnetite, it remains unclear whether SD or MD magnetite controls the AMS fabric.

The anisotropy of anhysteretic remanent magnetization (AARM) can be used to measure the preferred orientation of ferro/ferrimagnetic minerals capable of retaining a remanent magnetization in the absence of an applied magnetic field, which for most plutonic rocks is limited to magnetite. Furthermore, both elongate SD and MD magnetite grains will theoretically acquire a maximum remanence magnetization along their long axes, thereby alleviating the problem of inverse fabrics inherent in AMS studies (Jackson, 1991). Therefore, a comparison of AMS data with AARM data from the same sampling site allows the identification of inverse or intermediate AMS fabrics in plutonic rocks. These non-normal fabrics can then be discarded, or at least considered suspect, before interpreting magma flow directions.

Anhysteretic remanent magnetization (ARM) is acquired by samples subjected to a decaying alternating magnetic field and a superimposed weaker direct field. Minerals capable of retaining a remanent magnetization and with coercivities in the range of the alternating field will acquire a measureable artificial remanent magnetization. The ARM is proportional to the strength of the direct field by a proportionality constant analogous to the magnetic susceptibility, termed the anhysteretic susceptibility (King et al., 1982;

McCabe et al., 1985). Measuring the ARM of samples in different orientations in the direct field allows the determination of a second-rank tensor of anhysteretic susceptibility and an AARM ellipsoid (figure 28), with $AARM_1$, $AARM_2$, and $AARM_3$ axes similar to the AMS ellipsoid described above.

Geologic Background of the Sampling Areas

Samples for this study were taken from the Late Cretaceous Philipsburg Batholith in southwest Montana, the Early-Tertiary Shonkin Sag and Square Butte Laccoliths of north-central Montana, and three mafic dikes from the Mid-Tertiary Spanish Peaks Igneous Complex (SPIC) of southern Colorado. Thorough AMS studies of each of these intrusions have been conducted at the University of New Mexico Paleomagnetism Laboratory.

The Philipsburg Batholith is a 122 km^2 surface area, Late Cretaceous age intrusion within the Sevier fold-thrust belt of southwest Montana (Hyndman et al., 1982). The Philipsburg Batholith consists of granites, granodiorites, quartz monzonites and quartz monzodiorites, with an average granodiorite composition. Major silicate minerals include quartz, plagioclase and potassium feldspars, biotite, and hornblende. Biotite and hornblende range from 10 to 25 modal percent and biotite is typically more abundant than hornblende. There are no field relations that suggest post-emplacement deformation in the Philipsburg Batholith. Magmatic fabrics in the batholith are too weak to observe in the field. The orientations of mafic enclaves have previously been measured for some sites in the eastern part of the batholith, but these fabric markers are not present throughout most of the intrusion (O'Connell, 2000).

The Eocene Square Butte and Shonkin Sag Laccoliths in the Central Montana Alkalic Province were both emplaced in the Upper Cretaceous Eagle Formation. The Shonkin Sag Laccolith is 70 meters thick and both upper and lower contacts are well preserved. The Square Butte Laccolith is ~ 500 meters thick and has undergone significant erosion such that the upper contact is no longer present. Despite these differences in thickness, the Shonkin Sag and Square Butte Laccoliths are chemically very similar. Both intrusions are largely composed of shonkinite, a mafic rock consisting of augite, olivine, biotite and orthoclase, overlain by a thinner, less mafic syenite layer with similar mineralogy (Kendrick and Edmond, 1981). Field relations at the lateral margins of the Shonkin Sag Laccolith suggest that intrusion occurred as a series of rapidly emplaced sills.

Plutons, dikes, and sills of the mid-Cenozoic SPIC were emplaced into flat-lying strata of the Paleocene Poison Canyon Formation and the Eocene Cuchara and Huerfano Formations in the northern part of the Raton Basin of southern Colorado and northern New Mexico (Muggleton, 2006). The SPIC includes East Spanish Peak, West Spanish Peak, numerous smaller plutons and laccoliths, a radial dike swarm centered on West Spanish Peak, a smaller dike swarm centered on Silver Mountain, a set of east-west striking lamprophyre dikes, and a set of north-south striking, Rio Grande Rift parallel dikes and sills to the west of the Spanish Peaks. Two of the dikes in this study are part of the E-W set of lamprophyre dikes. The third dike is from the West Spanish Peak dike swarm.

Methods

AMS and AARM data were obtained for eight sites from the Philipsburg Batholith, four sites from the Square Butte Laccolith, eleven sites from the Shonkin Sag Laccolith, and three sites from dikes of the SPIC. Rock magnetic experiments were used to determine the magnetic mineralogy of the samples, and included the acquisition of isothermal remanent magnetization (IRM) to saturation, backfield demagnetization of saturation IRM, alternating-field (AF) demagnetization of IRM acquired in a 98 mT field, and AF demagnetization of ARM acquired in an AF field of 98 mT and a direct field of 0.1 mT. Hysteresis curves were measured for six Philipsburg Batholith samples. Additional rock magnetic data were obtained for sites for which AARM was not measured, in order to more fully characterize the magnetic mineralogy of the Philipsburg Batholith and the SPIC.

AMS Methods

AMS fabric data were obtained for 10-19 samples per site for all 26 sites. Samples were collected over a short distance (~50m^2). In all cases, AMS was measured before discrete specimens were demagnetized for AARM or rock magnetic measurements. All samples were collected using a portable-gas drill with a non-magnetic diamond-tipped drill bit and were oriented with magnetic and sun compasses. The samples were cut into 25 x 22mm right cylinder specimens with a non-magnetic diamond blade before measuring to best approximate the volume of a sphere. At least one specimen from each sample was measured using a Kappabridge KLY-4S. Susceptibility axes $K_1>K_2>K_3$, degree of anisotropy P', and shape parameter T were calculated using the Anisoft program (v4.2) from Agico Inc.

AARM Methods

AARM fabric data were obtained for four to eight samples per site for all 26 sites. One specimen was measured from each sample. AARM measurements were performed after specimens were AF demagnetized from a peak field of 100 mT. AARM specimens were cut to 15 x 13 mm right cylinders (~2.5 cm^3) in order to fit diagonally into a Schonstedt demagnetization unit. This was necessary to facilitate off-axis ARM positions required to calculate the anhysteretic susceptibility tensor. An ARM was imparted along the first of fifteen specific orientations in a direct field of 0.1 mT superimposed on an alternating field decaying from 100 mT. The remanent magnetization of the specimen was then measured with a 2G Enterprises superconducting rock magnetometer. An ARM was imparted and measured for each of the fifteen measurement orientations (figure 29) described in Tauxe (1998) and specimens were AF demagnetized from 100mT along three orthogonal axes after each measurement. The anhysteretic susceptibility tensor, the principal axes $AARM_1$>$AARM_2$>$AARM_3$, and the orientations of the AARM lineation and foliation were then calculated using the Jelinek method of linear perturbation analysis (Tauxe, 1998). Sample AARM ellipsoids were corrected to geographic coordinates before average site-level AARM ellipsoids were calculated. T and P' values for AARM ellipsoids were calculated as for AMS, following Jelinek (1978).

Partial AARM methods

Partial anisotropy of anhysteretic remanent magnetization (pAARM), which is measured by applying a direct field over a specific window of the decaying AF demagnetization field, was measured for two samples from site PB58 collected in the Philipsburg Batholith. The experimental setup was the same as for AARM

measurements, including all fifteen measured sample orientations (Tauxe, 1998). Low, middle, and high coercivities were activated by applying the 0.1 mT direct field during AF demagnetization windows of 0-30, 30-60, and 60-100 mT, respectively. Anhysteretic susceptibility tensors and pAARM ellipsoids were calculated as for AARM.

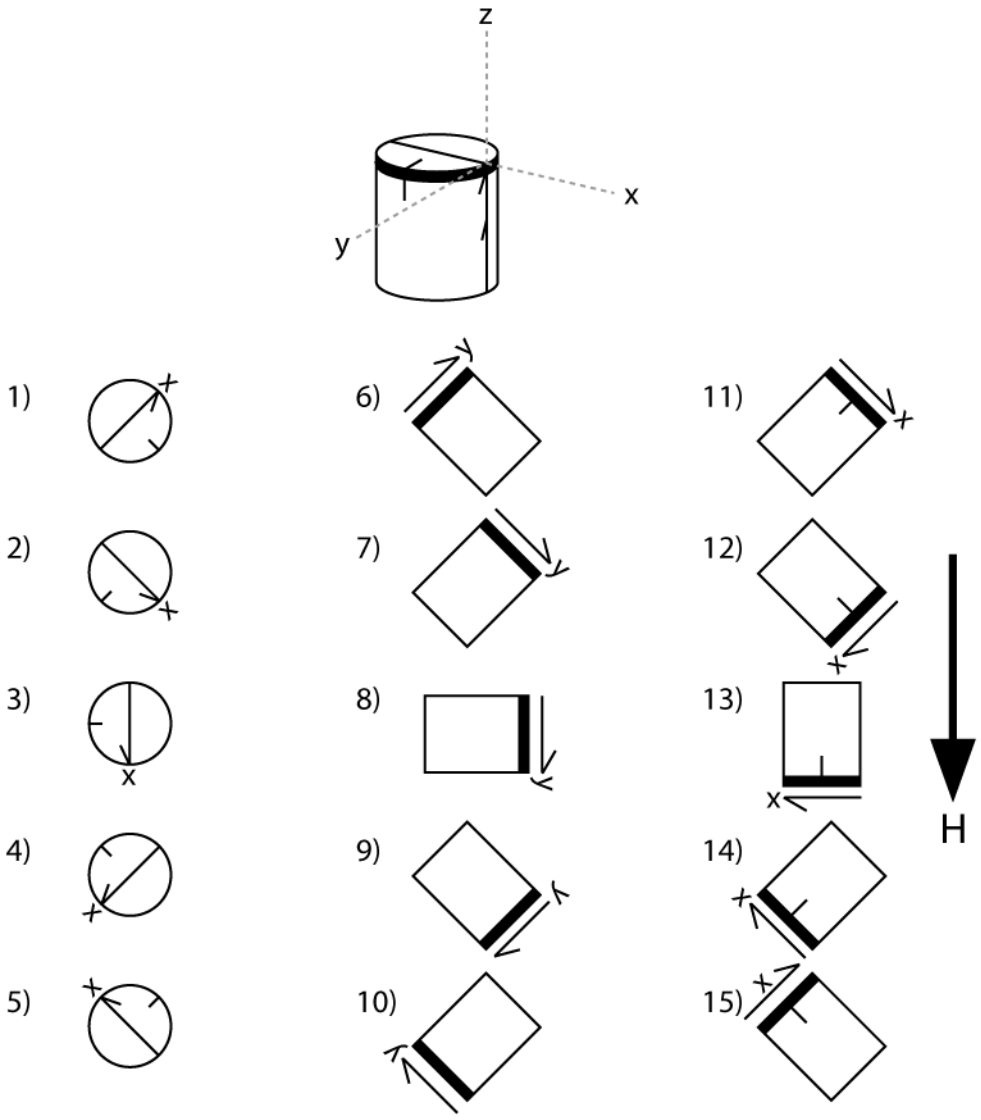

Figure 29. The fifteen measurement positions used for AARM and pAARM measurements. The positive z axis pointed down plunge during sample collection. The direct field is applied down in the diagram. Modified after Tauxe (1998).

Results

Average Bulk Susceptibility

Average bulk susceptibilities for all sites from the Philipsburg Batholith, Square Butte and Shonkin Sag Laccoliths, and SPIC dikes range from 1.19 to 6.86 x 10^{-2} (SI

unit/cm^3) with standard errors generally an order of magnitude lower, except for sites ss27, sp16, and sp81 (table 6).

Table 6 - Average bulk magnetic susceptibility for study sites

Site	Bulk K	+/- σ	Site	Bulk K	+/- σ
Philipsburg Bathoilth Samples			Shonkin Sag Laccolith Samples		
pb12	3.73	0.76	ss5	1.19	0.68
pb23	3.58	0.65	ss6	2.83	0.14
pb32	3.84	0.40	ss7	3.19	0.08
pb43	4.63	0.92	ss8	2.55	0.19
pb52	4.16	0.58	ss9	2.68	0.11
pb57	3.41	0.19	ss10	3.85	0.23
pb58	3.06	0.32	ss27	4.57	4.31
pb59	4.09	0.43	ss63	1.95	0.07
Square Butte Laccolith Samples			ss64	2.94	0.13
sb36	5.39	0.31	ss65	3.28	0.15
sb39	4.68	0.28	ss69	3.95	0.09
sb40	3.63	0.13	SPIC Dike Samples		
sb41	3.08	0.56	sp16	4.82	2.22
			sp73	5.68	0.45
			sp81	6.86	1.32

Bulk K and associated error reported in SI units/cm^3 x 10^{-2}

Rock Magnetic Results

Isothermal remanent magnetizations (IRM) imparted on selected Philipsburg Batholith specimens reach ~80 percent saturation in fields below 50 mT and reach complete saturation in fields below 150 mT. The low fields required for saturation of IRM, and the low coercivities of remanence calculated with backfield demagnetization of the saturation IRM (12 to 24 mT), suggest multi-domain (MD) magnetite is the dominant magnetic phase in the Philipsburg Batholith.

Modified Lowrie-Fuller tests, which compare AF demagnetization curves of ARM and 98 mT IRM, were used to determine the dominance of MD or SD magnetite in samples from the Philipsburg Batholith (Johnson et al., 1985). The field at which fifty percent of the ARM or IRM intensity remains is referred to as the median destructive field (MDF). MDF_{ARM}/MDF_{IRM} ratios less than one typify samples with dominantly MD

magnetite, and MDF_{ARM}/MDF_{IRM} ratios greater than one typify samples with a large population of SD or pseudo-single domain (PSD) magnetite (Dunlop and Ozdemir, 1997). MDF_{ARM}/MDF_{IRM} ratios for all Philipsburg Batholith samples are less than one (figure 30)., except for sample PB43j, which has a non-exponential ARM demagnetization curve.

Hysteresis curves were obtained using a vibrating sample magnetometer at the Institute for Rock Magnetism, University of Minnesota for samples from six Philipsburg Batholith sites for which AARM was measured. Saturation magnetization, M_s, ranges from 1.12 to 1.58 Am^2/kg, saturation remanence (M_{rs}) ranges from 0.009 to 0.021 Am^2/kg, coercivity (H_c) ranges from 0.8 to 1.5 mT, and coercivity of remanence (H_{cr}) ranges from 7.4 to 12.0 mT. Representative hysteresis loops for the Philipsburg Batholith show ramp-shaped curves that are typical of rocks dominated by MD magnetite grains (Dunlop and Ozdemir, 1997). The Philipsburg Batholith samples have low M_{rs}/M_s and high H_{cr}/H_c, which further suggest that the intrusion is dominated by MD magnetite (Day et al., 1977).

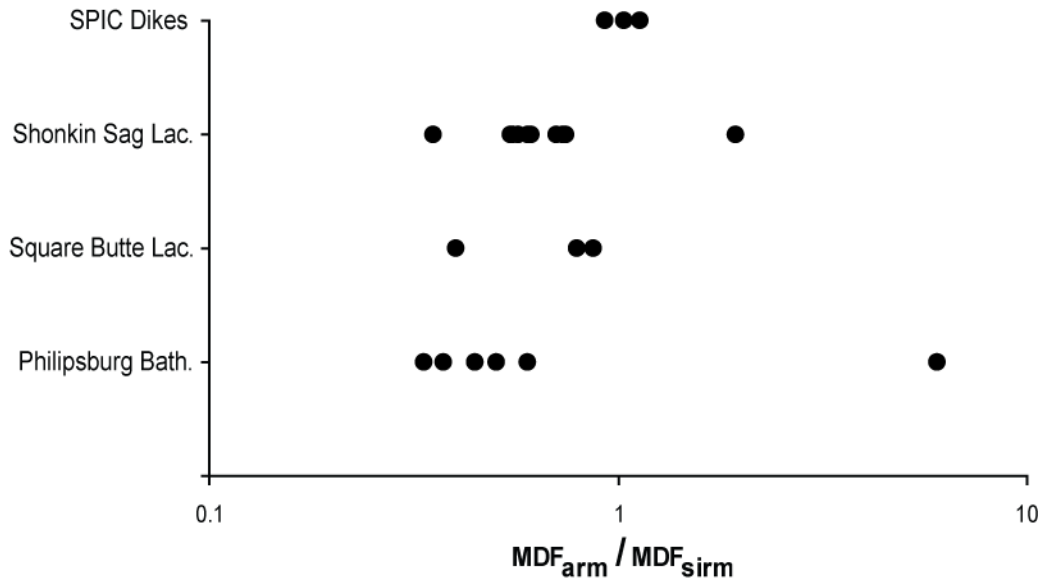

Figure 30. Mean destructive field ratio (MDF_{arm}/MDF_{irm}) for the 26 measured sampling sites. Values <1 indicate dominance of multi-domain magnetite and values >1 indicate dominance of single-domain magnetite.

Median destructive field ratios (MDF_{ARM}/MDF_{IRM}) for most samples from the Square Butte and Shonkin Sag laccoliths range from 0.35 to 0.86(figure 30), suggesting a large MD magnetite population. Sample SS5g has and MDF ratio of 1.9. This high ratio indicates the presence of SD/PSD magnetite in this sample. Three Shonkin Sag Laccolith and two Square Butte Laccolith samples have MDF_{ARM}/MDF_{IRM} ratios between 0.7 and 1, possibly suggesting a mixed population of MD and SD/PSD magnetite.

IRM acquisition experiments for 20 lamprophyre dike samples show nearly complete saturation between 90 and 300 mT, with an average around 150 mT. Backfield demagnetization of saturation IRM yields coercivites of remanence from 20 to 40 mT. MDF_{ARM}/MDF_{IRM} ratios for lamprophyre dike samples are all greater than one (figure 30), which indicates dominance by SD/PSD magnetite grains. Samples from both site

SP16 and SP 81, for which AARM fabrics were measured, had MDF_{ARM}/MDF_{IRM} ratios greater than one (figure 30), indicating dominance by SD/PSD magnetite.

Acquisitions of IRM in 21 radial dikes of the West Spanish Peak dike swarm reach saturation between 130 and 450 mT (Muggleton, 2006). Backfield demagnetization of saturation IRM yields coercivities of remanence between 20 and 50 mT. MDF_{ARM}/MDF_{IRM} ratios for radial dike samples are mostly greater than 1, indicating dominance of SD/PSD magnetite. A sample from site SP73, for which AARM fabrics were measured, had a MDF_{ARM}/MDF_{IRM} ratio of ~1, indicating a mixed population of MD and SD/PSD grains.

AMS and AARM Results

Site level mean AMS directions from the Philipsburg Batholith, Square Butte and Shonkin Sag Laccoliths, and SPIC dikes are generally well defined (figure 31). Individual sample data are either well clustered around three orthogonal directions, or data are tightly grouped in one principal susceptibility direction and dispersed in a plane perpendicular to this direction. Most sites from all three intrusions have positive T values, meaning strong AMS foliations and weaker lineations, or oblate fabrics (table 7). A few sites are prolate or triaxial. Degree of anisotropy, P', ranges from 1.05 to 1.32 for the Philipsburg Batholith, 1.01 to 1.03 for the Square Butte Laccolith, 1.01 to 1.10 for the Shonkin Sag Laccolith, and 1.02 to 1.05 for SPIC dike sites. These low P' values are expected for fabrics formed during magma flow (Hrouda, 1982). There is no relationship between T and P' values.

AARM data also have well defined mean principal anhysteretic susceptibility directions for sites from all four sampling localities, although individual sample

directions are not as tightly grouped as those for AMS directions (figure 32). For most sites, three groups of data define orthogonal directions, but it is not uncommon for sample axes to be interchanged compared to the mean direction (e.g. a few $AARM_2$ directions near the mean $AARM_3$ direction). Most sites have positive T values (oblate fabrics), except for the Shonkin Sag Laccolith, where about half the sites have prolate fabrics (table 7). Comparable to AMS data, there is no obvious relationship between AARM T and P' values.

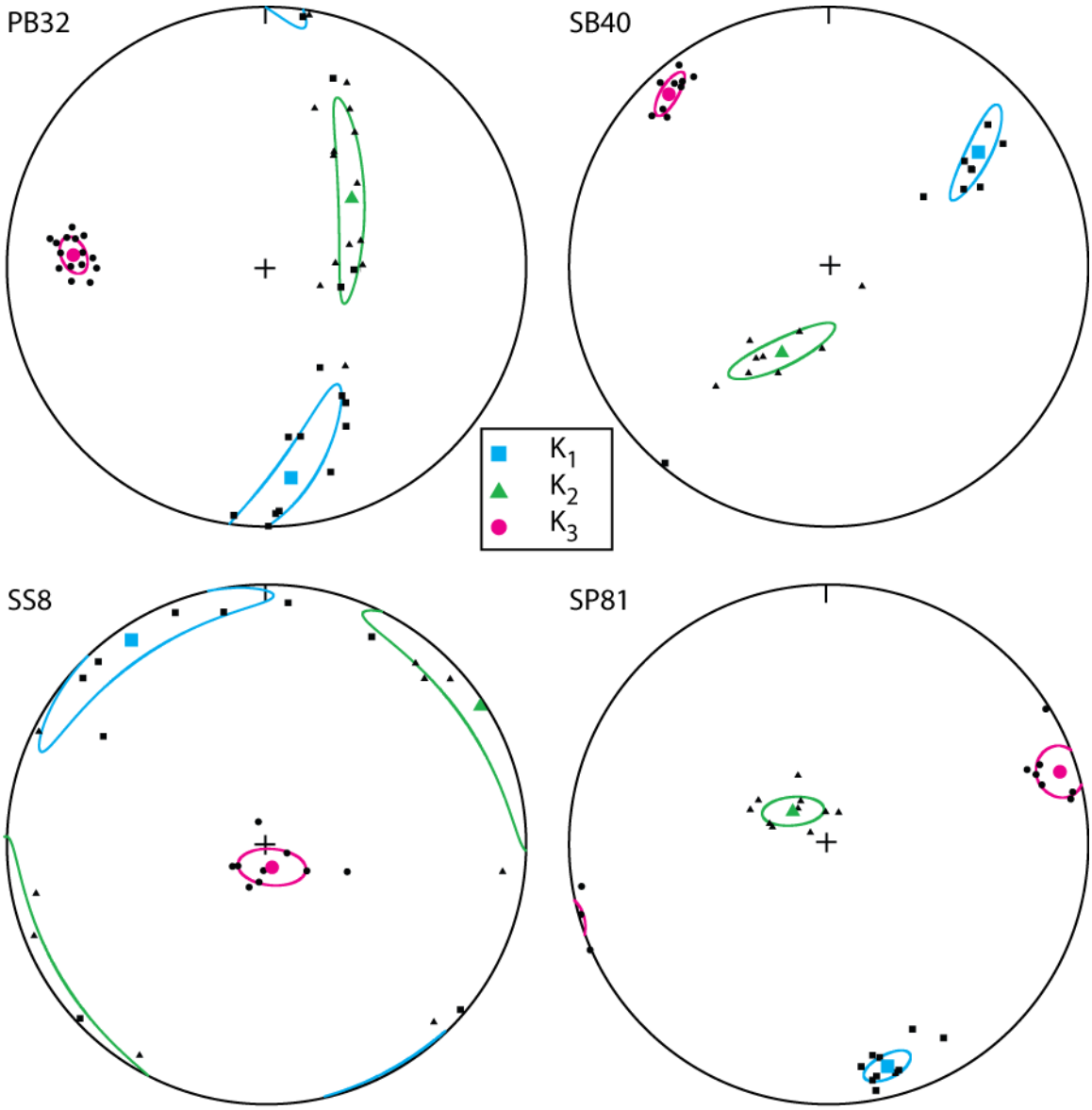

Figure 31. Representative AMS site data showing well defined principal AMS axes for the Philipsburg Batholith, Square Butte and Shonkin Sag Laccoliths, and dikes of the Spanish Peaks Igneous Complex.

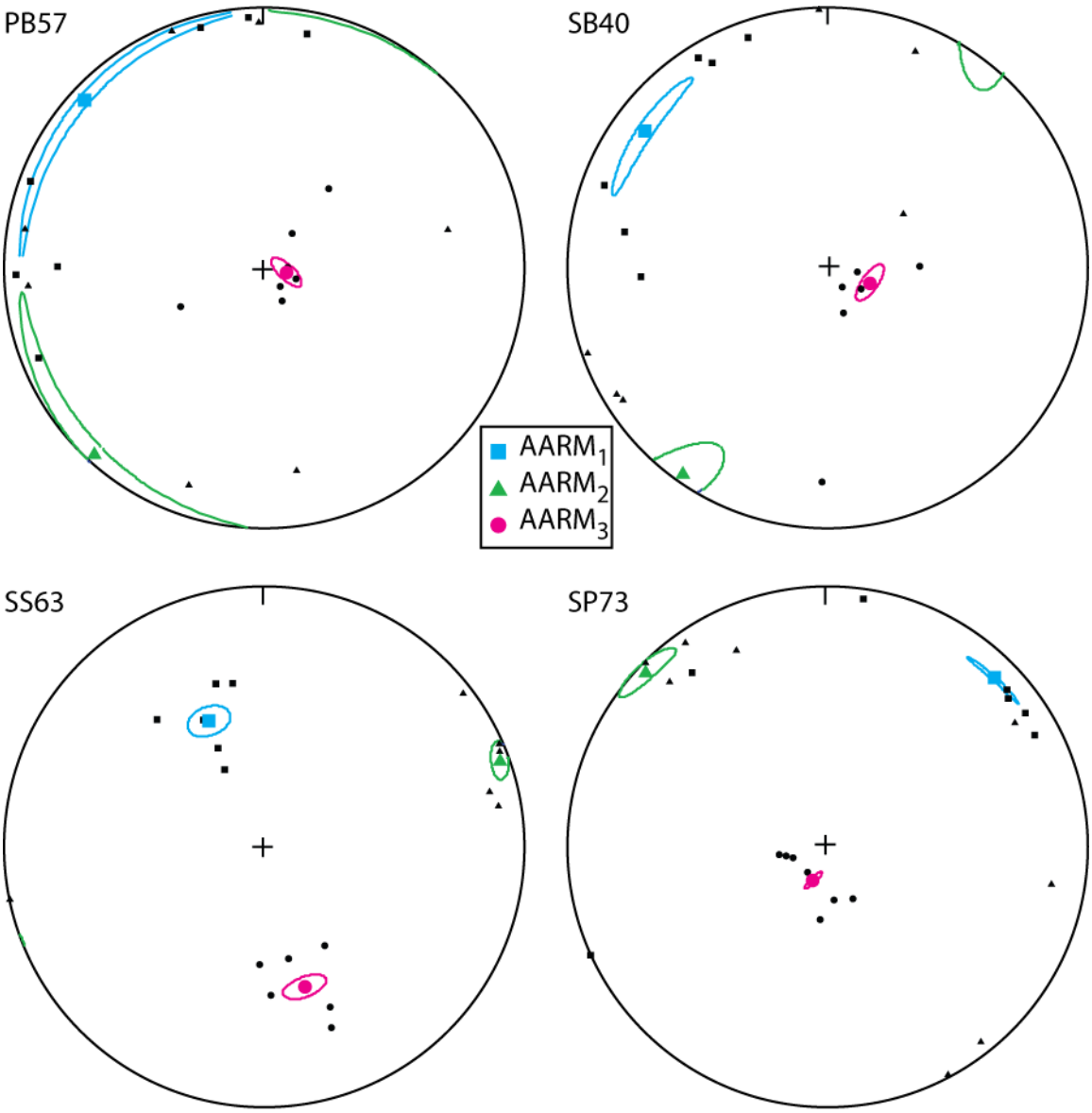

Figure 32. Representative AARM site data showing well defined principal AARM axes for the Philipsburg Batholith, Square Butte and Shonkin Sag Laccoliths, and dikes of the Spanish Peaks Igneous Complex.

Table 7 - Site mean AARM and AMS fabric data for comparisons of the two fabric measurements.

site	AARM Lineation	AARM Foliation	AMS Lineation	AMS Foliation	AARM T	AMS T	AARM P'	AMS P'	AARM/AMS Relationship
				Philipsburg Batholith Sites					
PB12	054.9/21.4	293.0/24.8	062.1/17.5	242.7/88.1	0.0214	-0.515	1.3392	1.326	intermediate
PB23	126.4/27.0	086.1/38.2	107.9/24.2	075.8/40.5	-0.0031	0.638	1.1419	1.123	normal
PB32	205.1/43.7	051.4/65.1	172.8/20.3	003.8/62.8	-0.5093	0.851	1.3957	1.215	oblique
PB43	185.5/67.6	132.9/71.9	193.7/80	150.8/83.1	-0.4036	-0.114	1.1968	1.056	normal
PB52	301.4/4.5	126.4/41.5	160.7/32.4	127/48.7	0.8154	0.224	1.2399	1.24	normal
PB57	313.1/6.0	189.1/7.3	314.7/0.2	135.3/15.2	0.8894	0.762	1.1632	1.086	normal
PB58	315.3/40.2	142.5/81.6	133/10	132/84.1	0.7307	-0.009	1.0906	1.081	normal
PB59	238.6/17.4	097.2/26.8	184.2/6.1	134.7/8	0.715	0.418	1.1064	1.061	normal
				Square Butte Laccolith Sites					
sb36	306.7/10.5	259.3/14.1	254.0/1.4	242.9/7.4	0.7191	0.747	1.0774	1.038	normal
sb39	315.0/8.6	135.5/86.4	214.2/9.3	034.7/87.2	-0.8638	0.317	1.0538	1.011	inverse
sb40	306.3/13.3	200.8/13.8	52.8/29.3	046.7/79.4	-0.0581	0.618	1.0859	1.02	inverse
sb41	285.0/9.8	269.9/33.4	125.8/3.8	111.8/15.5	0.2675	-0.546	1.0433	1.009	normal
				Shonkin Sag Laccolith Sites					
ss5	269.6/17.4	261.0/64.6	280.5/10.5	182.4/10.6	0.5297	0.046	1.0282	1.009	oblique
ss6	260.3/38.7	199.2/42.4	259.8/12.4	192.4/13.4	-0.0676	-0.114	1.027	1.011	oblique
ss7	064.9/21.0	016.2/27.1	242.7/13.5	242.3/88.2	0.2383	0.683	1.0316	1.011	intermediate
ss8	352.6/37.4	316.0/52.1	326.9/7.0	252.9/82.8	0.1144	0.634	1.108	1.02	oblique
ss9	034.3/66.7	276.8/69.0	170.4/9.0	088.9/9.1	-0.2303	0.263	1.0995	1.011	inverse
ss10	332.7/43.7	169.6/73.1	260.3/8.8	148.3/9.5	-0.5159	0.611	1.067	1.021	oblique
ss27	081.0/60.4	000.3/60.8	63.4/19.4	149.5/10.7	-0.5412	-0.050	1.0357	1.012	oblique
ss63	336.0/46.5	253.8/46.8	254.2/10.9	153.4/11.1	-0.2234	0.083	1.1305	1.099	oblique
ss64	299.1/81.4	128.7/88.6	243.2/20.2	120.0/23.7	-0.3176	0.750	1.0289	1.011	inverse
ss65	187.1/42.5	157.6/61.8	166.3/32.5	148.6/25.6	0.1751	0.573	1.059	1.01	normal
ss69	253.5/77.2	207.8/80.8	283.0/5.6	142.9/8.7	0.7713	0.862	1.0143	1.022	inverse
				Spanish Peaks Igneous Complex Dikes					
sp16	328.2/60.8	325.1/88.3	226/82	082/85	-0.46	0.954	1.0831	1.037	oblique
sp73	045.0/10.6	291.2/11.6	207/4	152/15	0.4492	-0.251	1.1016	1.019	normal
sp81	162.4/5.2	150.8/24.3	165/12	163/83	-0.6007	-0.455	1.0401	1.045	intermediate

Comparison of T and P' values from AMS and AARM Data

No obvious correlation exists between AARM P' and AMS P' values, except that AARM P' values are higher than AMS P' values for all but three sites, which have approximately equal AMS and AARM P' values (figure 33). Similarly, no trend was observed when plotting AARM T values against AMS T values (figure 34). Examination of T and P' relationships on the basis of location and fabric relationship type (described below) also yielded no significant relationship between T and P' values for AARM versus AMS.

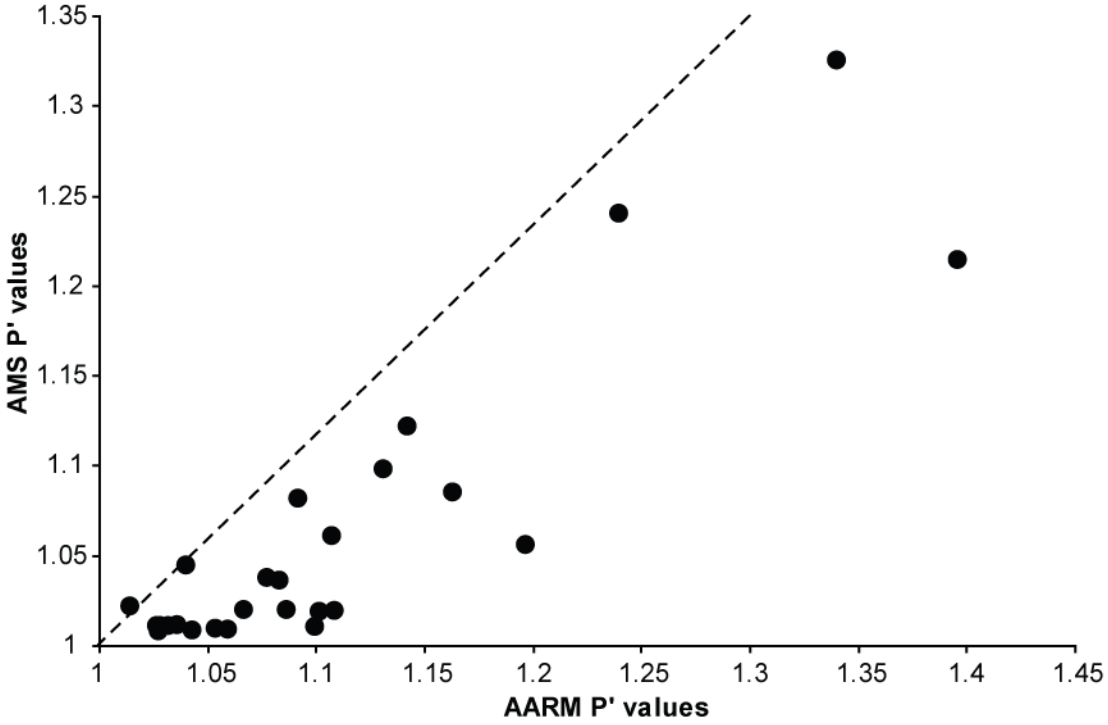

Figure 33. Comparison of degree of anisotropy (P′) values calculated for AARM and AMS ellipsoids from all 26 measured sites. AARM P′ are generally greater than AMS P′ values.

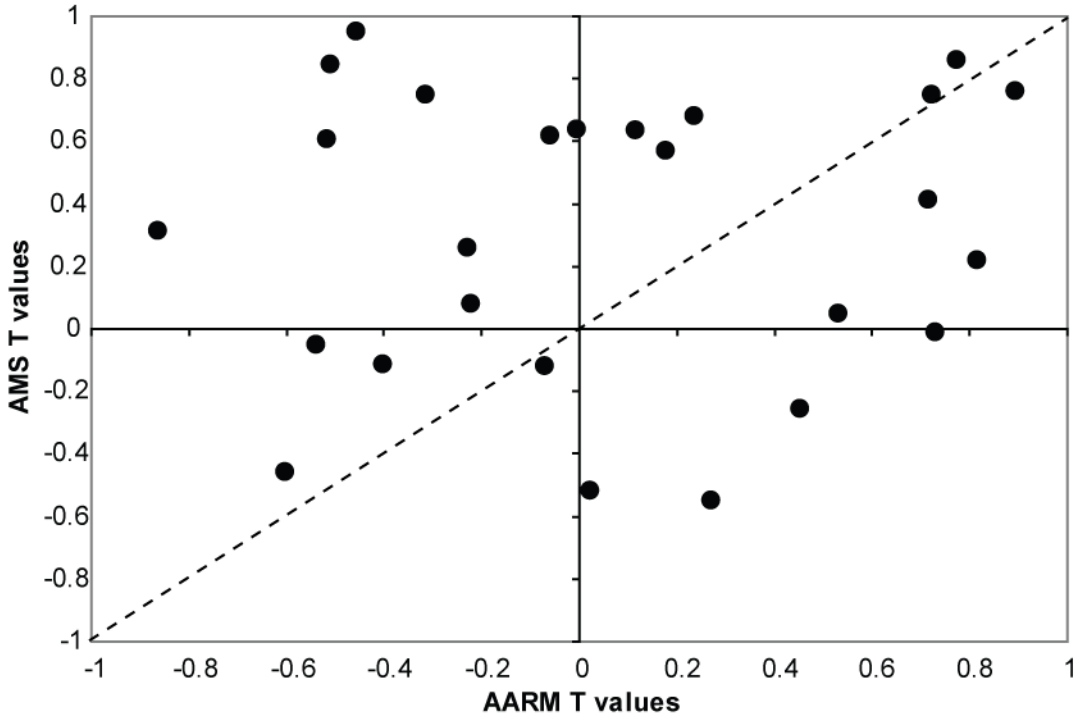

Figure 34. Comparison of the shape parameter (T) calculated for AARM and AMS ellipsoids from all 26 measured sites.

Comparison of AMS and AARM fabrics

Fabric Relationship Types

Four different relationships between AMS and AARM fabrics were observed in the 26 measured sampling sites (figure 35). The first observed fabric relationship is the case when all three principal axes of the AMS and AARM ellipsoids are coaxial. The second observed fabric relationship is characterized by an interchanging of the K_1 and K_3 axes of the AMS ellipsoid, with respect to the $AARM_1$ and $AARM_3$ axes of the AARM ellipsoid. The third fabric relationship is characterized by the interchanging of either the K_1 and K_2, or the K_2 and K_3 axes of the AMS ellipsoid with respect to the axes of the AARM ellipsoid. These three fabric relationships are analogous to the normal, inverse, and intermediate fabrics, repectively, that have been previously described when comparing AMS fabrics to petrofabrics in theoretical models (Rochette et al., 1992;

Ferre, 2002) and in AMS studies of dikes and lava flows (Rochette et al., 1999; Callot et al., 2001; Aubourg et al., 2002; Aubourg and Geoffroy, 2003), except that the AMS ellipsoid is compared to the AARM ellipsoid in the current study. The fourth observed fabric relationship is the case when the AMS and AARM ellipsoid axes are non-coaxial, and therefore the AMS foliation is oblique to the AARM foliation.

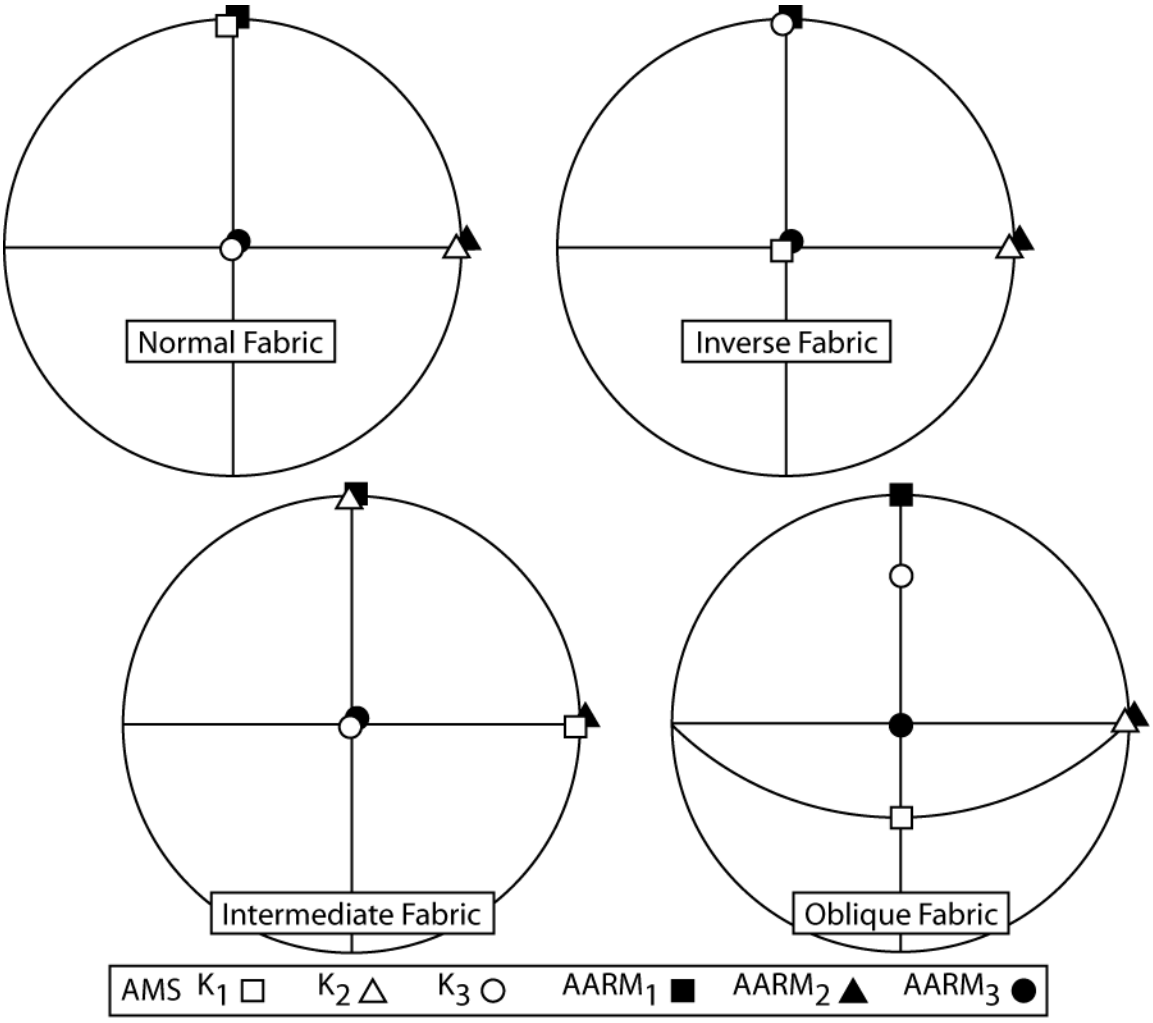

Figure 35. The four relationships between AARM and AMS fabrics observed in this study.

Philipsburg Batholith Fabrics

Three AMS and AARM fabric relationships were identified from eight sites in the Philipsburg Batholith (figure 36). Six sites have normal AMS/AARM fabric relationships. All of the normal sites have oblate or triaxial AMS and AARM ellipsoids, except site PB43, which has a prolate AARM ellipsoid and a triaxial AMS ellipsoid. Site PB12 has an intermediate fabric relationship, with parallel K_1 and $AARM_1$ directions, but an interchanging of the intermediate and minimum principal axes of the AMS and AARM ellipsoids. This is the only Philipsburg Batholith site that has a prolate AMS fabric. Site PB32 has an AMS fabric that is oblique to the AARM fabric. Additionally, these two non-normal sites have AMS P' values above 1.2 and AARM P' values greater than 1.3. All the sites with normal fabric relationships have P' values lower than 1.2, except for site PB52, with P' = 1.24 for both AMS and AARM ellipsoids.

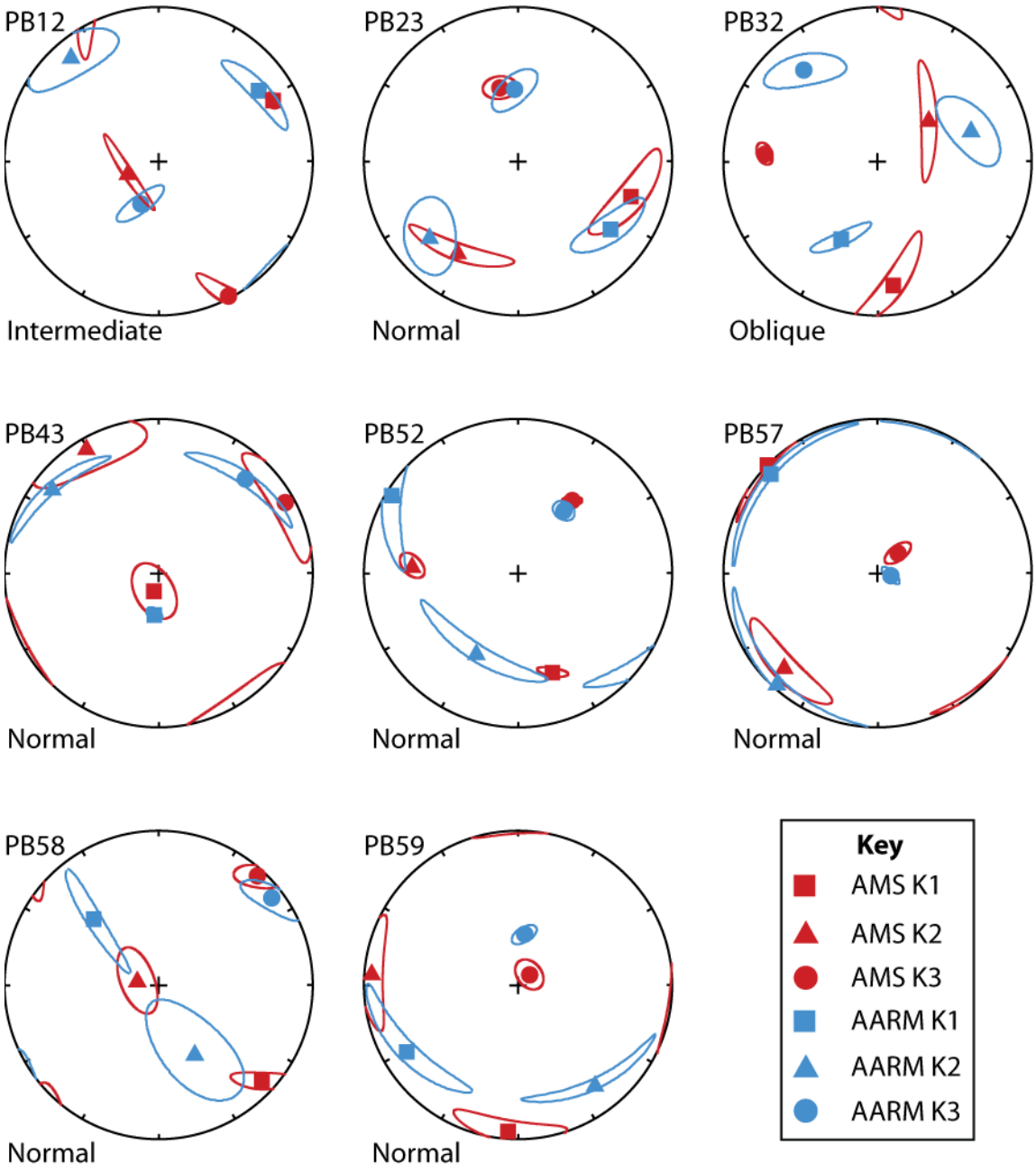

Figure 36. Fabric relationships between AARM and AMS fabrics in eight sites in the Philipsburg Batholith. Stereonets are equal-area plots. 95% confidence ellipses are plotted for each direction.

Square Butte and Shonkin Sag Laccolith Fabrics

Two sites from the Square Butte Laccolith have normal AMS/AARM fabric relationships and two sites have inverse fabric relationships (figure 37). Site SB36 is located in the capping syenite layer on the north side of Square Butte and has a normal

fabric relationship. The other three sites are main-phase shonkinites from the southeast side of Square Butte. Sites SB39 and SB40 have inverse fabric relationships and site SB41 has a normal fabric relationship. Both sites with inverse fabrics have prolate AARM ellipsoids, whereas the sites with normal fabrics have oblate AARM ellipsoids.

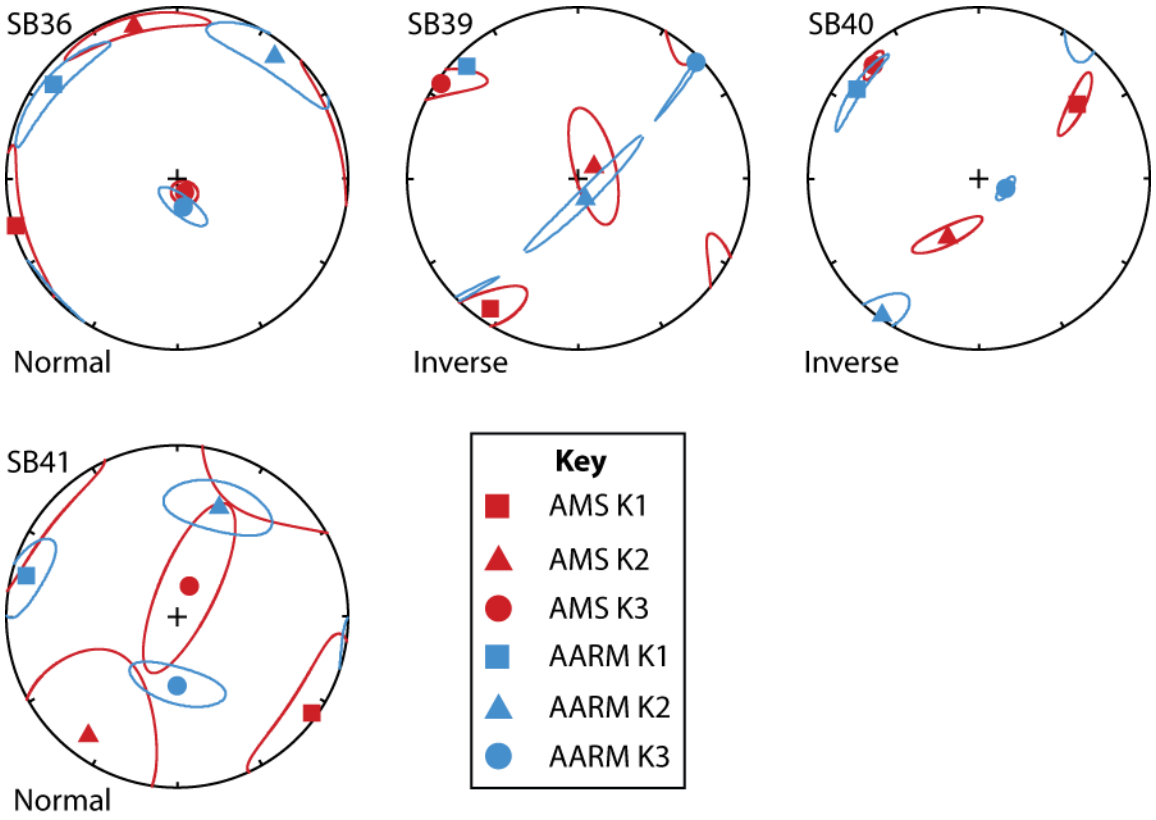

Figure 37. Fabric relationships between AARM and AMS fabrics in four sites in the Square Butte Laccolith. Stereonets are equal-area plots. 95% confidence ellipses are plotted for each direction.

The Shonkin Sag Laccolith (figure 38) has one normal site (SS65), three inverse sites (SS9, SS64, SS69), one intermediate site (SS7) and six sites with oblique fabric relationships (SS5, SS6, SS8, SS10, SS27, SS63). Site SS69, with an inverse relationship, and site SS10, with an oblique relationship, were collected in the syenite unit at the top of

the laccolith. The rest of the sites are shonkinite from a transect through the laccolith on its south side. There is no apparent relationship between T and P' values and fabric relationship type in the Shonkin Sag Laccolith.

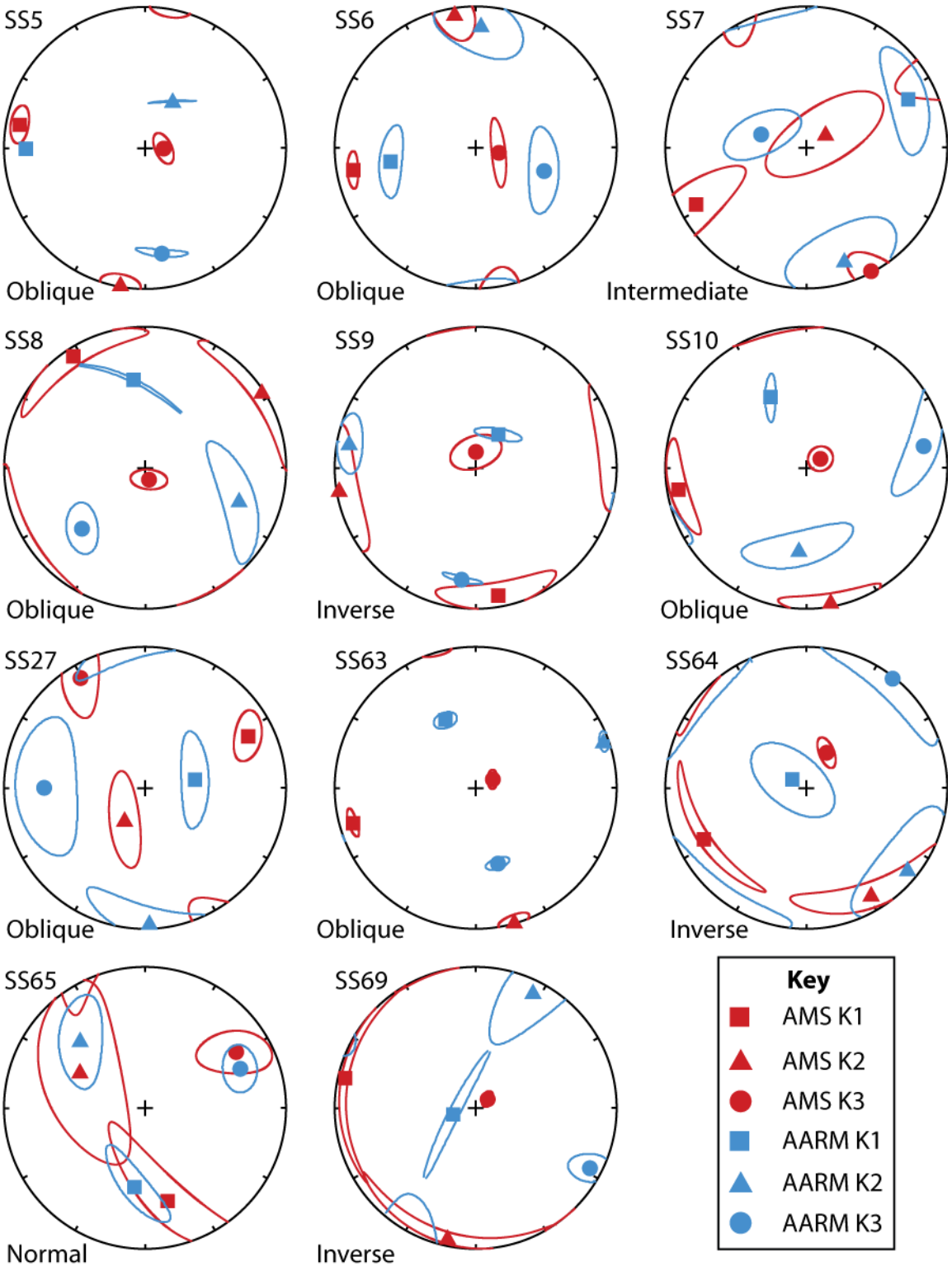

Figure 38. Fabric relationships between AARM and AMS fabrics in eleven sites in the Shonkin Sag Laccolith. Stereonets are equal-area plots. 95% confidence ellipses are plotted for each direction.

SPIC Dike Fabrics

The AMS foliation of one sampled lamprophyre dike (SP16) is parallel to the dike margin, typifying a normal relationship between the AMS ellipsoid and the dike margin. This site has an oblique relationship between AMS and AARM data (figure 39). The $AARM_3$ direction is about 30 degrees from the dike plane. The AMS lineation is perpendicular to the dike margin for the other lamprophyre dike (SP81), typifying an inverse dike margin fabric. The AMS/AARM relationship for SP81 is intermediate. The AARM lineation is also perpendicular to the dike margin, but the $AARM_2$ and $AARM_3$ directions are interchanged compared to the AMS K_2 and K_3 axes.

The AMS fabric of site SP73, from the West Spanish Peak radial dike swarm also has an inverse dike margin relationship. Interestingly, site SP73 has a normal AMS/AARM relationship and all three principal axes of both the AMS and AARM ellipsoids are very well defined, with confidence ellipses less than 20 degrees.

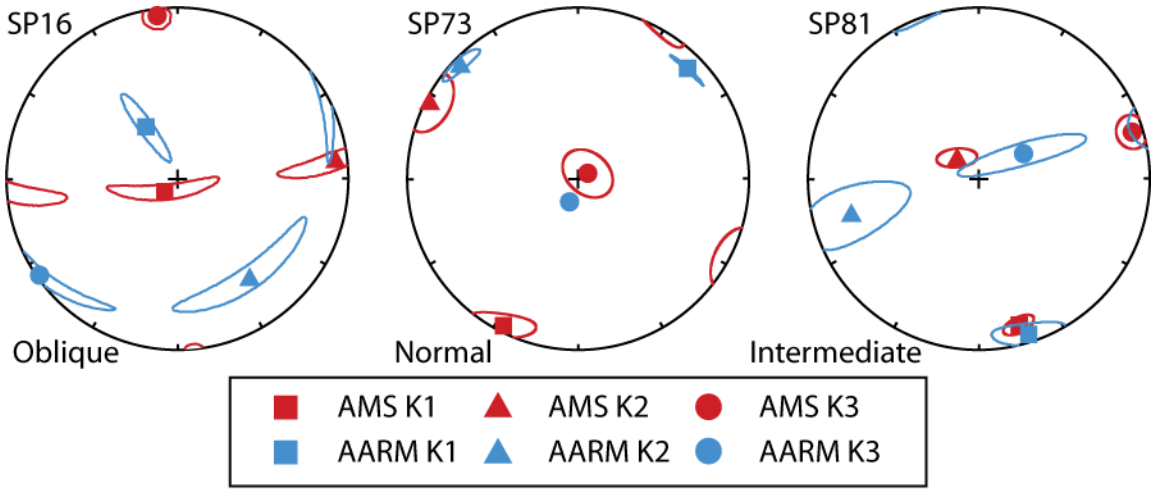

Figure 39. Fabric relationships between AARM and AMS fabrics in three sites in dikes of the Spanish Peaks Igneous Complex. Stereonets are equal-area plots. 95% confidence ellipses are plotted for each direction.

pAARM Results

Three pAARM ellipsoids were measured for two samples from site PB58, which has a normal AARM/AMS relationship. The anhysteretic susceptibilities due to the medium (30-60 mT) and high (60-100 mT) coercivity fractions are at least an order of magnitude less than the anhysteretic susceptibilities of the AARM for both samples PB58b and PB58h. This result shows that most of the AARM signal is controlled by low coercivity grains, likely controlled by the orientation of MD magnetite. The three principal axes of the low coercivity pAARM and the overall AARM ellipsoids are nearly coaxial for both samples (figure 40). The maximum principal axis of the medium coercivity pAARM ellipsoid is also nearly parallel to the $AARM_3$ axis of sample PB58h, and the two other axes of the medium pAARM lie in the AARM foliation plane. This is similar to an inverse relationship between two fabrics, as discussed above for AMS/AARM comparisons, and may indicate that the 30-60 mT pAARM records the same preferred orientation of magnetite as the overall AARM is recording, except the 30-60 mT pAARM is dominated by SD/PSD magnetite grains instead of MD grains.

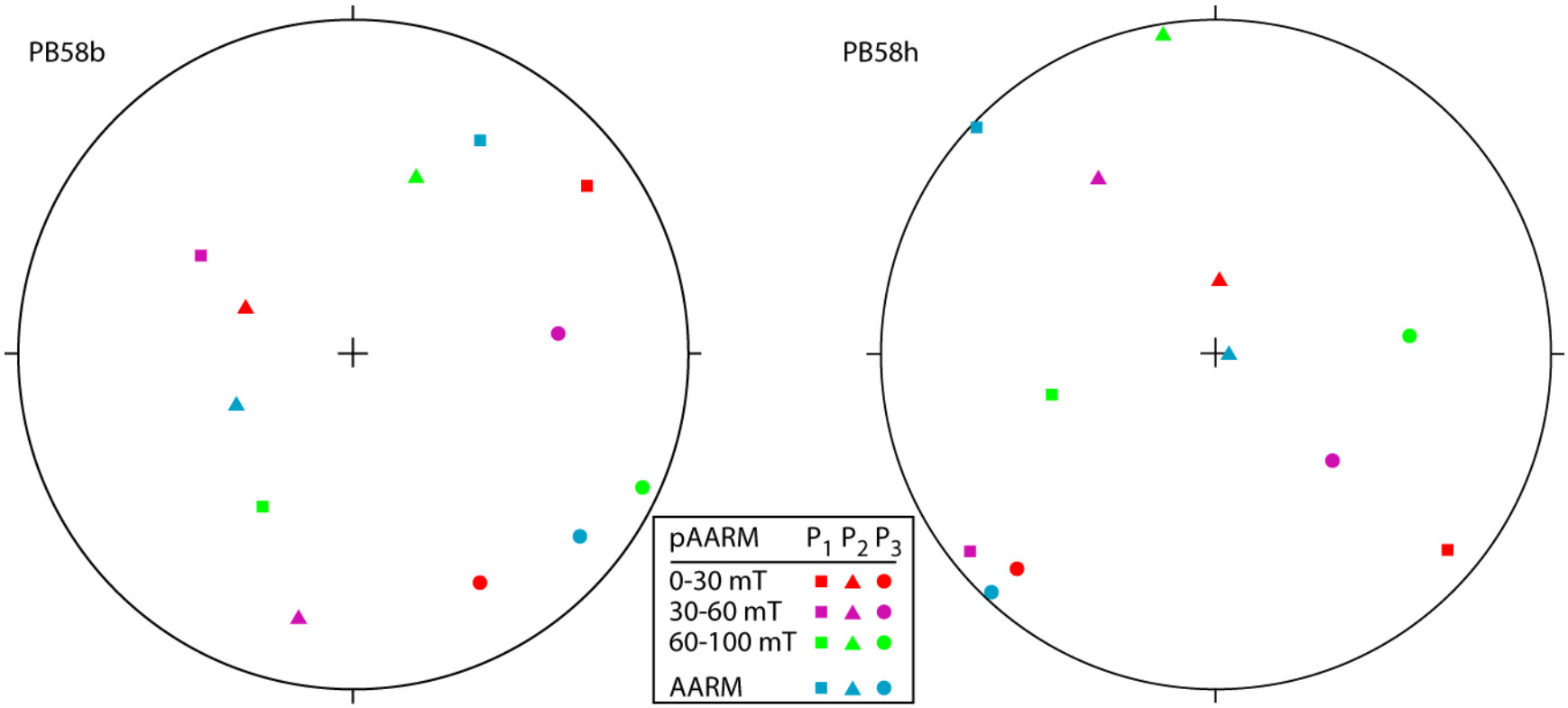

Figure 40. Partial AARM measurements for two samples from site PB58 in the Philipsburg Batholith showing the near parallelism of the preferred orientation of low coercivity (0-30mT) grains with the overall AARM ellipsoid.

Discussion

The high average bulk magnetic susceptibilities for all 26 sites examined in this investigation indicate that the AMS fabric from the all three plutons and the SPIC dikes is dominated by ferro/ferrimagnetic minerals, most likely magnetite. Susceptibility values above 10^{-2} preclude a large contribution to the AMS fabric from paramagnetic minerals, such as micas, amphiboles, or pyroxenes, which have susceptibilities between 10^{-5} and 10^{-4} SI volume (Hrouda, 1982).

The first three AMS-AARM fabric relationship types observed in this study (normal, inverse, and intermediate fabrics) have previously been attributed to the varying amounts of SD magnetite in the samples (Jackson, 1991; Rochette et al., 1992). The long axis of elongate SD magnetite grains is a minimum magnetic susceptibility direction and a maximum anhysteretic susceptibility direction (Jackson, 1991). Therefore, samples with predominantly MD magnetite should exhibit normal AARM/AMS fabric relationships and samples with predominantly SD magnetite should exhibit inverse AARM/AMS fabric relationships. Intermediate fabric relationships may result from a mixed population of MD and SD magnetite, and therefore a mixed population of normal and inverse fabrics (Rochette et al., 1992).

Rock magnetic tests indicate that magnetite in the Philipsburg Batholith is predominantly MD magnetite. If both the AMS and AARM fabrics are controlled by MD magnetite then a normal fabric relationship should exist between the AMS and AARM ellipsoids from Philipsburg Batholith sites. The six sites with normal AARM/AMS fabric relationships in the Philipsburg Batholith confirm MD magnetite as the principal control on both the AMS and AARM fabrics in most of the Philipsburg Batholith. Sites PB12

and PB32, with oblique and intermediate fabric relationships, respectively, are only distinguished from other Philipsburg Batholith samples by higher degrees of anisotropy (P' >1.20). These anisotropy values are slightly higher than normally expected for magma flow fabrics (Hrouda, 1982), which suggests that the AARM and/or AMS fabrics may reflect post-emplacement strain. However, no post-emplacement deformation of these rocks was observed in the field or in petrographic inspection.

Low MDF_{arm}/MDF_{irm} ratios of Square Butte samples also suggest an abundance of MD magnetite in the Square Butte, and AARM/AMS fabric relationships are expected to be normal. Two Square Butte sites do have normal fabric relationships, confirming the control of MD magnetite on the AARM and AMS fabrics. Two other Square Butte sites have inverse fabric relationships, implying that the AMS fabric is controlled by SD magnetite. However, the MDF ratios of these sites are both less than 1, indicating the dominance of MD magnetite.

Shonkin Sag Laccolith samples are also dominated by MD magnetite, as shown by low MDF_{arm}/MDF_{irm} ratios. One site has a normal fabric relationship and one site has an intermediate fabric relationship. Most sites have oblique or inverse fabric relationships, indicating that MD magnetite may not be the dominant control on AMS fabrics. Site SS5 is the only site with a high MDF ratio, indicating abundant SD/PSD magnetite. This site has an oblique fabric that is closer to intermediate than it is to normal or inverse.

Two of the sites from SPIC dikes have AMS foliations that are perpendicular to the dike margins. The other dike we examined has an AMS foliation parallel to the dike margin. Contrary to the expected alignment of elongate magnetite grains during magma

flow, none of the three dikes have margin parallel AARM. Rock magnetic tests indicate that site SP16 is dominated by SD/PSD magnetite, which should yield inverse fabrics. The AMS fabric for SP16 is normal to the dike margin, and the AARM/AMS relationship is oblique. Site SP81 has an inverse dike margin fabric, as predicted by the MDF ratio, and an intermediate AARM/AMS relationship. The most interesting site is SP73, which has an AMS fabric inverse to the dike margin and yet a normal AARM/AMS relationship. This site has a normal AARM/AMS relationship, which is expected for of the mixed assemblage of MD and SD/PSD magnetite identified at this site by rock magnetic tests. These results show that the relationships between AMS fabrics and dike margins may not always reflect contributions by SD magnetite on AMS fabrics.

The similarity of the low coercivity pAARM ellipsoids to the AARM ellipsoids for samples PB58b and PB58h confirms that the AARM signal at this site is dominated by the lowest coercivity magnetite grains, which are likely MD. The inverse relationship between the low and middle coercivity pAARM ellipsoids from sample PB58h indicates that a higher coercivity population is probably composed of SD/PSD magnetite that has the same preferred orientation as lower coercivity grains. We interpret these results to indicate that all size fractions of magnetite in site PB58 were oriented at the same time, probably due to magma flow during emplacement. Although we do not have pAARM data from other sites in the batholith, we infer that all sites in the Philipsburg Batholith probably record one preferred magnetite orientation.

Of the 16 sites in this study with non-normal AARM/AMS fabric relationships, 13 have MDF_{arm}/MDF_{irm} ratios less than 1, implying that magnetite at these sites is mostly MD magnetite. One possible explanation for this observation is that the dominant

size fraction of magnetite, which is MD, may not control the AMS fabric. It is possible that sites with inverse AARM/AMS relationships have a population of MD magnetite with a very weak preferred orientation (nearly isotropic) and a strong preferred orientation of elongate SD magnetite grains. AMS and AARM fabrics for these samples would be controlled by the orientation of SD grains and the resulting fabrics would exhibit an inverse relationship. Intermediate fabrics can similarly be explained by a mixture of a strongly anisotropic population of SD grains and a weakly anisotropic, but more abundant population of MD grains.

Although the mixture of different grain sizes of magnetite with differing anisotropies is a viable explanation for the observed inverse and intermediate AARM/AMS fabric relationships at sites dominated by MD magnetite, this explanation is notably further complicated when the degrees of anisotropy for normal and inverse sites from the same intrusion are compared. The four sites from the Square Butte Laccolith have half normal and half inverse AARM/AMS relationships. All four sites have very similar degrees of anisotropy (P') and are all dominated by MD magnetite. If the AMS from the inverse sites is due to the anisotropy of small populations of SD magnetite and nearly isotropic MD magnetite, then the SD populations must have very strong anisotropy in order to make the P' values for the inverse sites similar to the P' values of the normal sites, because all the magnetite size fractions are contributing to the AMS measurements relative to their volume. We have difficulty providing a mechanism affecting a single intrusion that would give a strong preferred orientation to SD magnetite but not MD magnetite at some sites, and a moderate preferred orientation to all magnetite size fractions at other sites.

Eight measured sites have AMS fabrics that are oblique to the AARM fabrics. These oblique fabric relationships cannot be explained by the mixing of SD and MD magnetite populations with a single preferred orientation. AARM fabrics oblique to AMS fabrics have been observed in mafic dikes from Salvador in NE Brazil and multiple preferred orientations of populations of magnetite with different grain sizes were suggested to explain these oblique fabrics, but this explanation was inconsistent with reported pAARM fabrics (Raposo and Berquo, 2008). It is possible that the AARM ellipsoid reflects the preferred orientation of magnetite, but that the AMS signal is controlled by a stronger preferred orientation of paramagnetic silicates. This model could explain oblique fabrics in samples with low bulk susceptibilities (~10^{-5} to 10^{-4} SI per cm^3) but is inconsistent with rocks exhibiting high bulk susceptibilities, such as those we observe in this study. Paramagnetic silicates account for less than one percent of the bulk susceptibility for samples with susceptibilities around 10^{-2} SI per cm^3, which would require very strong anisotropies in paramagnetic grains. The highest P' values of single crystals of pyroxenes and amphiboles only reach P = 1.4 (Hrouda, 1982), indicating that the anisotropy of perfectly aligned populations of paramagnetic minerals is certainly not strong enough to affect AMS of rocks of high bulk susceptibility. Even if our current estimates of the anisotropies caused by alignment of paramagnetic silicates are much lower than what is realistic, the alignment of paramagnetic silicates required to affect the AMS of samples examined in this study would surely make the fabrics visible at the outcrop or in thin section.

The results of this study indicate that AARM is a useful tool for assessing the validity of AMS fabrics in plutonic rocks. Most sites from the Philipsburg Batholith have

normal AARM/AMS fabric relationships indicating that AMS measurements are not complicated by the inverse effect of SD magnetite. The range of fabric relationships from the Square Butte and Shonkin Sag Laccoliths suggest that more detailed rock magnetic data and more petrographic observations are required to fully characterize the controls on AMS fabrics. For the Spanish Peaks dikes, the differences between AARM/AMS fabric relationships and comparisons of the AMS fabric to the dike margins imply that the inverse or intermediate dike margin relationships may not always be due to the inverse effect of SD magnetite and other mechanisms may result in dike margin perpendicular foliations developing during magma flow or after dike emplacement. More AARM measurements are required for a broader understanding of the relationship between AARM fabrics and the orientation of dike margins. Additional pAARM measurements are also required to clarify the influence of different magnetite size fractions on both AARM and AMS ellipsoids.

Conclusions

We have compared the AARM and AMS fabrics of 26 sampling sites from three intrusions and three dikes. Four AARM/AMS fabric relationships have been identified. These fabrics are termed normal, inverse, intermediate, and oblique fabrics, and are similar to previously described comparisons of AMS with dike wall orientations (e.g. Rochette, 1999). Multiple fabric relationships were found in all three intrusions examined, suggesting that the controls on AMS may vary within magma bodies. AARM/AMS relationships for three dikes are not the same as the relationship of AMS to the dike margins. Most notably, both AMS and AARM fabrics of dike SP73 have inverse relationships to the dike margin, implying that SD magnetite is not responsible for the

margin perpendicular AMS foliation. The non-parallel relationships between AARM foliations and dike margins suggest that the preferred orientation of ferro/ferromagnetic minerals in these rocks is not aligned parallel to flow, as often assumed in AMS studies. The assumption that AMS fabrics controlled by the preferred magnetite orientations are aligned by magma flow could also be questioned in larger intrusions, such as batholiths.

The varying AARM/AMS fabric relationships identified in a variety of intrusive igneous rocks indicate that more than one preferred orientation may be recorded in magnetic fabric studies, which may complicate the interpretation of magma flow paths in intrusive rocks. If more than one preferred magnetite orientation is present in igneous rocks, AMS fabric interpretations from plutons may be erroneously based on a non-magmatic alignment of a subpopulation of magnetite grains or on a combination of two preferred fabrics. It is therefore important to compare AMS fabrics to AARM fabrics and, ideally, to petrofabrics determined in outcrop, thin section, or image analysis in order to test the underlying assumption that AMS data reflect petrofabric orientations.

Partial AARM ellipsoids measured for two samples from site PB58 in the Philipsburg Batholith over three coercivity windows show that the axes of the pAARM ellipsoid for the lowest coercivity window are nearly coaxial with the axes of the AARM ellipsoid for both samples, confirming that the AARM is controlled by MD magnetite. We suggest that AARM and pAARM are important tools for understanding the controls of AMS in plutonic rocks.

Chapter Two Acknowledgements

We would like to thank Dr. Mike Jackson for help with hysteresis measurements at the University of Minnesota Institute of Rock Magnetism. We are grateful to Jack Grow and Christina Carr for field assistance during the summer of 2007. We would also like to thank Will Woodruff for assistance with rock magnetic experiments for the

Shonkin Sag Laccolith and Nick George for assistance with sample preparation and AMS measurements of the Shonkin Sag and Square Butte Laccoliths. This project was funded by grants to T. Naibert from the Geological Society of America, the Office of Graduate Studies and Dept. of Earth and Planetary Sciences at the University of New Mexico. A UNM Research Allocations Committee award to J. Geissman supported the field sampling of the Square Butte and Shonkin Sag laccoliths.

References Cited

Aranguren, A., Cuevas, J., Tubia, J.M., Roman-Berdiel, T., Casas-Sainz, A., Casas-Ponsati, A., 2003, Granite laccolith emplacement in the Iberian arc: AMS and gravity study of the La Tojiza pluton (NW Spain): Journal of the Geological Society London, v. 160, p. 435-445.

Aubourg, C., and Geoffroy, L., 2003, Comment on paper: Magnetic fabric and inferred flow direction of dikes, conesheets and sill swarms, Isle of Skye, Scotland: Journal of Volcanology and Geothermal Research, v. 122, p. 143-144.

Aubourg, C., Giordano, G., Mattei, M., Speranza, F., 2002, Magma flow in sub-aqueous rhyolite dikes inferred from magnetic fabric analysis (Ponza Island, Italy): Physics and Chemistry of the Earth, v. 27, p. 1263-1272.

Bouchez, J.-L., 1997, Granite is never isotropic: an introduction to AMS studies of granitic rocks, *in* Bouchez, J.-L., Hutton, D.H.W., and Stephens, W.E., eds., Granite: from segregation of melt to emplacement fabrics: Dordrecht, Holland, Kluwer Academic Publishers, p. 95-112.

Bouchez, J.-L., Gleizes, G., Djouadi, T., Rochette, P., 1990, Microstructure and magnetic susceptibility applied to emplacement kinematics of granites: the example of the Foix pluton (French Pyrenees): Tectonophysics, v. 184, p. 157-171.

Bulter, R.F., 1992, Paleomagnetism: magnetic domains to geologic terranes: Boston, Massachusetts, Blackwell Scientific Publishing. 336 p.

Callot, J.-P., Geoffrey, L., Aubourg, C., Pozzi, J.-P., Mege, D., 2001, Magma flow directions of shallow dikes from the East Greenland volcanic margin inferred from magnetic fabric studies: Tectonophysics, v. 335, p. 313-329.

Day, R., Fuller, M., Schmidt, V.A., 1977, Hysteresis properties of titanomagnetites: grain size and compositional dependence: Physics of the Earth and Planetary Interiors, v. 13, p. 260–267.

Dunlop, D.J., and Özdemir, Ö., 1997, Rock Magnetism: Cambridge, United Kingdom, Cambridge University Press, 596 p.

Ferre, E., 2002, Theoretical models of intermediate and inverse AMS fabrics; Geophysical Research Letters, v. 29, p. 31-1-4.

Gebelin, A., Martelet, G., Chen, Y., Brunel, M., Faure, M., 2006, Structure of late Variscan Millevaches leucogranite massif in the French Massif Central: AMS and gravity modeling results: Journal of Structural Geology, v. 28, p. 148-169.

Hrouda, F., 1982, Magnetic anisotropy of rocks and its application in geology and geophysics: Geophysical Surveys, v. 5, p. 37-82.

Hyndman, D.W., Silverman, A.J., Ehinger, R., Benoit, W.R., Wold, R., 1982, The Philipsburg Batholith, Western Montana: Montana Bureau of Mines and Geology Memior, v. 49, p. 1-37.

Jackson, M., 1991, Anisotropy of magnetic remanence: a brief review of mineralogical sources, physical origins, and geological applications, and comparison with susceptibility anisotropy: Pure and Applied Geophysics, v. 136, p. 1-28.

Jelinek, V., 1978, Statistical processing of magnetic susceptibility measured in groups of specimens: Studia Geophysica et Geodaetica, v. 22, p. 50–62.

Kendrick, G.C., and Edmond, C.L., 1981, Magma immiscibility in the Shonkin Sag and Square Butte laccoliths: Geology, v. 9, p. 615-619.

King, J., Banerjee, S.K., Marvin, J., Ozdemir, O., 1982, A comparison of different methods for determining the relative grain size of magnetite in natural sediments: some results from lake sediments: Earth and Planetary Science Letters, v. 59, p. 404-419.

McCabe, C., Jackson, M., Ellwoods, B., 1985, Magnetic anisotropy in the Trenton limestone: results of a new technique, anisotropy of anhysteretic susceptibility: Geophysical Research Letters, v. 12, p. 333-336.

Muggleton, S.R., 2006, Paleomagnetism and anisotropy of magnetic susceptibility of the Spanish Peaks igneous complex, south-central Colorado: implications for the North American mid-Cenozoic reference paleomagnetic pole and magma emplacement mechanisms [M.S. Thesis]:Albuquerque, University of New Mexico, 195 p.

O'Connell, M.P., 2000, Geometry, kinematics, and emplacement mechanisms of the Philipsburg Batholith within the Sevier fold-and-thrust belt, Flint Creek Range, western Montana [M.S. Thesis]: Bozeman, Montana State University, 99 p.

Raposo, I., and Berquo, T., 2008, Tectonic fabric revealed by AARM of the proterozoic mafic dike swarm in the Salvador city (Bahia State): Sao Francisco Craton, NE Brazil: Physics of the Earth and Planetary Interiors, v. 167, p. 179-194.

Rochette, P., Jackson, M., Aubourg, C., 1992, Rock magnetism and the interpretation of anisotropy of magnetic susceptibility; Review of Geophysics, v. 30, p. 209-226.

Rochette, P. Aubourg, C., Perrin, M., 1999, Is this magnetic fabric normal? A review and case studies in volcanic formations: Tectonophysics, v. 307, p. 219-234.

Tauxe, L., 1998, Paleomagnetic principals and practice: Dordrecht, Holland, Kluwer Academic Publishers, Modern Approaches in Geophysics, v. 17, 299 p.

Titus, S.J., Clark, R., Tikoff, B., 2005, Geological and geophysical investigation of two fine-grained granites, Sierra Nevada batholith, California: evidence for structural controls on emplacement and volcanism: Geological Society of America Bulletin, v. 117, p. 1256-1271.